NOVA SCHOOL OF SCIENCE & TECHNOLOGY

DEPARTMENT OF PHYSICS

INÊS CAROLINA DOS SANTOS RODRIGUES

BSc in Biomedical Sciences

# SYNTHESIS AND CHARACTERIZATION OF STIMULI-RESPONSIVE MESOPOROUS SILICA NANOPARTICLES

MASTER IN BIOMATERIALS AND NANOMEDICINE

NOVA University Lisbon
September, 2023

DEPARTMENT OF PHYSICS

# SYNTHESIS AND CHARACTERIZATION OF STIMULI-RESPONSIVE MESOPOROUS SILICA NANOPARTICLES

**INÊS CAROLINA DOS SANTOS RODRIGUES**

BSc in Biomedical Sciences

**Advisor:** Drª Sandra Gago
*Assistant Researcher, NOVA University Lisbon*
**Co-advisor:** Dr Nuno Basílio
*Assistant Researcher, NOVA University Lisbon*

**Examination Committee:**
**Chair:** Dr Jorge Carvalho Silva
*Associate Professor, NOVA University Lisbon*
**Rapporteurs:** Drª Carina Crucho
*Junior Researcher, Instituto Superior Técnico*
**Adviser:** Drª Sandra Gago
*Associate Researcher, NOVA University Lisbon*

MASTER IN BIOMATERIALS AND NANOMEDICINE

NOVA University Lisbon
September, 2023

**SYNTHESIS AND CHARACTERIZATION OF STIMULI-RESPONSIVE MESOPOROUS SILICA NANOPARTICLES**

# ACKNOWLEDGMENTS

Começo por agradecer aos meus orientadores, Drª. Sandra Gago e Dr. Nuno Basílio, por me guiarem nesta minha escolha, diria ousada, com certeza com muita paciência. Acabei por aceitar o desafio e explorar um tema muito ligado à Química que, apesar das bases adquiridas na licenciatura, se afasta um pouco da minha área de formação. Agradeço imenso aos restantes integrantes do grupo de Fotoquímica, que sempre se mostraram disponíveis em ajudar, respondendo às dúvidas e curiosidades que me foram surgindo. Agradeço em especial à Patrícia e à Mariana porque em conjunto, e com muitas risadas nas horas livres, conseguimos tornar tudo um pouco mais fácil. Foi ótimo podermos discutir e debater ideias, algo que adoro fazer. Agradeço também muito à minha família e amigos. Pelo apoio que me foi dado durante este percurso de um ano, tanto nos momentos altos como nos baixos. Por fim, e nao menos importante, agradeço ao coordenador do curso, Dr. Jorge Carvalho Silva, e aos restantes professores do mesmo, que foram quem o tornou possível.

Este ano foi, sem dúvida, um grande desafio, cheio de emoções e aprendizagens, que não teria sido o mesmo sem o contributo e apoio de todos. Foram muitas as trocas de ideias, as dicas e os conhecimentos transmitidos.

“A ship is always safe at the shore, but that is not what it is built for”

Albert Einstein

# ABSTRACT

Mesoporous silica nanoparticles (MSNs) are among the most widely used materials in biomedicine, due to their high biocompatibility and easy functionalization that allow the development of promising nanocarriers able to react to different stimuli. This thesis focused on the synthesis and characterization of Spiropyran (SP) derivatives, a class of light-sensitive molecules that exhibit thermal stability and undergo reversible switching between two spectrally well-separated states. One model compound and its heterogeneous counterpart based on functionalized MSNs (MSN-SP) were prepared and studied. Their interaction with cucurbit[7]uril (CB7) was also investigated to create a nanovalve system regulated by light-activated protonation and deprotonation processes. Spiropyran exhibits higher stability at pH=4, when in its protonated merocyanine form, and its $pK_a$ values are near 7, even in the presence of CB7. However, when in suspension, the MSN-SP complex barely remains stable, although CB7 and an acidic pH seem to enhance it. ITC calorimetry tests enabled the determination of the SP-CB7 complex binding affinity ($K_A$) values, which were found to be $1.445 \times 10^7$ $M^{-1}$, at pH=4.2, and in the order of $10^5$ $M^{-1}$, for pH=7.5. Another system based on ammonium functionalized MSNs (MSN-TESPAI) was prepared, and its DNA adsorption capacity or desorption in the presence of CB7 were studied by UV-Vis spectroscopy and DLS analysis. All compounds and materials prepared were characterized by several techniques ($^1$H NMR, FTIR, $N_2$ adsorption, Elemental analysis, XRD and TGA) that confirm their successful synthesis and functionalization, with loadings of ≈0.55mmol/g and ≈3.6mmol/g for MSN-SP and MSN-TESPAI, respectively.

**Keywords**: Mesoporous Silica Nanoparticles, Spiropyran, cucurbit[7]uril, Nanovalve system, Controlled drug release, DNA adsorption

# RESUMO

As Nanopartículas de silica mesoporosa (MSNs) são dos materiais mais utilizados na biomedicina por serem biocompatíveis e de fácil funcionalização, o que lhes permite desempenhar o papel de transportadores, responsivos a diversos estímulos. Esta tese teve como foco a síntese e caracterização de derivados de Espiropirano (SP), uma classe de moléculas sensíveis à luz, estável termicamente e com propriedades reversíveis. Preparou-se um composto modelo e o seu heterogéneo correspondente baseado em MSNs funcionalizadas (MSN-SP) para a realização dos estudos em solução e suspensão, assim como a sua interação com o cucurbit[7]urilo (CB7) de modo a se criar um sistema de nanoválvula. Este sistema seria regulado por processos de protonação e desprotonação ativados por luz. Os SP mostraram maior estabilidade a pH=4, quando na sua forma de merocianina protonada, e possuem valores de $pK_a$ proximos de 7, mesmo na presença de CB7. No entanto, o complexo MSN-SP dificilmente permanece estável em suspensão, mesmo que tanto o CB7 como a criação de um meio acídico o pareçam potenciar. Testes de calorimetria por ITC permitiram averiguar que o complexo SP-CB7 possui uma constante de afinidade ($K_A$) de $1.445x10^7$ $M^{-1}$, a pH=4.2, e na ordem dos $10^5$ $M^{-1}$, a pH=7.5. Foi também preparado outro sistema baseado em MSN funcionalizadas com amónios (MSN-TESPAI), para que testes por espectroscopia UV-Vis e DLS permitissem explorar a capacidade de adsorção e desadsorção de DNA na presença de CB7. Todos os compostos e materiais produzidos foram caracterizados recorrendo a várias técnicas ($^1$H NMR, FTIR, $N_2$ adsorption, Elemental analysis, XRD and TGA) que permitiram confirmar o sucesso da síntese e da funcionalização, apresentando valores a rondar os 0.55 e os 3.6 mmol/g para MSN-SP e MSN-TESPAI, respetivamente.

**Palavras-chave**: Nanopartículas de Silica Mesoporosa, Espiropiranos, cucurbit[7]urilo, Sistema de nanoválvula, Libertação controlada de fármacos, Adsorção de DNA

# CONTENTS

# LIST OF FIGURES

# LIST OF TABLES

# ABBREVIATIONS AND ACRONYMS

| | |
|---|---|
| **(3-chloropropyl)triethoxysilane** | CPTES |
| **Acetonitrile** | ACN |
| **Absorption, distribution, metabolism, excretion** | ADME |
| **Cetyltrimethylammonium Bromide** | CTAB |
| **Cucurbit[7]uril** | CB7 |
| **Deoxyribonucleic acid** | DNA |
| **Dichloromethane** | DCM |
| **Diethyl ether** | $Et_2O$ |
| **Dimethyl sulfoxide** | DMSO |
| **Drug delivery system** | DDS |
| **Dynamic light scattering** | DLS |
| **Ethanol** | EtOH |
| **Focused ultrasounds** | FUS |
| **Fourier-transform infrared** | FTIR |
| **Isothermal titration calorimetry** | ITC |
| **Merocyanine** | MC |
| **Mesoporous silica nanoparticles** | MSNs |
| **Methanol** | MeOH |
| **Mobil composite material number 41** | MCM-41 |
| **Molecular weight** | MW |
| **Nanoparticles** | NPs |
| **Nuclear magnetic resonance** | NMR |
| **Phosphate buffer solution** | PBS |
| **Polyethylene glycol** | PEG |

| | |
|---|---|
| **Proton nuclear magnetic resonance** | $^{1}$H NMR |
| **Protonated Merocyanine** | MCH |
| **Ribonucleic acid** | RNA |
| **Spiropyran** | SP |
| **Tetraethyl orthosilicate** | TEOS |
| **Thin Layer Chromatography** | TLC |
| **Toluene** | MePh |
| **Transmission Electron Microscopy** | TEM |
| **Triethanolamine** | TEA |
| **Ultraviolet** | UV |
| **Ultraviolet-visible** | UV-Vis |
| **U.S. Food and Drug Administration** | FDA |
| **X-ray diffraction** | XRD |
| **zeta potential** | ζ-potential |

# SYMBOLS

| | |
|---|---|
| $H^+$ | Protons |
| **ppm** | Parts per million |
| **rpm** | Rotations per minute |
| $\bar{\nu}$ | Wavenumber |
| $\nu$ | Stretching |
| $\nu_s$ | Symmetric stretching |
| $\nu_{as}$ | Asymmetric stretching |
| $\delta$ | Bending |
| $\lambda$ | wavelength |
| **A** | Absorbance |
| $h\nu$ | Energy of a photon |
| $C_f$ | Final concentration |
| $C_o$ | Initial concentration |
| **p.a** | "para análise" (for analysis) |
| **kc** | Thermal ring-closure |
| **ko** | Thermal ring-opening |
| $K_a$ | Acid dissociation constant |
| $K_A$ | Binding affinity |
| $K_D$ | Dissociation constant |
| $p/p^o$ | Relative pressure |
| $A_{BET}$ | Specific surface area obtained from BET's method |
| $D_p$ | Pore diameter |
| $V_p$ | Cumulative pore volume |

| | |
|---|---|
| $\mathbf{n_{abs}}$ | Nitrogen adsorption |

# 1. INTRODUCTION

## 1.1 Drug delivery systems

In biomedicine, the route chosen for drugs' administration affects their absorption, distribution, metabolism, and excretion (ADME) within the body. These four parameters correspond to drugs' pharmacokinetics which also affects the bioavailability of the administered substance [1] hence the success of the therapy. To overtake this problem, throughout the years there has been an increase in drug delivery systems (DDS) development and use. These systems have been designed using a wide array of materials and chemical strategies functioning as carriers that can remain in the body system for prolonged periods of time and reach targeted locations enhancing therapies' success [2].

One area that has significantly gained attention over the last two decades, and is progressively being used in DDS, is Nanotechnology. This field is defined as the engineering and manipulation of particulate matter into a physical state between 1 and 100nm that can be rearranged into nano-systems (nanomaterials) with improved functions [3]. This optimal value considers that smaller particles are quickly excreted and those bigger could be blocked on blood vessels [4], where there is no defined optimum value. Some studies suggest that 50nm is an optimum particle size for efficient cell uptake, in comparison to larger or smaller ones [5]–[7]. Other studies involving amine-functionalized and polyethylene glycol (PEG)-coated MSNs reported that 100−150nm MSNs could be more efficiently taken up by cells, even when compared with 50-55nm NPs [5], [8], [9]. Nanoparticles (NPs) in particular are increasingly being explored for their promising application as carriers in DDS [10].

NPs' surfaces are feasible to be modified and gain specific surface properties, allowing them to have selective targeting, increased efficacy and reduced drugs' side effects [10]. They are also managed to release their cargo in a controlled manner, allowing a sustained drug delivery over time [10]–[12]. Controlled release is an important feature that therapeutic systems may have, so it can be adaptable and customizable to a certain person or a certain type of disease (personalized medicine) [13]. This can be achieved for example using nanovalved-systems responsive to external stimuli [14], [15].

## 1.2 Silica Nanoparticles

There are several types of NPs and, based on their composition, they are generally placed into three major classes: organic, carbon-based, and inorganic NPs [16]. Inorganic nanoparticles have earned significant attention for their potential application in DDS owing to their unique characteristics [17], and they include metal-based and metal oxide-based NPs [16].

Within the nanocarriers already developed in the field of nanomedicine, mesoporous silica materials, namely Mesoporous Silica Nanoparticles (MSNs), have gained recognition as one of the most promising nanomaterials for drug delivery applications due to their high *in vitro* and *in vivo* biocompatibility, tunable particle size, versatile surface chemistry and high surface area and pore volume, providing the possibility to transport large quantities of drugs [5], [18]–[20]. The non-polar cavities of these particles are suitable for hydrophobic drugs, preserving them in a non-crystalline state and promoting drug dissolution [21]–[23]. This type of NPs is included in inorganic nanomaterials as they are made of silica dioxide ($SiO_2$). In addition, silica has already gained the status of "Generally Recognized as Safe" by the U.S. Food and Drug Administration (FDA) [24].

The main challenge of MSNs is the design of carriers to bind more specifically and/or accumulate on target tissues. This can be achieved considering size, and surface chemistry characteristics, namely charge [5]. Another challenge is preparing well-ordered MSNs with a uniform size distribution, to obtain stable colloidal suspensions [7], although particles usually tend to adopt a spherical shape during synthesis to minimize the surface energy [25].

There are also other options that have similar features and are easier to produce, manage and functionalize [26], [27], namely Mobil composite material number 41 (MCM-41), which is one type of ordered mesoporous silica materials [18]. MCM-41 has a hexagonal pores' structure [28], [29], as shown in **Figure 1.1**, the great characteristics listed before and their pores' diameter ranges between 1.5 and 10nm [30], [31].

### 1.2.1 Nanoparticles's Synthesis

MSNs can be synthesized through several methods. Sol-gel chemistry, in particular, enables the production of a wide range of materials, including silica. This method involves the formation of a sol that is subjected to a series of chemical reactions, leading to the formation of a gel network through a process called gelation. In the context of MSNs, the sol contains silica precursors, which can be tetraethyl orthosilicate (TEOS) or even a sodium silicate solution. During this process, the silica precursors undergo hydrolysis and condensation reactions, resulting in silica NPs within a three-dimensional network. The addition of a surfactant template to the sol is the general method that enables the generation of particles' pores. The surfactants that can be used are, for example, Cetyltrimethylammonium Bromide (CTAB) and Pluronic F127, which are cationic and nonionic, respectively [32]. After the gelation process, the system can be treated with calcination (high temperature) to remove micellar templates for obtaining the final MSNs. Calcination is commonly used due to its ease of operation and efficiency and for requiring simple equipment [33]. Catalysts are also needed in this type of reaction which is possible through agents with the ability to provide basic conditions, e.g. triethanolamine (TEA), which functions as a growth inhibitor [5].

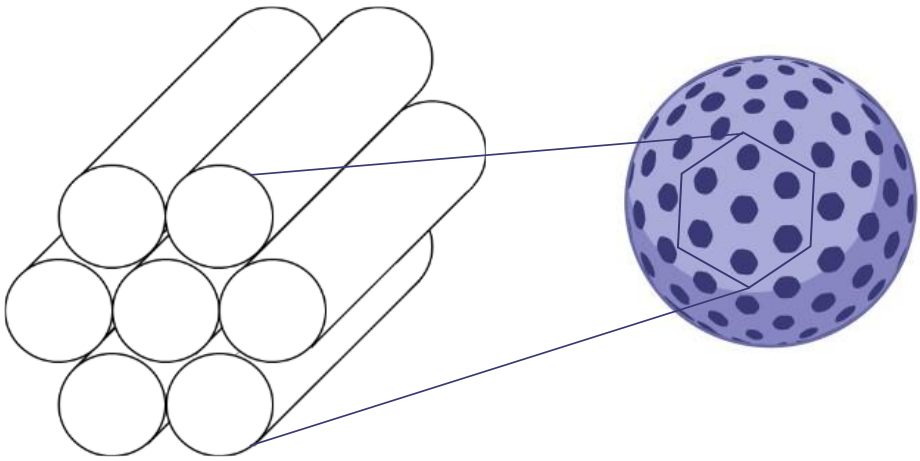

**Figure 1.1** Hexagonal pores' structure of some mesoporous silica materials.

## 1.3 Silica Nanoparticles in controlled-release systems

Mesoporous silica materials have been widely reported for being used in many controlled-way drug delivery systems functioning according to several stimuli: external or internal [18], [34]. The stimulus can be temperature, pH, light, magnetic and electric fields, ultrasounds, redox agents, glucose, or enzymes, due to the high range of possible functionalizations.

### 1.3.1 pH as a stimulus

pH is one of the key factors of biological fluids, blood stream and body tissues, changing depending on the condition and/or organelle. So, in delivery systems, it can be managed to adapt and control the drug release, which is why it's probably the most used stimulus. It was also reported that functionalizing MSNs' surface with molecules containing the carboxylic acid (COOH) or amine groups may introduce pH-responsive moieties to MSNs [34].

### 1.3.2 Light as a stimulus - Spiropyrans

Light, in particular, has been widely used due to its ease of control, extremely high spatial and temporal precision and its broad range of wavelength and intensity. There are many light-sensitive molecules which exhibit structural changes after exposure to light and that can be used to functionalize the NPs [34]. This structural alteration is reflected in a reversible change of the absorption spectrum and, in consequence, in a change of the colour [35]. This feature is named Photochromism [36] which often comes along with a change in physical and chemical properties [35].

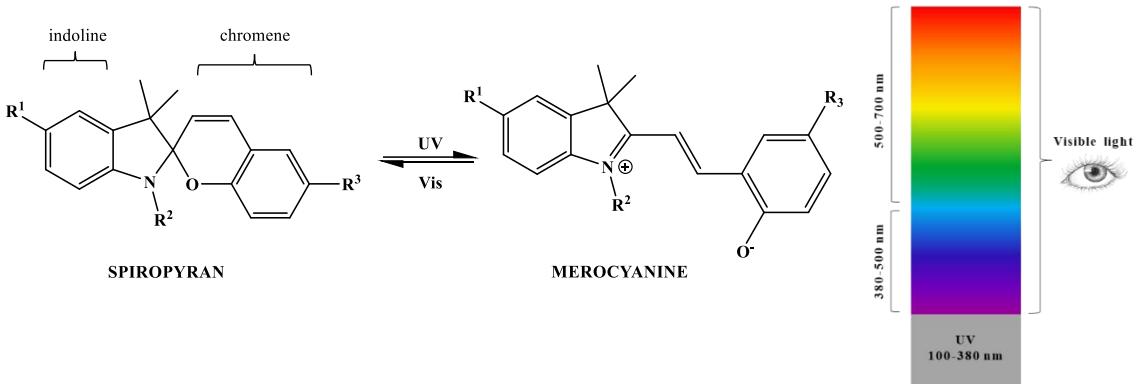


**Figure 1.2** SP spectrally well-separated states: SP (closed) in their original form and its reversible conversion into Merocyanine (open) upon UV irradiation. SP molecule possesses two main aromatic regions, an indoline and a chromene, bound together via a spiro junction.

Spiropyrans (SP) derivates are one of the most promising and well-studied classes of organic photochromic compounds [37], [38] and are characterized by two spectrally well-separated states (closed and open) that are thermally stable and can switch between each other [39].

The SP molecule itself corresponds to the hydrophobic colourless closed state and includes an indoline and a chromene moiety bound together via a spiro junction (C-O bond), as illustrated in **Figure 1.2** [40]. Upon Ultraviolet (UV) light exposure, the molecule undergoes a photochemical transformation into its coloured open hydrophilic form, Merocyanine. When there is no longer that exposure, or an exposure to visible light, there is a reversion of the process. This behaviour resembles that of a reversible photoswitch, which can transition between different forms or states depending on the wavelengths of light [41].

In the dark, SP derivatives exist predominantly in 3 forms: protonated merocyanine (MCH), deprotonated merocyanine (MC) and spiropyran (SP) - **Figure 1.3**. MC undergoes thermal ring-closing (kc) being converted into SP form, which can ring-open (ko), due to its reversibility capacity. This thermal equilibrium is inherently linked to the protonation equilibrium, also known as acid dissociation constant ($K_a$), between MCH and MC. Thus, MCH and MC forms exist depending on the pH and, when the MC form predominates, SP also exists in equilibrium. So, in addition to being photochromic, SP reversible isomerization can be obtained by other independent stimuli including temperature (thermochromism) and pH (acidochromism) [40], [42]. MCH can be thus described as a Photoacidic compound considering that it releases a proton after optical excitation/ irradiation (*hv*), therefore being able to control protonation and deprotonation [41]. MCH is also the most thermodynamically stable photochromic form in aqueous solutions presenting a yellow-colored solution. Upon irradiation at around 410nm, the solution gets bleached, reaching its colourless SP form. A change in pH or the photoexcitation of MCH, and

consequent absorption of energy, triggers the release of the proton ($H^+$) creating a redshifted fluorescence band corresponding to MC emission [42], [43].

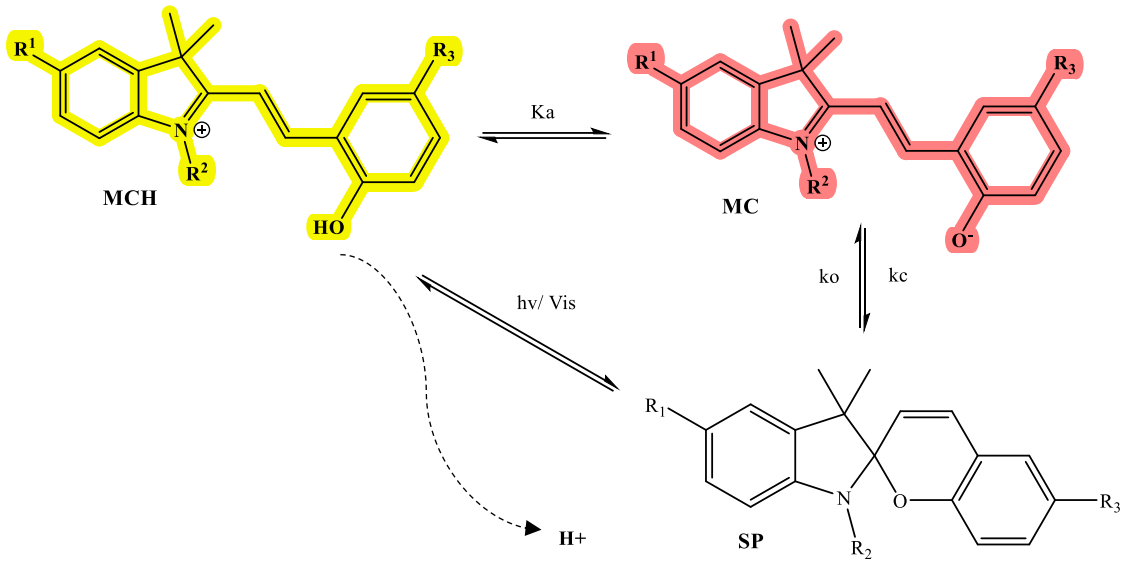


**Figure 1.3** Merocyanine photoacid and (photo)thermal equilibrium.

In summary, the reversibility of this process is promising to create switchable DDS and enable the creation of costume-made therapies, also decreasing the likelihood of toxicity.

## 1.4 Nanovalves - cucurbituril family

Nanovalves are cyclic molecules that slide along a thread-like structure, acting as a gate. They are able to block the escape of guest molecules from the interior of the particle's pores and enable their release when there is a stimulus [18], [44]. One of the most widely used types of nanovalves is that of the cucurbituril family (cucurbit[n]uril), whose shape resembles a pumpkin [45], [46] as represented in **Figure 1.4**.

Cucurbit[n]urils are unusual macrocyclic hosts due to the high equilibrium constants that can be achieved for their host-guest complexes [47]. Several types of cucurbiturils differ in the number (n) of glycoluril monomers, namely CB6, CB8, CB5 and CB7, where the first two are insoluble in water and the last ones are reportedly soluble [18], [45]. Nevertheless, according to literature, CB7 has superior solubility in aqueous solutions [18], [48] in addition to the fact that, among cucurbituril homologs, it can bind guest molecules with extremely high binding affinities [49], [50].

These molecules have cation receptor properties [45], [51] and as there is an increase in the size of the molecules' strand, there is also an increase in the binding affinity constant ($K_A$) [52]. This happens because cucurbituril hosts feature two symmetry-equivalent ureidyl carbonyl portals, which are electrostatically negative and guard the hydrophobic cavity [50].

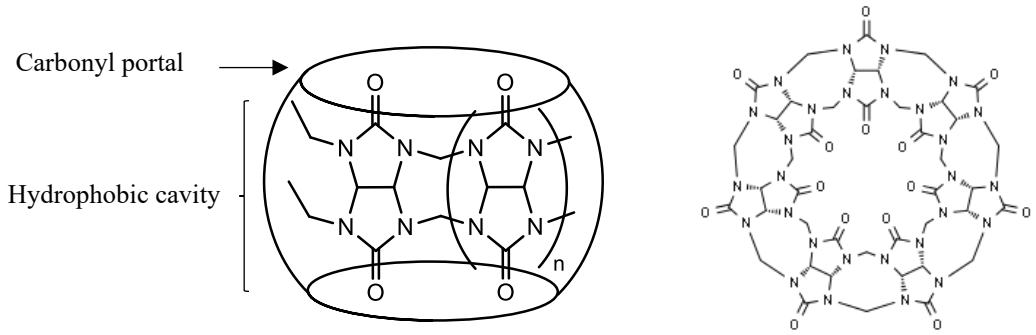


**Figure 1.4** Cucurbituril general structure at the left: n glycoluril monomers bonded by pairs of methylene bridges to form a rigid, annular and hollow cavity. At the right, there is CB7 chemical structure and its molecular formula is $C_{42}H_{42}N_{28}O_{14}$ (Molecular Weight (MW) = 1163 mol/g).

Regarding CB7 dimensions, it owns 5.4Å of portal diameter, measures 9.1Å in height, 7.3Å in cavity diameter and has an internal cavity with 279Å$^3$ of volume [53]. CB7 molecular size allows the accommodation of a variety of small aromatic or ring-structured organic compounds [54], [55]. Competitive studies by isothermal titration calorimetry (ITC) and Proton nuclear magnetic resonance ($^1$H NMR) revealed that these CB7 host-guest complexes have extremely high binding affinities in aqueous solutions ($10^9$-$10^{17}M^{-1}$) [54], [56].

As cucurbiturils have high affinity for cationic molecules, they can be associated with cationic thread-like molecules, as represented in **Figure 1.5**, functioning as a gate slider.

The highest $K_A$ measured with cucurbiturils was observed with the complexation of CB7 with diamantane diammonium ion which showed an extremely high binding constant of up to $7\times10^{17}$ $M^{-1}$ [49], [50]. This result exceeded nature's strongest binding constant of $1\times10^{15}$ $M^{-1}$ achieved by the avidin-biotin system [57], [58]. It is important to mention that the "perfect" size-shape complementarity not only ensures a strong hydrophobic interaction but also results in the removal of water molecules trapped inside CB7 to overcome the enthalpy-entropy compensation [54], [59]. CB7 host-guest complexes have the advantage of being less influenced by biological media, high temperature, and organic solvents. In fact, CB7 degradation temperature is only at 643 K (≈370 ºC) [60]. Moreover, varying the condition of the solution, in terms of ionic strength and solvent type for example, it is possible to create variations in their binding affinities [54], [61].

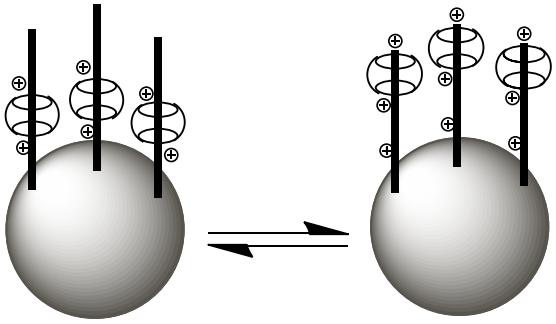

**Figure 1.5** CB7 affinity to cationic molecules.

## 1.5 Gene therapy

In gene therapy, NPs are also being used to encapsulate Ribonucleic and Deoxyribonucleic acids (RNA and DNA, respectively) [10], [62]. Gene therapy involves the manipulation of gene expression or the modification of the biological characteristics of living cells for therapeutic use. This promising technique uses genetic material (nucleic acids) as functional molecules for the treatment of a wide range of medical conditions. Nucleic acids have been attracting increasing attention due to the human genome elucidation together with recent discoveries such as RNA interference (RNAi) and CRISPR-based genome editing and with the fact that a single treatment can achieve a durable and even curative effect [63]. Nevertheless, a successful delivery of nucleic acids into their active site inside the cell is still challenging. They have low stability in vivo, rapid clearance and, due to their negative charge coming from their phosphate groups, hydrophilicity, and high molecular weight, have limited permeability through the cell membrane [63], [64]. So, tailored systems that allow their entrance to the cells are desired, namely resorting to nanomaterials. Owing to their tunability with diverse physicochemical properties, they can be functionalized with any type of molecule, performing a selective targeting and helping in cellular internalization [63].

# 2. PROJECT OVERVIEW

In the first instance, the main goal of this project was the production and study of a nanovalved-system based on MSNs, functionalized with SP derivatives, and capped with CB7, so it could be loaded with neuromodulators for neurological diseases' treatment. This system was thought to be applied, in the future, together with mechanoluminescent NPs that could convert focused ultrasounds (FUS) into visible light to, in consequence, activate the main delivery system, as represented in **Figure 2.1**. As this one-year thesis progressed, we realized the ambitious nature of the project, leading us to prioritize the thorough preparation and study of each component before proceeding to the integrated system.

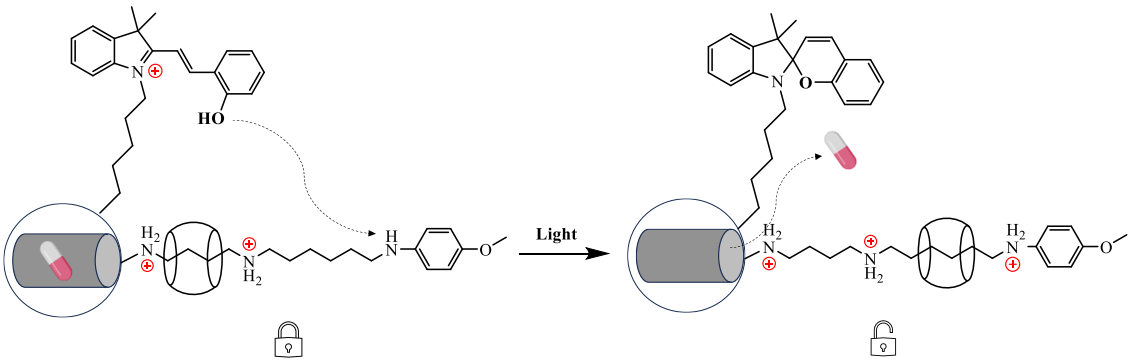


**Figure 2.1** General mechanism of a photochromic nanovalve. When the MCH molecule (at the left) is converted into SP (right), it releases a $H^+$ that can be captured from other molecules that become protonated. That protonation can promote CB7 sliding and pores uncovering, making it able to release drugs.

Taking this into account, we produced the main components of the system. This included a model compound representing SP derivatives and two distinct heterogeneous systems based on functionalized MSNs: one with the SP analogue and the other with ammonium groups.

We conducted a series of experiments to investigate the pH and light responsiveness of the system involving SP derivatives, with and without the presence of CB7, as well as their stability in aqueous solutions and suspensions.

Recognizing the potential applications of gene therapy in treating various diseases, we extended our studies to nucleic acids. Given DNA's negative charge, systems with SP derivates can enhance its adsorption onto the surface and allow its delivery on target. To explore this, we used the material functionalized with ammonium groups and aimed to determine whether the DNA effectively adsorbed onto the NPs' surface and whether the introduction of CB7 led to competition with DNA, potentially allowing its release.

# 3. MATERIALS AND METHODS

## 3.1 Solvents and Reagents

All solvents and reagents were used as received from commercial sources. Sodium Silicate Solution (8% $Na_2O$, 27% $SiO_2$), Cetyltrimethylammonium Bromide (CTAB, Alfa Aesar, 98%), Pluronic F127 (BASF), Triethanolamine (TEA, Alfa Aesar), Tetraethyl orthosilicate (TEOS, Alfa Aesar, 98%), (3-chloropropyl)triethoxysilane (CPTES, Sigma-Aldrich, 95%), 1,4 - diaminobutane (Alfa Aesar, 98%), Calcein (mixture of isomers, TCI), (3-Iodopropyl)trimethoxysilane (Sigma-Aldrich), Triethylamine (Sigma-Aldrich, 99%), Deoxyribonucleic acid (DNA low molecular weight, from salmon sperm, Sigma-Aldrich), 2,3,3 - trimethyl - 3H - indole (Alfa Aeser, 98%), 1,6 - Dibromohexane (Sigma-Aldrich, 96%), Sodium carbonate solution ($Na_2CO_3$, PanReac AppliChem 99.5%), Magnesium sulfate ($MgSO_4$, PanReac AppliChem 96%), Salicylaldehyde (Fluka, >98%), 4-(dimethylamino)-N,N,N-trimethylbutan-1-ammonium iodide (available in the Photochemistry and Supramolecular Chemistry Lab of FCT NOVA and purified), N,N-Diethyl-3(trimethoxysilyl)propan-1-amine (FluoroChem, 95%), 1,3,5-trioxane (Sigma-Aldrich, >=99% and Fluka), 1-Adamantanamine hydrochloride (Alfa Aeser, 99%), KBr (Merck, 99.9%), NaCl (Honeywell ≥99.5%), KCl (Sigma-Aldrich, ≥99.5%), $Na_2HPO_4$ (Thermo Fisher Scientific 98+%), $KH_2PO_4$ (Merck 99%).

Deuterium oxide ($D_2O$, Euriso-top, 99.90% D), Deuterated Dimethyl sulfoxide (DMSO d6, Euriso-top, 99.80% D), Deuterated Chloroform ($CDCl_3$, Euriso-top, 99.80% D), Deuterated Methanol ($CD_3OD$, Euriso-top, 99.80% D), Diethyl ether ($Et_2O$, LabChem), n-hexane (Carlo Erba), Toluene (MePh, LabChem), Anhydrous MePh (Sigma-Aldrich), Dried MePh (with molecular sieves), Acetonitrile (ACN) p.a. (Carlo Erba), Dried ACN (with molecular sieves), Dichloromethane p.a. (DCM, Carlo Erba), Ethanol (EtOH) p.a. (Honeywell Riedel-de Haën), Methanol (MeOH) p.a. (Honeywell Riedel-de Haën).

Phosphate buffer solutions (PBS) where prepared at **1)** pH=6.5 and **2)** pH=7.4:

**1)** NaCl (68.44mmol), KCl (1.34mmol), $Na_2HPO_4$ (5.07mmol), $KH_2PO_4$ (0.88mmol); 1L

**2)** NaCl (34.22mmol), KCl (0.67mmol), $Na_2HPO_4$ (2.54mmol), $KH_2PO_4$ (0.44mmol); 250mL

## 3.2 Equipment and Characterization Techniques

### Nuclear Magnetic Resonance (NMR)

$^1H$ NMR spectra were obtained on a Bruker AMX 400 instrument operating at 400.13 MHz at the NMR Lab of the Chemistry Department of FCT NOVA University.

$^1$H NMR was also used to characterize and quantify the organic loading obtained by their functionalization. A known amount of 1,3,5-trioxane was added as an internal standard, as described in the literature [65]. Samples were prepared in an Eppendorf by dispersing 5 mg of NPs in 0.6 mL of $D_2O$/NaOH, the dissolution of the silica matrix was enhanced through sonication and then the sample was added to an NMR tube.

**Transmission Electron Microscopy (TEM)**

TEM images were obtained using a Hitachi H-8100 electron microscope with thermionic emission (LaB6) and an acceleration voltage of 200kV and 20uA at MicroLAb in partnership with Instituto Superior Técnico. The samples were supported on a Formvar/carbon-coated copper grid (200 mesh), dried before the examination and the size of the nanoparticles was determined by manual counting using the Image J software.

**UV-Visible (UV-Vis) spectroscopy**

UV-Vis spectra were taken using a Cary 100 Bio spectrophotometer.

**Dynamic Light Scattering (DLS)**

For DLS analyses, a Nano Particle Analyzer SZ-100 from Horiba Scientific was used with the following parameters: Nanoanalysis mode in measurement mode settings, detector position at 90º and polydisperse form of distribution. For size analysis disposable cells with four openings were used while folded capillary cells (electrode cell, carbon 6mm) were used to measure zeta-potential (ζ-potential).

**Nitrogen adsorption-desorption isotherms, textural and pore X-ray diffraction (XRD), Elemental analysis (EA) and Thermogravimetric analysis (TGA)**

Nitrogen adsorption–desorption isotherms were determined at 77 K on a Quantachrome Autosorb iQ system, equipped with a turbomolecular pump, using helium (for dead space calibration) and nitrogen of 99.999% purity. Previously to the measurements, the samples were outgassed for 8h at 180 °C using a heating rate of 1 °C min$^{-1}$ to achieve the final temperature. XRD measurements were carried out on a Bruker AXS-D8 Advance powder diffractometer, using CuKα radiation (40 kV, 30 mA), a step size of 0.01º (2θ) and 5s per step. Regarding EA, a Thermo Finnigan Flash EA 112 series was used. Finally, TGA analysis were performed on a PerkinElmer STA6000 system with a heating rate of 10 °C min$^{-1}$ and under a 20mL min$^{-1}$ flow of helium. All these tests were performed in partnership with the University of Évora.

**Fourier-transform infrared (FTIR) spectroscopy**

FTIR spectra were recorded on a PerkinElmer Spectrum Two FT-IR equipment, in the 400-4000 cm$^{-1}$ region, using KBr pellets.

**Isothermal titration calorimetry (ITC)**

MicroCal PEAQ-ITC from Malvern Panalytical. All conditions were analyzed at 25 ºC with 25 points per injection.

**Microwave-assisted synthesis**

Microwave irradiation was performed using an Anton Paar Monowave 450 oven with potency control.

**Fluorescence Spectroscopy**

Emission spectra were recorded on a PerkinElmer LS 45 Luminescence Spectrometer.

**Irradiation Experiments**

Irradiation experiments were carried out in a spectrofluorometer (SPEX Fluorolog 1681 0.22m) equipped with a 150 W Xe-Hg lamp as the light source and using maximum slit width, with the following conditions: $\lambda_{irr}$=420nm.

In this experimental work, complementary equipments were also used: Centrifuges (20.000 rpm, Beckman Avanti J-25 Centrifuge; DMO412 from LabTechniques); Muffle (Nabertherm L5/11/C6D); Oven (Memmert UE 500 Lab Oven with Stainless Steel Tray); pH values were measured with a Crison pH-Meter BASIC 20+; Scales (Sartorius R200D and Sartorius Basic B610); Ultrasonic Bath (Elma S 100H Elmasonic) and Vortex Mixer (Janke & Kunkel IKA Labortechnik VF2).

## 3.3 Synthesis of Mesoporous silica materials

### 3.3.1 MCM-41

This material was prepared using a sol-gel method described in the literature [18], [66]. Specifically, 10 g of sodium silicate were dissolved in 30 mL of Milli-Q water in a beaker. Then, 7.5 g (21 mmol) of CTAB were also dissolved in 80 mL of Milli-Q water and both solutions were mixed and left under stirring for 30 min. After that time, the pH was adjusted to 10, using a 2M sulfuric acid ($H_2SO_4$) solution previously made, the time under stirring was extended to more 30 min and a new adjustment of the pH to 10 was performed. The white gel prepared was transferred to a Teflon-coated autoclave and heated in an oven at 100 ºC for 48h. After that time a filtration under vacuum was made and the resulting product was washed several times with water. The white solid was dried at 80 ºC for 24h and then calcinated at 560 ºC for 6h (using a heating ramp of 1 ºC $min^{-1}$ under air) to remove the surfactant.

**FTIR** (KBr, $\bar{\nu}$/cm$^{-1}$): 3468 (s, νOH), 2925-2856 (w), 1637 (m, δOH), 1400 (m), 1085 (s, $\nu_{as}$ Si-O-Si), 967 (w, νSi-OH), 800 (w, $\nu_s$ Si-O-Si), 460 (m, δSi-O-Si).

### 3.3.2 MSN 45nm

This material was also prepared using a sol-gel method following a procedure described in the literature [5]. A mixture of 1.33 g (4 mmol) of CTAB, 5.36 g (0.43 mmol) of Pluronic F127, 31.28 g (210 mmol) of TEA, 114 mL of ethanol (EtOH) and 250 mL of Milli-Q water was prepared and stirred overnight, at room temperature. After that, 5.12 mL (23mmol) of TEOS were slowly added under vigorous stirring using a pipette and the mixture was left under static conditions for more 24h. On the next day, 200 mL of EtOH were added to the suspension previously obtained to facilitate the centrifugation step. The suspension was centrifuged (in cycles of 17 000 rpm for 15min), the supernatant was removed by decantation and the resultant precipitate was washed with EtOH. In the end, the solid was dried in an oven at 100 ºC for 24h and calcined at 560 ºC for 6h (using a heating ramp of 1ºC min$^{-1}$ under air).

**FTIR** (KBr, $\bar{\nu}$/cm$^{-1}$): 3460 (m, νOH), 2925-2856 (w, νCH), 1634 (w, δOH), 1401 (w, δCH), 1094 (s, $\nu_{as}$ Si-O-Si), 968 (w, νSi-OH), 798 (w, $\nu_s$ Si-O-Si), 465 (m, δSi-O-Si).

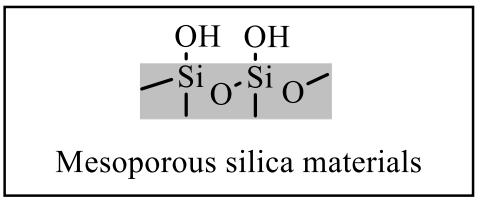


## 3.4 Synthesis of functionalized MCM-41

### 3.4.1 MCM41-CPTES

Also based on the method reported by Liu and Du [18], 0.5 g of MCM-41 were dried under vacuum at 150 ºC. Then, 15 mL of MePh and 0.5 mL (2.08 mmol) of CPTES were added and the mixture was stirred under reflux for 24h. After that time, the solution was filtered and washed with ACN. The product obtained was then dried at 80 ºC to obtain a chloro-functionalized MCM-41 (MCM41-CPTES).

**$^1$H NMR** (400 MHz, $D_2O$+NaOH): δ3.55 (2H, H5), 1.79 (m, 2H, H4), 0.51 (t, J = 8.4 Hz, 2H, H3) ppm; *Extra-protons at 3.56 and 1.12 ppm corresponding to extra H1 and H2; Organic loading: 1.932mmol/g. **FTIR** (KBr, $\bar{\nu}$/cm$^{-1}$): 3436 (m, νOH), 2925-2856 (w, νCH), 1637 (w, δOH), 1398 (w, δCH), 1238 (m), 1083 (s, $\nu_{as}$ Si-O-Si), 967 (w, νSi-OH), 798 (w, $\nu_s$ Si-O-Si), 698 (w, νC-Cl), 457 (m, δSi-O-Si).

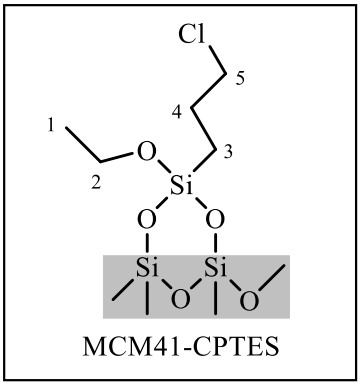

MCM41-CPTES

### 3.4.2 MCM41-Butanediamine

0.4 g of MCM41-CPTES were transferred to a round-bottom flask and suspended in a solution with 15 mL of MePh and 0.5 mL (5 mmol) of 1,4 - diaminobutane. The mixture was stirred under reflux under nitrogen and the resultant solid was filtered, washed with MePh, and dried at 80 ºC in an oven.

**$^1$H NMR** (400 MHz, $D_2O$+NaOH):δ2.53 (t, J = 6.8 Hz, 2H, H5), 1.46 (m, 2H, H4), 0.39 (t, J = 8.4 Hz, 2H, H3) ppm; *Extra-protons at 3.56 and 1.13 ppm corresponding to H1 and H2; Organic loading: 2.159 mmol/g. **FTIR** (KBr, $\bar{\nu}$/cm$^{-1}$): 3436 (m, νOH), 2925-2856 (w, νCH), 1634 (w, δOH), 1468 (w, δNH), 1402 (w), 1076 (s, $\nu_{as}$ Si-O-Si), 967 (w, νSi-OH), 795 (w, $\nu_s$ Si-O-Si), 698 (w, νC-Cl), 459 (m, δSi-O-Si).

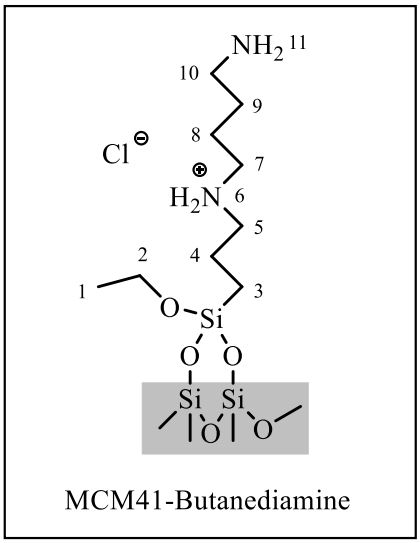

MCM41-Butanediamine

## 3.5 Synthesis of functionalized MSN

### 3.5.1 N,N,N-triethyl-3-(trimethoxysilyl)propan-1-ammonium iodide

This compound was synthesized by microwaved-assisted reaction using a mixture of (3-Iodopropyl)trimethoxysilane and triethylamine in a 1:1 proportion (5.107 mmol) into a wide-neck glass microwave tube. The mixture was stirred (600 rpm) at 80 ºC for 3h. After that time, a viscous white oil was obtained. The product was dissolved in just the right amount of DCM and then precipitated with $Et_2O$. Hereafter the N,N,N-triethyl-3-(trimethoxysilyl)propan-1-ammonium iodide will be named TESPAI ("TE" represents the "triethyl" part of the compound; "SP" the "silyl propan" part; and "AI" the "ammonium iodide" part of the compound).

**$^1$H NMR** (400 MHz, $CDCl_3$): δ 3.56 (s, 9H, H1), 3.44 (t, 2H, H5), 3.28 (m, 2H, H4), 1.79 (m, 2H, H3), 1.39 (t, J = 7.2 Hz, 9H, H6), 0.73 (t, J = 7.2 Hz, 2H, H2) ppm; *Extra-protons at 3.44 and 1.23 ppm corresponding to remaining $Et_2O$ and at 1.79 and 1.39 ppm perhaps regarding remaining Triethylamine; Yield: 32%.

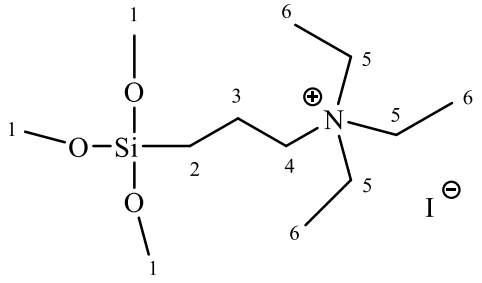


N,N,N-triethyl-3-(trimethoxysilyl)propan-1-ammonium iodide

MW = 391.37g/mol

### 3.5.2 MSN-TESPAI

400 mg of MSN were left drying/activating under vacuum at 150 ºC for 2h. The activated NPs were left with the produced TESPAI (1.6mmol) under reflux in 1 mL of dry MePh and 3 mL of ACN at 120 ºC overnight. On the following day, the refluxed NPs were washed with ACN p.a three times, another one with EtOH p.a. and finally left to dry in the oven.

**$^1$H NMR** (400 MHz, $D_2O$+NaOH): δ 3.15 (m, 6H, H5), 3.02 (t, J = 8.8 Hz, 2, H4), 1.62 (m, 2H, H3), 1.14 (t, J = 6.8 Hz, 9H, H6), 0.33 (t, J = 8 Hz, 2H, H2); *Extra protons at 5.11 ppm corresponding to extra H1; extra protons at 3.53 and 1.05 corresponding to remaining EtOH; Organic loading: 3.636mmol/g; **FTIR** (KBr, ν/$cm^{-1}$): 3460 (m, νOH), 2985-2851 (νCH), 1612

(w, δOH), 1461 (w), 1397 (w, δCH), 1094 (s, $\nu_{as}$ Si-O-Si), 1014 (w, νSi-OH), 777 ($\nu_s$ Si-O-Si), 447 (m, δSi-O-Si).

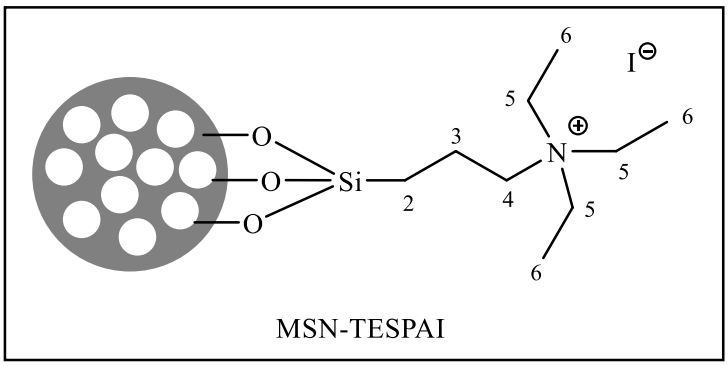


### 3.5.3 SP Synthesis

Three experimental protocols were conducted to achieve the desired SP structure, but only the third protocol was successful.

#### 3.5.3.1 Synthesis of Compound 1

2,3,3 - Trimethyl - 3H - indole (2.02 mL; 12,56 mmol) and 1,6 - Dibromohexane (8.02 mL; 62.6 mmol) was left under stirring at 110 ºC for 12h and under solvent-free conditions, according to a method reported in the literature [67]. Then, $Et_2O$ together with n-hexane were added to precipitate the oily product (**Compound 1**) which was washed several times with n-hexane and dried under vacuum.

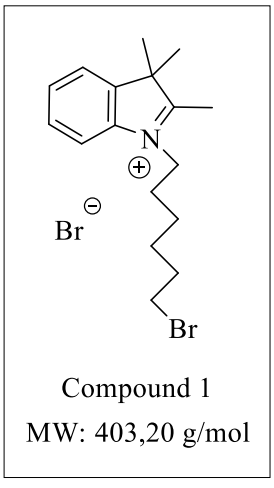


#### 3.5.3.2 Synthesis of Compound 2

Based on Rad *et al.*'s article [68], **Compound 1** (17.93 mmol) was dissolved in Milli-Q water (67 mL) in an Erlenmeyer and a $Na_2CO_3$ solution previously prepared in water (for 20.78 mmol of

$Na_2CO_3$ were added 41 mL of water), was added dropwise under stirring and left under agitation for more 15min, in agreement with the proportions applied on the article mentioned. The product obtained (**Compound 2**) was extracted with $Et_2O$ (3x20 mL) using a separating funnel and, after 3 cycles, the extract was dried with $MgSO_4$, filtrated, and concentrated under reduced pressure in the evaporator. Then, it was also dried in the vacuum line. Finally, the product was purified by a chromatography column using n-hexane and $Et_2O$ as eluents in a 9:1 proportion, respectively, and the collected fractions were monitored through Thin Layer Chromatography (TLC) and $^1$H NMR.

**$^1$H NMR** (400 MHz, $CDCl_3$): δ7.11 (m, 2H, H3 e H4), 6.75 (t, J = 7.2 Hz, 1H, H2), 6.51 (d, J = 8 Hz, 1H, H5), 3.85 (d, J = 11.2 Hz, 2H, H6), 3.49 (t, J = 7.2 Hz, 2H, H12), 3.41 (m, 2H, H7), 1.84 (m, 2H, H11), 1.67 (m, 2H, H10), 1.48 (m, 2H, H9), 1.38 (m, 2H, H8), 1.33 (s, 6H, H1) ppm; *Extra-protons at 0.88 and 1.26 ppm corresponding to n-hexane and at 3.48 and 1.02 ppm corresponding to $Et_2O$; Yield: ≈43%.

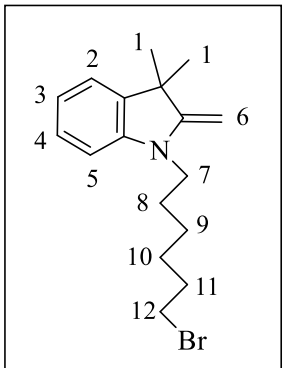


Compound 2
MW: 322,29 g/mol

### 3.5.3.3 Synthesis of Compound 3

Compound 2 (1.76 g; 5.50 mmol) and salicylaldehyde in EtOH were stirred under reflux to obtain **Compound 3**. The salicylaldehyde was added in 1.05 equivalents with a proportion of 5.46 mmol of salicylaldehyde for 5.2 mmol of Compound 2 [68]. The residue was then purified by column chromatography using n-hexane:$Et_2O$ 9:1 as eluent. As the product was not miscible in the eluent, it was dissolved in $Et_2O$, silica was added to the round-bottom flask and the mixture formed was dried under reduced pressure in the evaporator. As done before, the collected fractions were monitored through TLC and then $^1$H NMR.

**$^1$H NMR** (400 MHz, $CDCl_3$): δ7.15 (t, 1H, H18), 7.04 (t, J = 7.6 Hz, 4H, H2, 4, 8 e 11), 6.81 (t, J = 10 Hz, 3H, H3, 9 e 10), 6.68 (d, J = 8.4 Hz, 1H, H7), 6.52 (d, J = 8 Hz, 1H, H5), 5.67 (d, J = 10.4 Hz, 1H, H6), 3.36 (t, J = 6.8 Hz, 2H, H17), 3.22 (m, 1H, H12), 3.09 (m, 1H, H12), 1.8 (m,

2H, H16), 1.63 (m, 2H, H13), 1.41 (m, 4H, H14 e 15), 1.29 (s, 3H, H1), 1.16 (s, 3H, H1); *Extra-protons at 0.88 and 1.26 ppm corresponding to n-hexane; Yield: ≈27%.

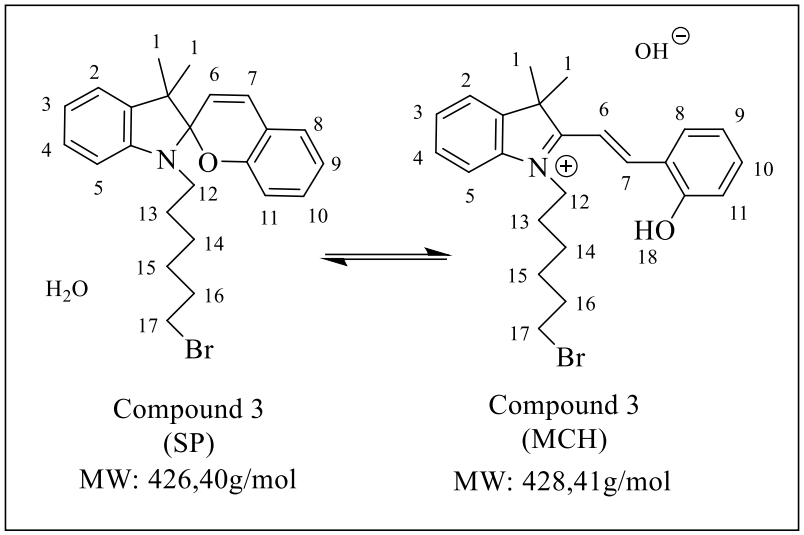


### 3.5.3.4 Synthesis of Compound 4

Compound 3 (0.6 g; 0.14 mmol) and 4-dimethylamino-butyl)-trimethyl-ammonium iodide (ammonium iodide) were stirred in 3 mL of ACN under reflux for 24h to obtain **Compound 4**. The proportion of reagents used was 1:0.9. Some crystallizations and washes with $Et_2O$ were performed and then the remaining ammonium iodide was removed using EtOH. Washes in ACN were also done, where the desired compound should be on the supernatant.

**$^1$H NMR** (400 MHz, DMSO d6): δ7.17 (d, J = 7.2Hz, 1H, H11), 7.08 (m, 3H, H3, 4 e 8), 7.00 (d, J = 10.4 Hz, 1H, H7), 6.84 (t, J = 7.2 Hz, 1H, H10), 6.75 (t, J = 7.2 Hz, 1H, H9), 6.65 (d, J = 8 Hz, 1H, H5), 6.54 (d, J = 8 Hz, 1H, H2), 5.76 (d, J = 10.4 Hz, 1H, H6), 3.44 (m, 12H, H13-16 e 20-21), 3.08 (s, 9H, H23), 3.06 (t, J = 4 Hz, 8H, H12, 17, 19 e 22), 3.00 (s, 3H, H18), 2.98 (s, 3H, H18'), 1.20 (s, 3H, H1), 1.09 (s, 3H, H1'); *Extra-protons at 2.10 ppm corresponding to ACN; Yield: ≈100%.

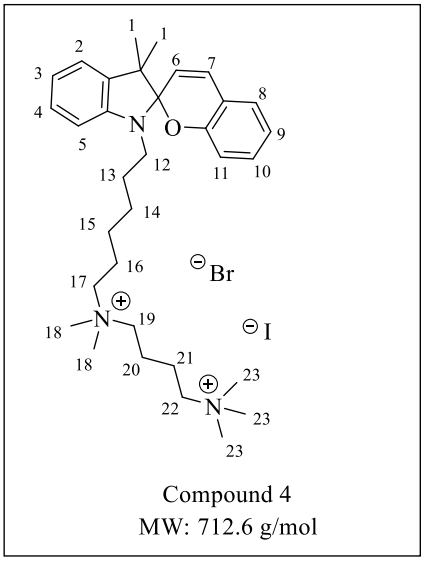

Compound 4
MW: 712.6 g/mol

### 3.5.3.5 Synthesis of Compound 5

Also using Compound 3, it was produced **Compound 5** with N,N-Diethyl-3-(trimethoxysilyl)propan-1-amine to make the structure able to be functionalized by the silica NPs. Now on, this reagent will be denominated DAPTS (“D” represents the "diethyl" part of the compound; “A” the "amino" part; “P” the "propyl" part; “T” the “trimethoxy” part; and “S” the “silane” part of the compound).

A mixture of Compound 3 and DAPTS (1:10) in ACN (4 mL) was poured into a wide-neck glass microwave tube and stirred (600 rpm) at 100 ºC, under microwave irradiation, for 3 cycles of 1h. After that time, the solvent was dried under the vacuum line and the product was recrystallized with $Et_2O$. The precipitate was dried again and analyzed through $^1H$ NMR.

**$^1$H NMR** (400 MHz, DMSO d6): δ7.16 (d, J = 7.2Hz, 1H, 11), 7.08 (m, 3H, H3, 4 e 8), 6.99 (d, J = 10.4 Hz, 1H, H7), 6.83 (t, J = 7.2 Hz, 1H, H10), 6.74 (t, J = 7.2 Hz, 1H, H9), 6.64 (d, J = 8 Hz, 1H, H5), 6.53 (d, J = 8 Hz, 1H, H2), 5.75 (d, J = 10.4 Hz, 1H, H6), 1.20 (s, 3H, H1), 1.08 (s, 3H, H1') *Extra-protons at 2.08 ppm corresponding to ACN. Yield: ≈32%.

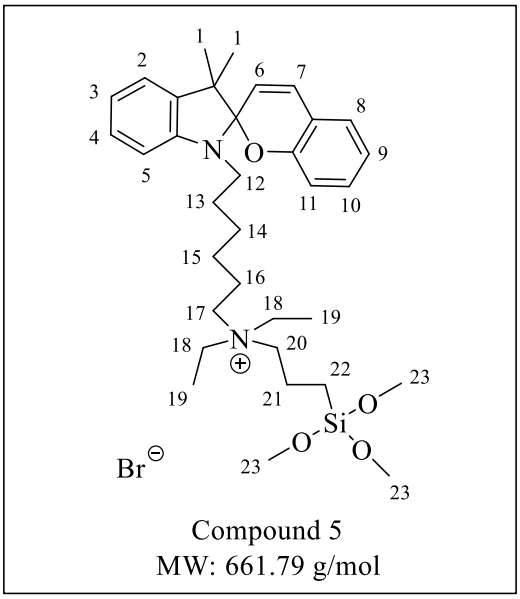


Compound 5
MW: 661.79 g/mol

### 3.5.4 MSN-Compound 5

The functionalization of MSNs with Compound 5 was performed twice using two different protocols: the first one using microwave-assisted heating (M/W) and the other with heating under reflux.

#### 3.5.4.1 Microwave-assisted heating

120 mg of MSNs were dried/activated under vacuum at 150 ºC for 2h and poured into a wide-neck glass microwave tub with Compound 5 (30 mg; $4.5x10^{-5}$ mmol) in 5 mL of dried MePh and stirred (600 rpm) at 120 ºC, under microwave irradiation, for 2h. Then, the product was centrifuged and washed twice with anhydrous MePh and one time with EtOH p.a. Finally, it was dried in an oven at 80 ºC. The final product will be called MSN-Compound 5-M/W.

**$^1$H NMR** (400 MHz, $D_2O$+NaOH): δ 3.61 (m, 2H, H21), 2.51 (m, 4H, H18), 2.40 (t, J = 7.6 Hz, 2H, H20), 1.17 (t, J = 6.8 Hz, 3H, H19), 1.00 (t, J = 7.2 Hz, 3H, H19'), 0.37 (t, J = 8.4 Hz, 2H, H22); *Extra-protons at 1.17 and 3.61 ppm corresponding to EtOH. Organic loading: 0.466 mmol/g; **FTIR** (KBr, ν/$cm^{-1}$): 3436 (s, νOH), 3184 (s), 2925-2852 (s, νCH), 1741 (s), 1636 (s, δOH), 1462 (s), 1400 (s, δCH), 1383 (s), 1087 (m, $\nu_{as}$ Si-O-Si), 959 (s, νSi-OH), 798 (s, $\nu_s$ Si-O-Si), 459 (s, δSi-O-Si).

#### 3.5.4.2 Reflux

250 mg of MSNs were activated as above described, mixed with 120 mg (0.18 mmol) of Compound 5 and stirred overnight under reflux (120 ºC) in 10 mL of anhydrous MePh. The solid was centrifuged, washed with anhydrous MePh and dried at 80 ºC in an oven. The final product will be called MSN-Compound 5-R.

**$^1$H NMR** (400 MHz, $D_2O$+NaOH) δ 3.58 (m, 2H, H21), 2.46 (m, 4H, H18), 2.36 (t, J = 7.6 Hz, 2H, H20), 1.11 (t, J = 6.8 Hz, 3H, H19), 0.93 (t, J = 7.2 Hz, 3H, H19'), 0.34 (t, J = 8.4 Hz, 2H, H22; Organic Loading: 0.5439 mmol/g; Elemental analysis (%) found: C 12.78, N 1.56, H 1.69. **FTIR** (KBr, ν/cm$^{-1}$): 3444 (s, νOH), 3138 (s), 2964-2856 (s), 1738 (s), 1633 (s), 1400 (s),1386 (s), 1091 (s, $\nu_{as}$ Si-O-Si), 949 (s, νSi-OH), 798 (s, $\nu_s$ Si-O-Si), 459 (s, δSi-O-Si).

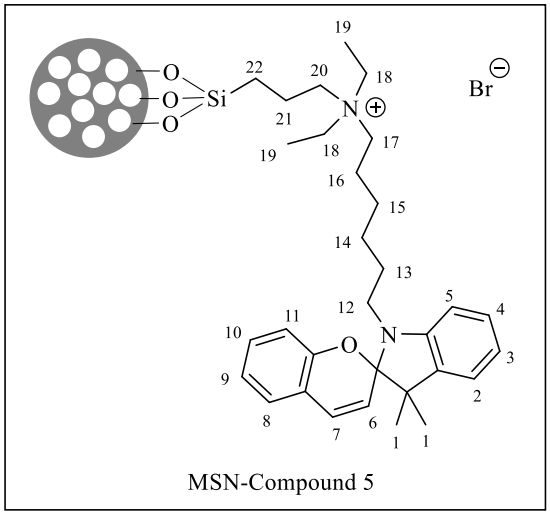

MSN-Compound 5

## 3.6 Loading and Release tests

Loading and Release experiments were performed using the prepared MCM-41 nanoparticles and considering Liu and Du's article published in 2009 [18].

### 3.6.1 CB7 attatchment

At this point, two batches were prepared: in the first experiment, our goal was to recreate and verify the protocol reported by Liu and Du, whereas in the second one, we introduced some modifications, including reducing the amount of NP and increasing the proportion of CB7.

**First batch:** 20 mL of PBS pH≈6.5 together with 1.5 mL of a ≈2 mM solution of CB7 and 20 mg of MCM41-butanediamine was sonicated followed by stirring at room temperature overnight. After that time, the suspension created was subjected to centrifugation, washed 3 times with PBS and a UV spectrum was performed. Forward to that, the supernatant was removed, the sample was dried and a $^1$H NMR analysis was prepared, before and after that triple washing.

**Second batch:** 5 mg of MCM41-butanediamine were suspended in 5 mL of CB7 and PBS pH≈6.5. In this case, we added 4 mL of PBS which was the enough amount of buffer to make the suspension reach a pH of approximately 6.5.

### 3.6.2 Release tests at different pHs

Then, a similar experimental protocol was prepared but this time using calcein as a fluorescent probe. In 3 different glass flasks, 20 mg of MCM41-butanediamine, 20 mL of PBS and 2.5 mg of calcein were left stirred at room temperature overnight. The CB7 (1.5 mL) was only added on the following day, when 3 different **conditions** were set: [**1**] no washes; [**2**] washed 3 times; [**3**] washed 5 times. All conditions were transferred to falcons and washed as mentioned, performing cycles of vortex and centrifugation. Finally, their supernatants were removed, and the samples were left to dry in an oven.

To perform the release tests with calcein, UV-Vis spectroscopy was used in the first instance to detect if there was calcein releasing through pH changes by adding NaOH in distinct quantities and concentrations (10 and 15 µL, at 1 M). This analysis was made to the **condition 3**, i.e., for the condition subjected to 5 washes.

### 3.6.3 Fluorescence

We also used a spectrofluorometer to examine the release profile of the NPs through calcein's emitting fluorescence. To draw up this experiment, **condition 3** was used as well as a new suspension only with MCM-41 and calcein which will be named **condition 4**. This new condition was prepared having in mind the preparation mentioned above but washed until it had no absorbance in UV spectroscopy. Then, 3 µL of a 0.859 M 1-Adamantanamine hydrochloride solution was added to both conditions.

As calcein's excitation and emission wavelengths are around 458 nm and 520 nm, respectively [18], the samples were excited at 450 nm.

**NOTE:** These tests were performed with a MCM-41 nanovalve system reported in the literature [18]. However, the results obtained, included in the appendix (**Figure A.15-A.17**), were not conclusive.

## 3.7 DNA tests

A new protocol was prepared based on some articles related to DNA adsorption [69]–[72].

DNA stock solutions were made in PBS pH=7.4 at different concentrations: 5000, 2000, 500, 100 and 10 µg/mL, and UV-Vis spectra were recorded for all of them, so a calibration plot could be done and the adsorption percentage calculated.

From each solution, 4 mL were poured into a falcon together with 5 mg of the MSN-TESPAI, previously grinded, and the suspension was dispersed for a while in a vortex. DLS analysis for both the size and the ζ-potential were done. After that, the suspension was stirred overnight, keeping in mind that the temperature must not overtake 25 ºC due to DNA degradation. The next

day, a DLS analysis was done to compare with the previous results. The suspension was centrifugated and the supernatant was analysed by UV-Vis spectroscopy. Finally, a double washing with PBS pH=7.4 was done and the precipitate was dried under vacuum. The solid was resuspended in PBS and analysed by DLS. At a certain point, 500 µL of CB7 ≈2 mM was added to the suspension to observe its effect.

## 3.8 SP Solution studies

### 3.8.1 Photochemistry vs Kinetics

To prepare the solution, Compound 4 was dissolved in Milli-Q water and its absorbance was recorded in a UV-Vis spectrophotometer, at different pHs (9.5-1.5) with a 0.5 interval. The solution with pH=4 was irradiated at 420 nm during periods of 30s, 1min and 25min and, after each irradiation, a UV-Vis spectrum was recorded. The recovery kinetics was followed for 100min (every 2min a UV-Vis spectrum was recorded).

### 3.8.2 With CB7

Another solution with an absorbance below 1 was prepared, and a ≈2 mM CB7 solution was added. For the tests, 2 mL of the solution prepared were diluted in a UV-Vis cuvette with 250 µL of water and 250 µL of a 0.1 M citrate buffer solution. Its behaviour was observed at different pHs from 9.5 to 1.5 with a 0.5 interval.

### 3.8.3 Degradability and Stability

The stability of Compound 4 was studied in $D_2O$ and $CD_3OD$ solutions by $^1H$ NMR spectroscopy. Both solutions were also analysed after a few days (3 and 13 days, respectively).

## 3.9 Spectral variations with pH and photochemistry of MSN-Compound 5

10 mg of the MSN-Compound 5 were poured into 25 mL of Milli-Q water and left a long time under sonication so a well-prepared suspension could be obtained. For the tests, 2 mL of the suspension prepared was diluted in a UV cuvette with 250 µL of water and 250 µL of 0.1 M citrate buffer. Several UV-Vis spectra were recorded from pH=1 to pH=9, adjusting the pH with HCl solutions of 1 and 0.1 M.

A suspension at pH=4 with 5 mg of the MSN-Compound 5 and 10 mL of Milli-Q water was also prepared.

## 3.10 DLS: stability and size

Suspensions of the starting MSNs and both MSNs-TESPAI and MSN-Compound 5-M/W were prepared in Milli-Q water.

Into a falcon, 2 mg of the NPs were poured together with 4 mL of filtered water. It is important to greatly grind the NPs before the suspensions' preparation. All suspensions needed long periods under vortex and sonication so the NPs could be well dispersed and not precipitate easily. This means high-speed vortex for 30min and 15-30min of sonification, twice, followed by another vortex [5]. A DLS equipment was used to verify NPs' size, hydrodynamic diameter and ζ-potential.

## 3.11 MSN-Compound 5 in a PBS suspension

The behaviour in suspension of the MSN-Compound 5 was observed firstly by preparing 5 mg of those NPs in 4 mL of PBS pH=7.4. Observations were also done for lower pHs (4 and 1), and, to the suspension with pH=1, a ≈2 mM CB7 solution was gradually added.

A less concentrated suspension was also prepared mixing 2 mg of the NPs with 4 mL of PBS pH=7.4. Its behaviour was observed as the pH was being decreased 1 by 1.

## 3.12 ITC

For the calorimetry tests through ITC, a stock solution of Compound 4 in MeOH was done. Again, the solution was prepared taking into account not to overtake an absorbance of 1 in a UV-Vis spectrophotometer. From that stock solution, 1 mL was taken, dried and reserved for the next experiments.

Three different conditions of ligand and sample solutions were prepared for the analysis in three different Eppendorfs: **[1]** From the dried solution, 100 µL were taken and dissolved in 900 µL of Milli-Q water to preface 1 mL (sample solution). A 1 mM CB7 solution was used as ligand solution; **[2]** 40 µL of the dried solution dissolved to complete 1 mL was used as sample and a 2 mM CB7 solution as ligand solution; **[3]** 20 µL of the dried solution dissolved to preface 1 mL was used as sample and a 1 mM CB7 solution as ligand. Both solutions had their pH adjusted to 4.

A stock solution of Adamantane 0.1 M was prepared using 1-Adamantanamine hydrochloride and, from that stock, a $5x10^{-4}$ M solution was also managed. That Adamantane solution was used as the sample solution whereas a 50 µM CB7 solution operated as ligand solution.

# 4. RESULTS AND DISCUSSION

## 4.1 Spiropyran in solution

Spiropyran (SP) was synthesized following the steps represented in **Figure 4.1**, where Compound 4 was obtained and used as a model compound for the following experiments. Throughout its production steps, different reaction yields were obtained: 43% (Compound 2), 27% (Compound 3) and 100% (Compound 4), where the lower yields are due to the chromatography columns performed.

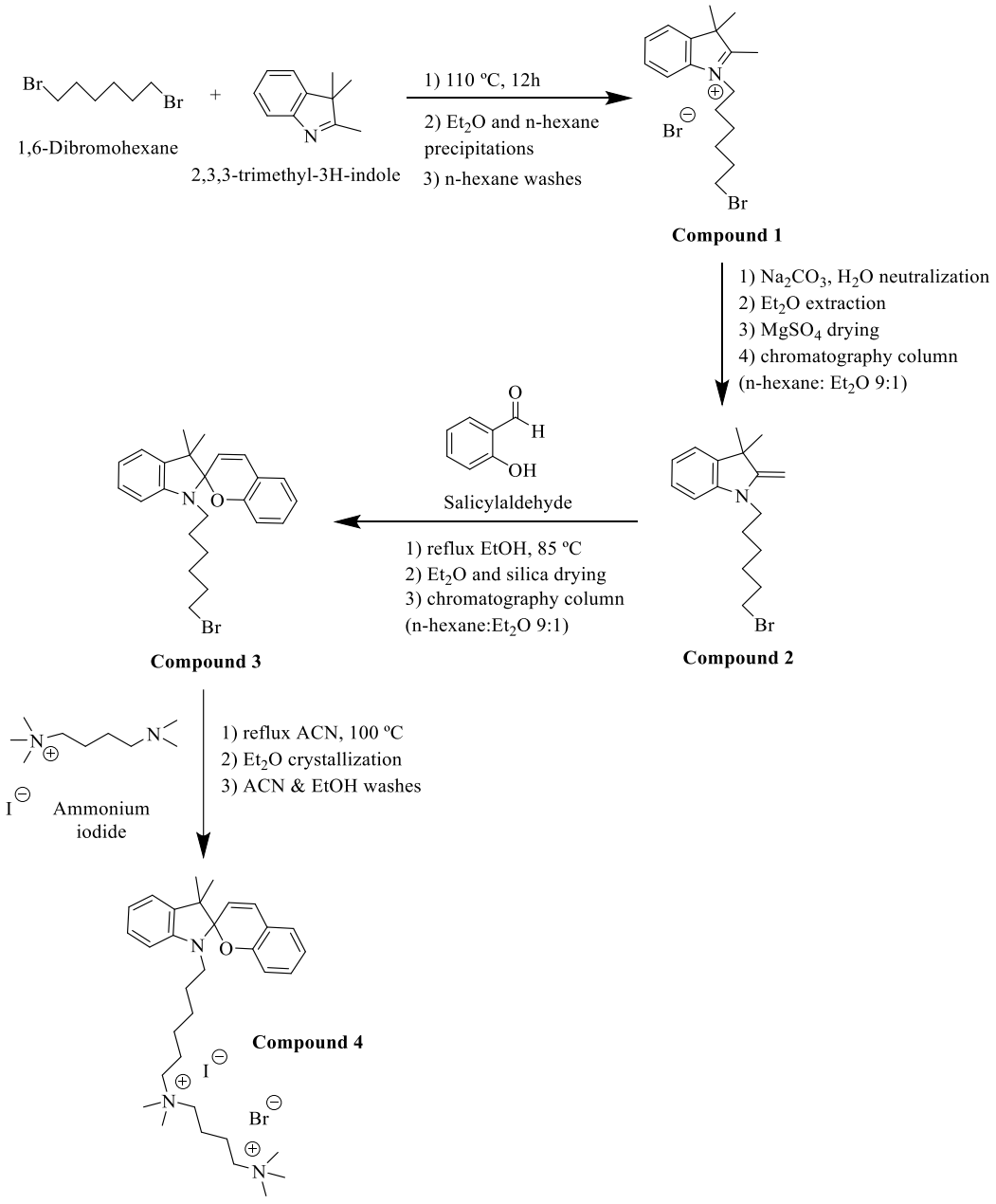


**Figure 4.1** Synthetic strategy leading to the production of Compound 4.

The synthesized product was analysed by $^{1}$H NMR spectroscopy. In **Figure 4.2**, Compound 4's aromatic region (corresponding to indoline and chromene moieties) can be well observed and is according to COSY and NOESY spectrums in that region (**Figure A.3**). The rest of the spectrum is not so clear, although the peaks' integration is in agreement with Compound 4 structure.

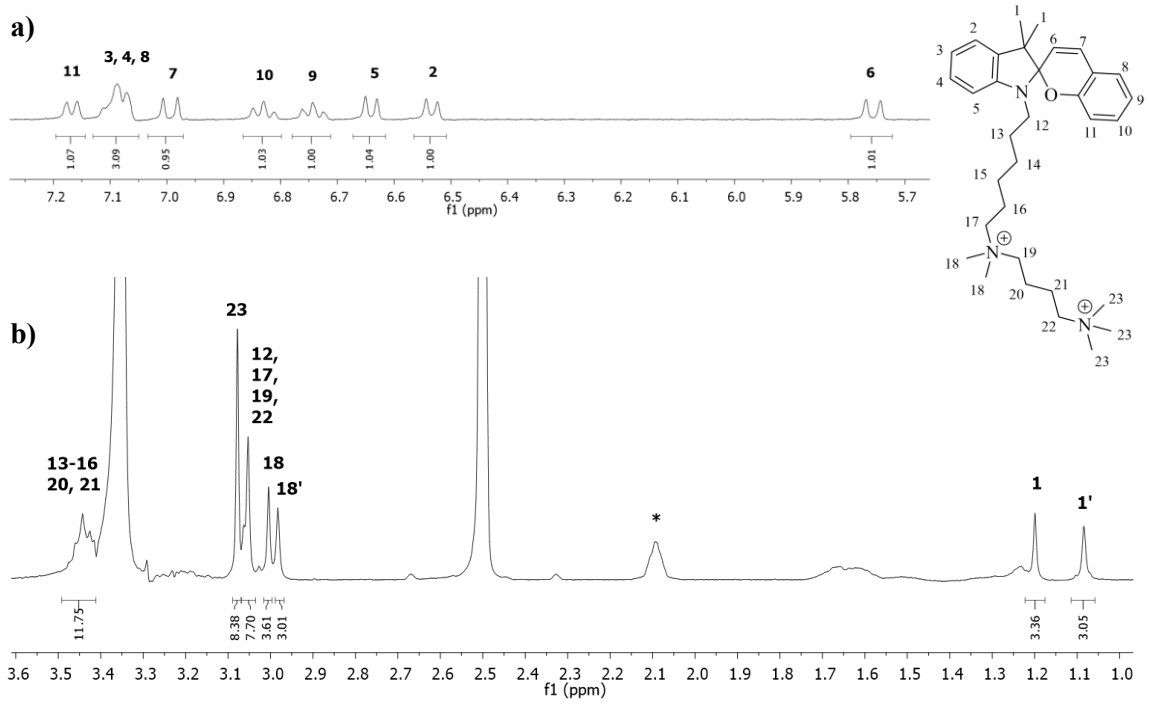


**Figure 4.2** $^{1}$H NMR of Compound 4 in DMSO d6. Spectrum **a)** corresponds to the aromatic attribution while **b)** to the remaining molecule's attribution; solvent peaks are marked with a *.

## 4.1 Photochemical and acid-base behaviour

The behaviour of Compound 4 upon gradual pH variations (from pH=1.5 to pH=9.5) was studied by UV-Vis spectroscopy (**Figure 4.3**). The changing colours correspond to the distinct forms assumed by the molecule at different pH values, illustrating the acid-base equilibrium behaviour of the model compound.

Acidic solutions, represented as yellow, have an absorption maximum wavelength ($\lambda_{max}$) at ≈420nm while basic solutions, represented as pink/red, have their absorption maximum at ≈530nm. The first $\lambda_{max}$ corresponds to MCH species and the second one to MC species, since an acidic medium causes protonation. These results are in agreement with what was already reported, where the maximum absorbance peaks for each species were $\lambda_{MCH}$ = 442nm and $\lambda_{MC}$ = 538 nm, the first form at a lower pH and the second one at a higher pH, in the dark [42]. SP molecule, due to its main aromatic regions, shows two bands at ≈300 and 370nm, a slight deviation from the values reported in the literature [40].

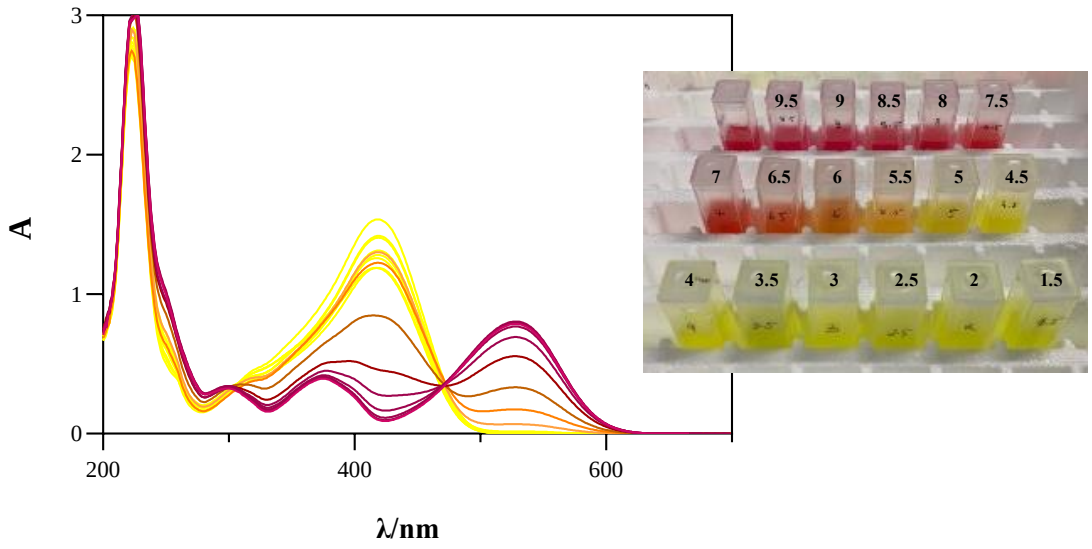


**Figure 4.3** UV-Vis spectra of Compound 4 as a function of pH, at different pHs in water, from pH = 1.5 to pH = 9.5, and the progression of colours respective to the different forms that this molecule can have. The colour of each UV-Vis spectrum is represented with the corresponding coloured solution (yellow at a lower pH – higher absorbance at 420nm – and pink/red at a higher pH – higher absorbance at 530nm).

In addition, the solutions prepared were tracked for a few days to analyze their stability and degradation (**Figure A.4**) and the most stable solution seems to be between pH = 4 and pH = 4.5. Similar experiments, in the same pH range, were performed in the presence of a ≈2mM CB7 solution and the results show almost the same curve pattern as the initial solutions, as represented in **Figure 4.4**, which means that it has little impact on its isomerization, as already reported [43]. As well as for the initial solutions, their stability and degradation tests (**Figure A.5**) showed higher stability at pH around 4 (3.5<pH<4). However, other authors reported that MCH is the thermodynamically most stable photochromic form both in water and CB7 cavity at pH 2.35 [43].

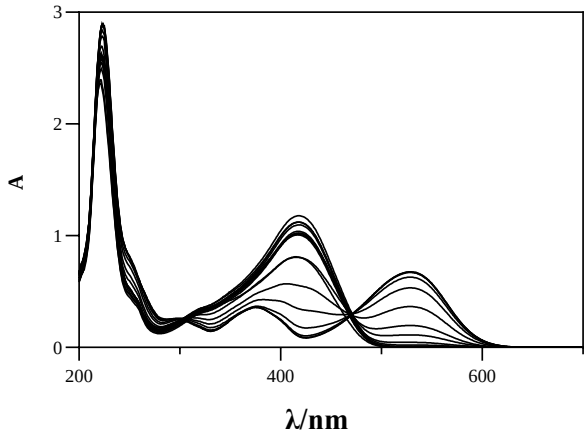


**Figure 4.4** Spectral variations of Compound 4 observed as a function of pH in the presence of a ≈ 2 mM CB7 solution, in aqueous solution.

An important parameter to consider in these experiments is the $pK_a$, since it provides a convenient way to express the acidity of a compound on a logarithmic scale. The $pK_a$ values obtained (**Figure 4.5**) were found to be 6.65 and 6.98 for the free compound and the CB7 complex, respectively. We can thus conclude that CB7 has little effect on the acidity of SP species. These results mean that, at a pH near 7, the molecule will exist in equilibrium between the two forms of merocyanine. Since physiological mediums have different pHs depending on the organ and on the condition (e.g. cancer), this characteristic must be taken into account to ensure the presence of the MCH form and the desired behaviour of the system.

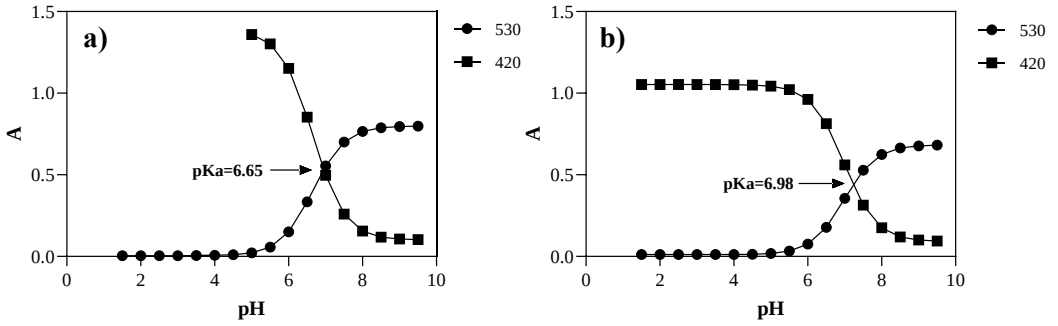


**Figure 4.5** The acid−base dissociation equilibria of **a)** the free Compound 4 and **b)** the Compound 4-CB7 complex.

For the following studies we intended to guarantee the presence of the MCH form. In **Figure 4.5** can be seen that, until pH≈5, MCH is predominant. Taking this, and the performed stability and degradation tests, into consideration, we decided to use a pH=4 solution.

Compound 4 was, therefore, irradiated in aqueous solution at pH=4 and the resultant UV-Vis spectra are represented in **Figure 4.6a**. After an irradiation at 420 nm for 25min, the initial absorbance (black curve) was reduced to its half (orange curve), which can be indicative of MCH's convertion into SP, which does not absorb in the visible region of the spectrum. Interestingly, just 30s (purple curve) were enough to considerably change the molecule and, in consequence, its absorbance.

In addition, **Figure 4.6b** represents the thermal recovery after irradiation followed over 100min (50 cycles of 2min) to inquire what is the behaviour of the molecule and how long it takes to recover its initial MCH form. It can be observed that not only it could achieve its initial absorbance completely (black bold curve), but also that required between 8 to 10min.

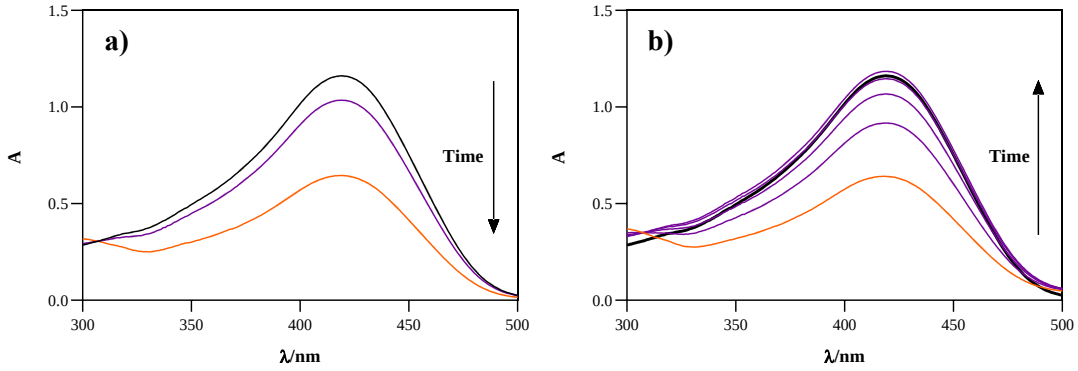


**Figure 4.6 a)** Irradiation at 420nm of an aqueous solution of Compound 4 at pH = 4 and its absorbances over time: initial spectrum (black curve), after 30s of irradiation (purple curve) and after 25min of irradiation (orange curve); **b)** Thermal recovery in the dark at room temperature: UV-Vis spectra recording for 100min, every 2min.

### 4.1.2 Degradability and Stability

**Figure 4.7** reveals a comparison of Compound 4's behaviour in different polar solvents: $CD_3OD$ (deuterated MeOH) and $D_2O$, through $^1H$ NMR. Spectrum **a)** corresponds to the spectrum performed in DMSO after its synthesis and will serve as a means of comparison. In spectra **b)** and **c)** we can see that, even after 13 days, the solution remained stable, with the same peaks' distribution. The major difference is detected in the peak at ≈5.7 ppm, which is due to an exchange of hydrogen atoms with the $CD_3OD$ deuterium used. Regarding $D_2O$, represented in spectrum **d)**, we can immediately observe an alteration in the peaks' pattern as well as a huge modification. After 3 days, in **spectrum e)**, there is an alteration in the previous spectrum.

These results might suggest that Compound 4 remains more stable in methanol.

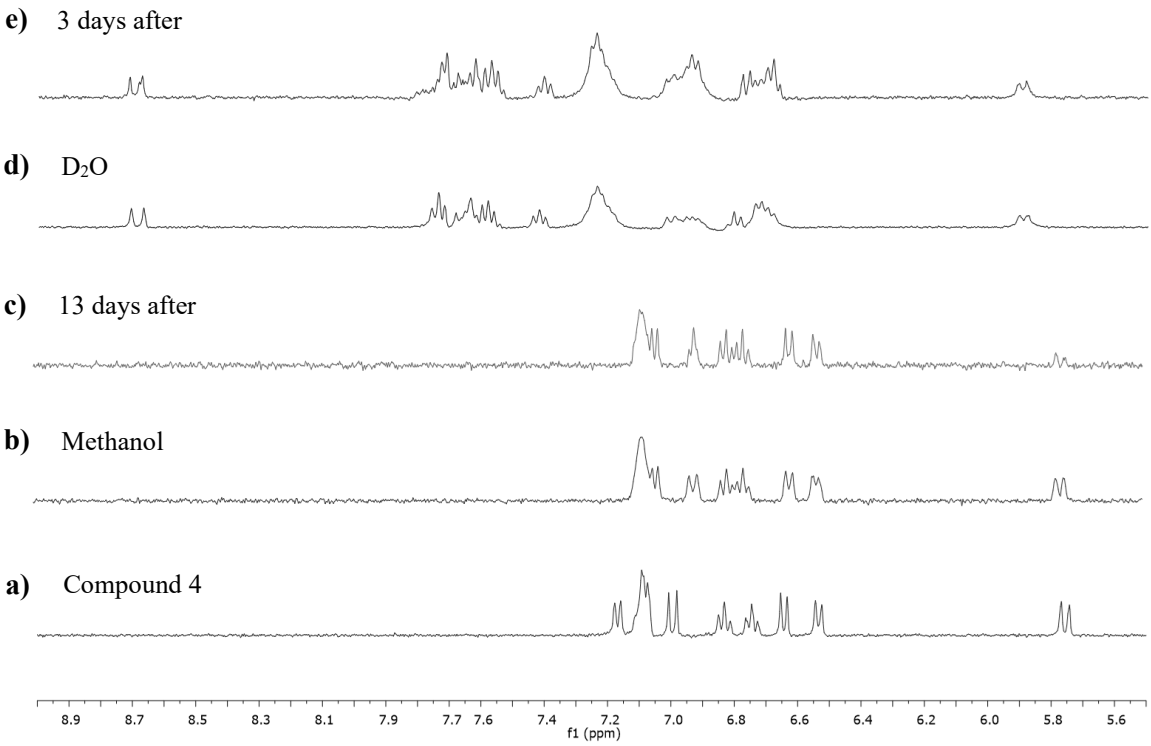


**Figure 4.7** $^{1}$H NMR spectrum of Compound 4 in three different solvents: DMSO, $CD_3OD$ and $D_2O$. **a)** Compound 4 after its synthesis and analysis in DMSO; **b)** Compound 4 in MeOH; **c)** sample of spectrum "b" after 13 days; **d)** Compound 4 in $D_2O$; **e)** sample of spectrum "d" after 3 days. All spectrums were magnified to the range of ppm respective to Compound 4's aromatic ring (between 8.9 and 5.5 ppm).

### 4.2.3 Spiropyran interaction with CB7

The ITC calorimetry data are compiled in **Table 4.1** and the titration curves are in the appendix (**Figures A.10-A.14**). This analysis is used to study binding interactions, and their thermodynamic properties, giving essential insights into the energetics of molecular interactions and the strength and stability of binding between molecules, ligands and receptors [73]. In this case, the tests performed will give insights into SP interaction with CB7.

**Table 4.1** Thermodynamic parameters obtained for the formation of CB7 inclusion complexes with Compound 4. **[A]** 0.2mM of Compound 4 as sample and 1mM of CB7 as ligand, at pH 7.5; **[B]** 0.2mM of Compound 4 as sample and 2mM of CB7 as ligand, at pH 7.5; **[C]** 0.1mM of Compound 4 as sample and 1mM of CB7, at pH 4.2.

| | System | pH | $K_D$ (M) | ΔH (kJ/mol) | TΔS (kJ/mol) | ΔG (kJ/mol) |
|---|---|---|---|---|---|---|
| **A** | Compound 4 + CB7 | 7.5 | $1.04\pm0.08\times10^{-6}$ | -31.5±0.3 | 2.73 | -34.2 |
| **B** | Compound 4 + CB7 | 7.5 | $2.90\pm0.07\times10^{-6}$ | -31.4±0.5 | 5.96 | -37.4 |
| **C** | Compound 4 + CB7 | 4.2 | $6.92\pm4.15\times10^{-8}$ | -30.9±1.0 | 10.00 | -40.9 |

Looking at enthalpy (ΔH) and entropy (ΔS) columns, we are able to see that conditions A, B and C have a ΔH<0, indicating an exothermic reaction, and a ΔS>0, which means there is energy being released throughout the process and there are molecular rearrangements, probably due to the interactions. This means that the complexation process is both entropically and enthalpically favourable. However, it is considered enthalpically driven since the magnitude of ΔH is greater than TΔS. The observed positive value of ΔS may be due to the release of a large number of water molecules from inside the CB7 hydrophobic cavity when interacting with Compound 4 [74].

Knowing that the binding affinity constant ($K_A$) is the inverse of the dissociation constant ($K_D$), the $K_A$ values obtained for the three first conditions were $9.615x10^5$, $3.448x10^5$ and $1.445x10^7$ $M^{-1}$, respectively. Condition C has a higher affinity constant when compared to the other three conditions because, at pH 4, Compound 4 is in its MCH form, meaning it has an extra available cation to interact more easily with CB7, as represented in **Figure 4.8**. At the same time it provides an electrostatic force of attraction, the hydrophobic cavity of CB7 provides hydrophobic force to attract the guest molecule [74], [75].

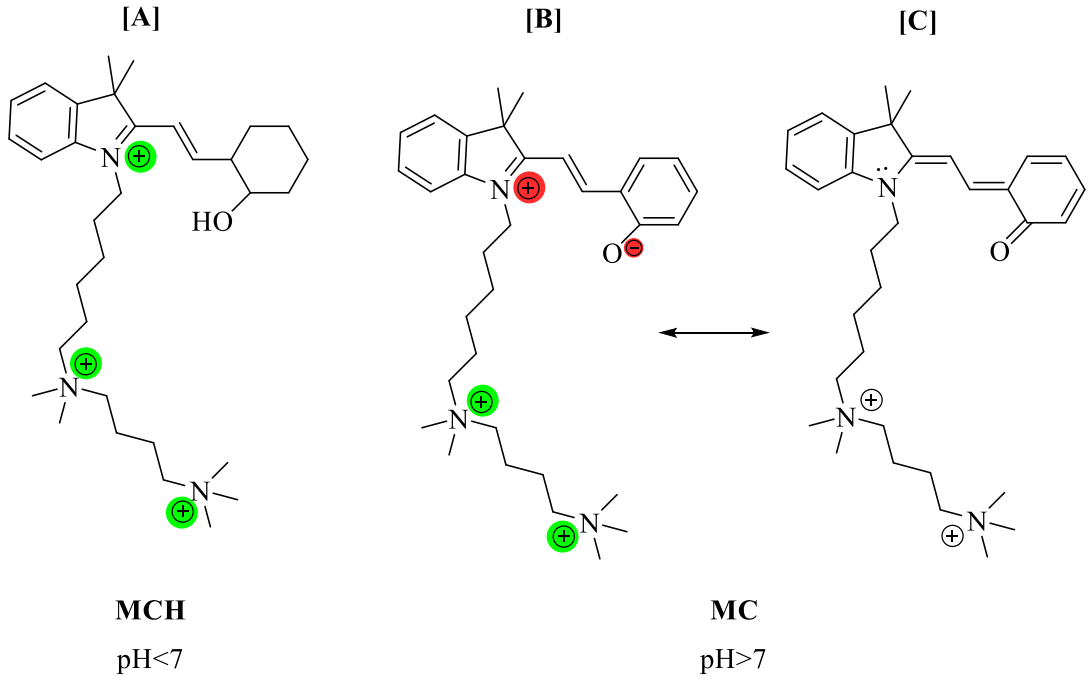


**Figure 4.8 [A]** MCH chemical structure (existing at acidic pH); MC structure is represented in its **[B]** zwitterionic and **[C]** quinoid forms (existing at basic pH). The available cations are at green while the cations already establishing electrostatic interactions are red. MCH possesses three available cations while MC form just has two in that condition.

As shown previously in the Project Overview section (**Figure 2.1**), the final system also includes another cationic molecule where the CB7 must slide to provide the desired controlled release. Therefore, in future tests, the $K_A$ results obtained for SP and CB7's interaction must be considered when analysing the affinity of CB7 to the other cationic molecule. If, for some reason, the $K_A$ is lower than the obtained in this work, the amount of CB7 added should be higher.

Binding affinity is also related to the Gibbs free energy (ΔG). As the results show (**Table 4.1**), when the binding constant is higher, ΔG is more negative [76] and the binding process is more thermodynamically favourable.

## 4.2 MSN 45nm functionalization and characterization analysis

The precursor MSNs were synthesized following a sol-gel method described in the literature, according to **Figure 4.9** scheme.

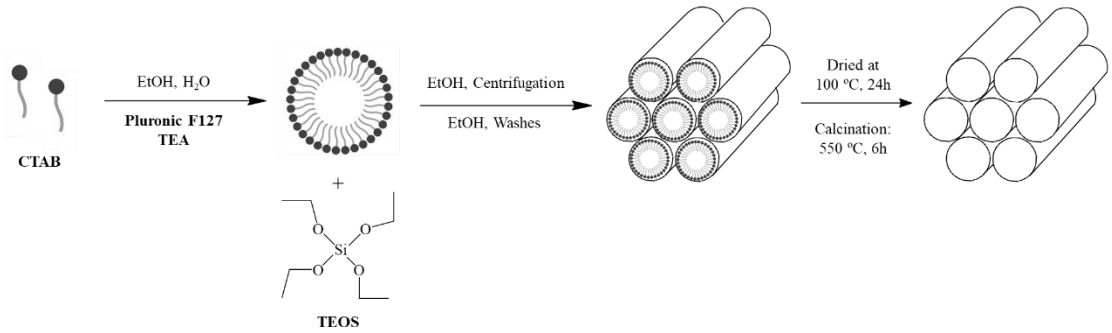


**Figure 4.9** Scheme of MSN 45nm synthesis.

After its synthesis, the precursor MSNs were functionalized with two different molecules: Compound 5 (the SP molecule able to functionalize the MSNs) and TESPAI (the molecule used for the DNA tests).

### 4.2.1 Compound 5 characterization

Compound 5 was produced following the steps represented in **Figure 4.10**, from the microwave-assisted heating (M/W) of Compound 3 with DAPTS. The production yield was considerably low (32%), which means the amount of time under microwave-assisted heating may not have been enough.

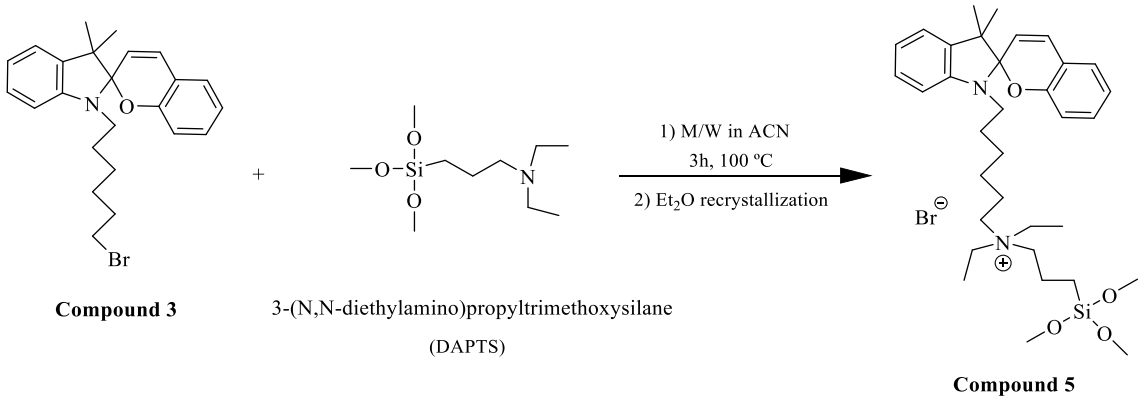


**Figure 4.10** Synthetic strategy leading to the production of Compound 5.

The product obtained was analysed by $^{1}$H NMR spectroscopy, and its spectrum can be observed in **Figure 4.11**. The peaks in the range 7.3-6.5 ppm can be assigned to the aromatic protons of Compound 5 (corresponding to indoline and chromene moieties), while the rest of the spectrum cannot be analysed with the same clarity, due to some peak overlap.

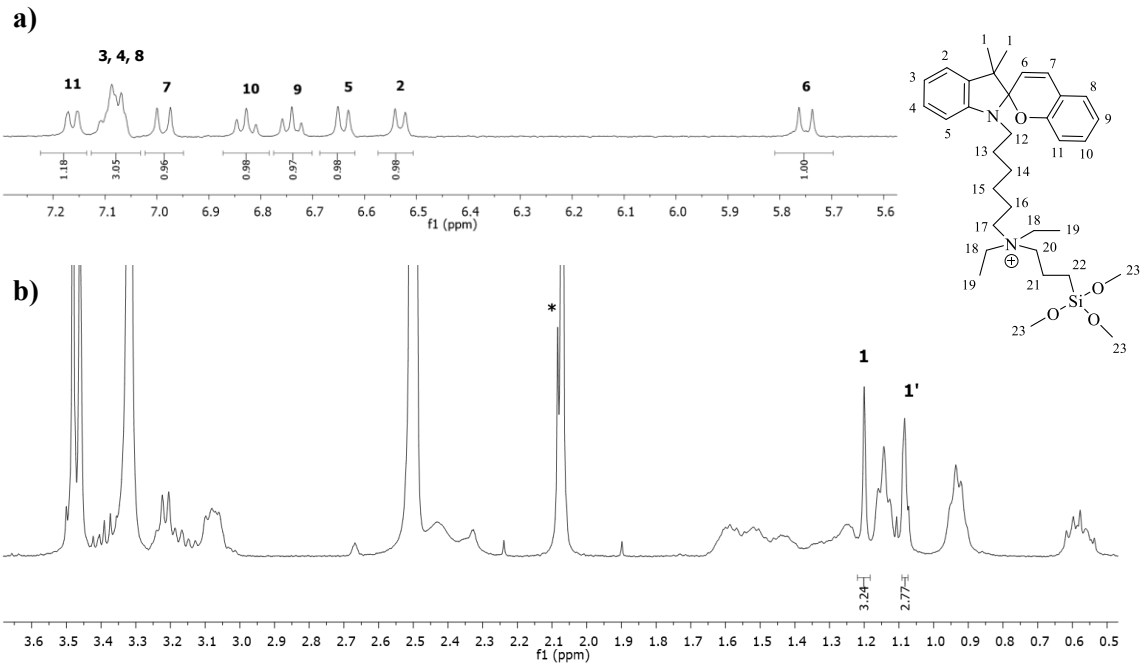


**Figure 4.11** $^{1}$H NMR of Compound 5 in DMSO d6: Spectrum **a)** corresponds to the aromatic attribution while **b)** to the remaining molecule's attribution; solvent peaks are marked with a *.

## 4.2.2 TESPAI characterization

TESPAI was synthezied following the steps represented in **Figure 4.12**, from the microwave-assisted heating of (3-Iodopropyl)trimethoxysilane and Triethylamine.

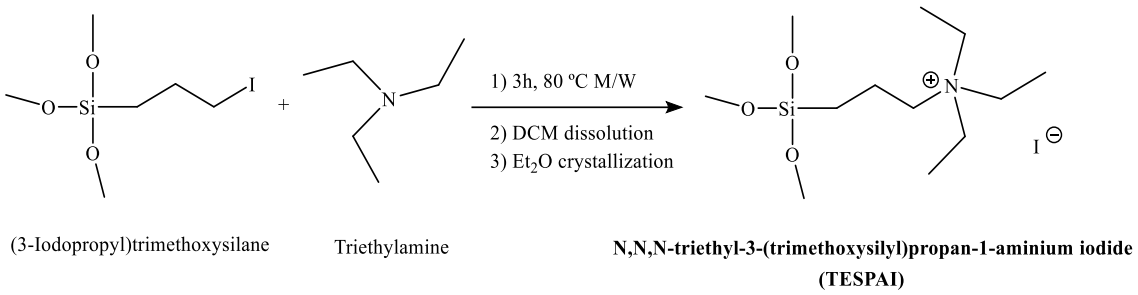


**Figure 4.12** Synthetic strategy leading to the production of TESPAI.

The product obtained was analysed by $^{1}$H NMR spectroscopy (**Figure 4.13**), and the assignment seems to be in agreement to what is expected. However, the reaction yield was considerably low (32%), suggesting that the amount of time under microwave-assisted heating may not have been enough.

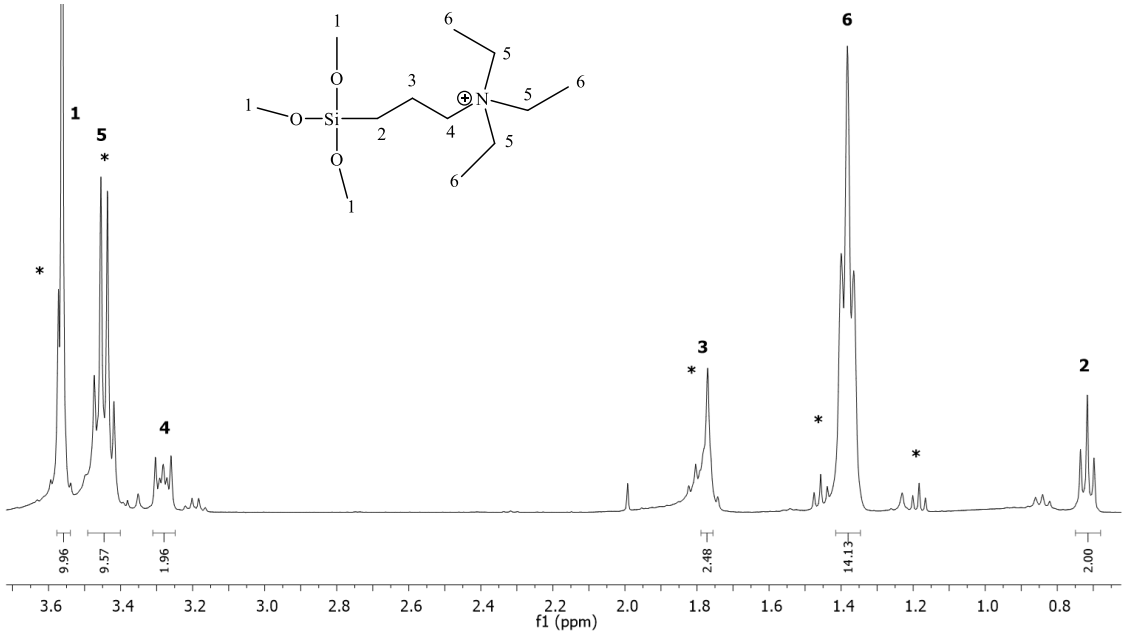


**Figure 4.13** $^{1}$H NMR of TESPAI in $CDCl_3$; solvent peaks and remaining reagents are marked with a *.

## 4.2.3 MSNs functionalization

MSNs were functionalized with Compound 5 through two distinct methods: microwave-assisted heating (M/W) and heating under reflux. Both methods are schematized in **Figure 4.14**.

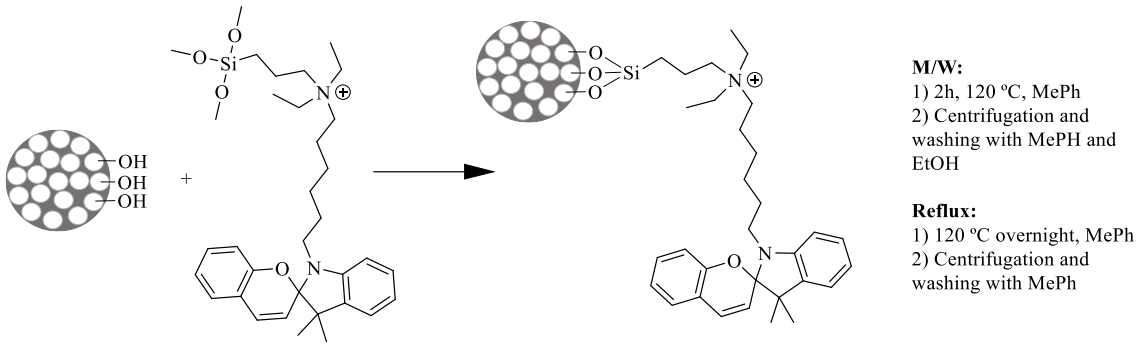


**Figure 4.14** MSN-Compound 5 production scheme.

Then, the precursor MSNs were also functionalized with TESPAI as represented in Figure **4.15 scheme**.

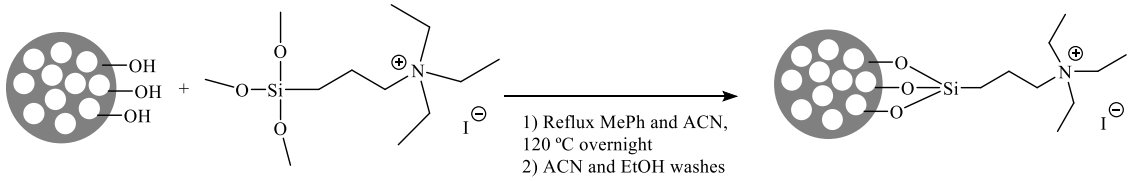


**Figure 4.15** MSN-TESPAI production schemes.

## 4.2.4 MSN characterization

All functionalizations (MSN-Compound 5 and MSN-TESPAI) were characterized by FTIR, $^{1}$H NMR, Nitrogen adsorption, XRD, Elemental analysis, TGA, TEM and DLS.

In **Figure 4.16**, FTIR spectra show silica characteristic peaks at around 790, 970, and 1090 $cm^{-1}$ owing to Si-O-Si symmetric stretching ($\nu_s$), Si-OH stretching ($\nu$), and Si-O-Si asymmetric stretching vibrations ($\nu_{ss}$), respectively. Also, a peak at 460 $cm^{-1}$ corresponds to Si-O-Si bending vibrations ($\delta$) [77]. The bands at around 3447 and 1627 $cm^{-1}$ are related to the stretching and bending vibrations of surface hydroxyls (O-H) and/or adsorbed water, respectively [18]. For both materials functionalized with Compound 5 and TESPAI, C-H bending vibrations at 1400 $cm^{-1}$ are observed [78]. The absorption peaks between 2850 and 3000 $cm^{-1}$ are due to the C–H stretching vibrations [79].

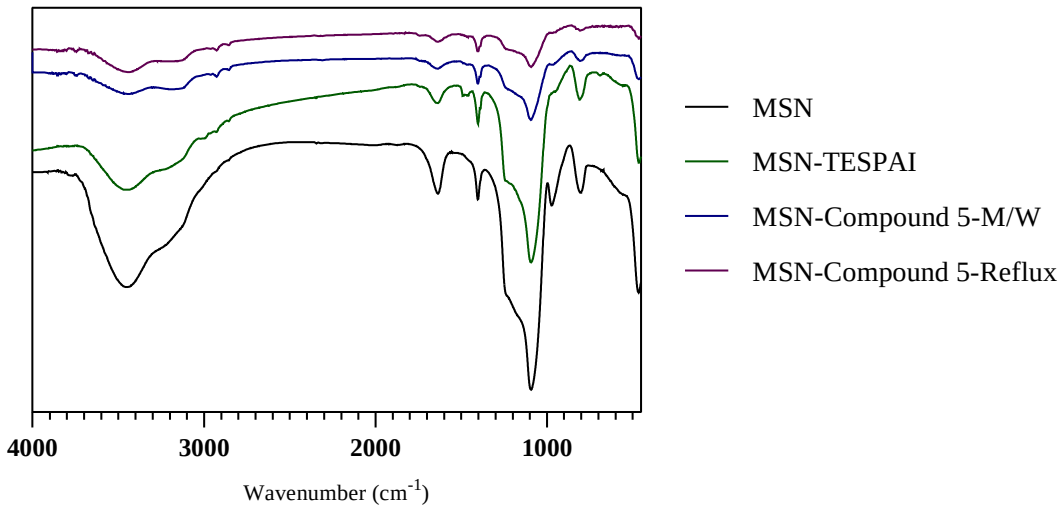


**Figure 4.16** FTIR spectra of **a)** the precursor MSNs, **b)** MSN-TESPAI, **c)** MSN-Compound 5-M/W and **d)** MSN-Compound 5-Reflux.

$^{1}$H NMR spectroscopy was used mainly for the quantification of the molecules functionalized onto MSNs' surface, which was 3.636, 0.466 and 0.5439 mmol/g for TESPAI, Compound 5-M/W and Compound 5-Reflux, respectively (**Figures 4.17 and 4.18**). The attribution was done considering the peak at 0.35 ppm as a reference, according to Crucho *et al.* 2017 [80].

**Figure 4.17**, in particular, respective to MSNs functionalizations with Compound 5, shows a degradation that might have occurred during the preparation of the sample with $D_2O$+NaOH, mainly in its aromatic region. This can be due to the high basic pH of the solution. In addition, the ammonium derivative present in Compound 5 can decompose giving the tertiary amine and influencing the appearance of the spectrum.

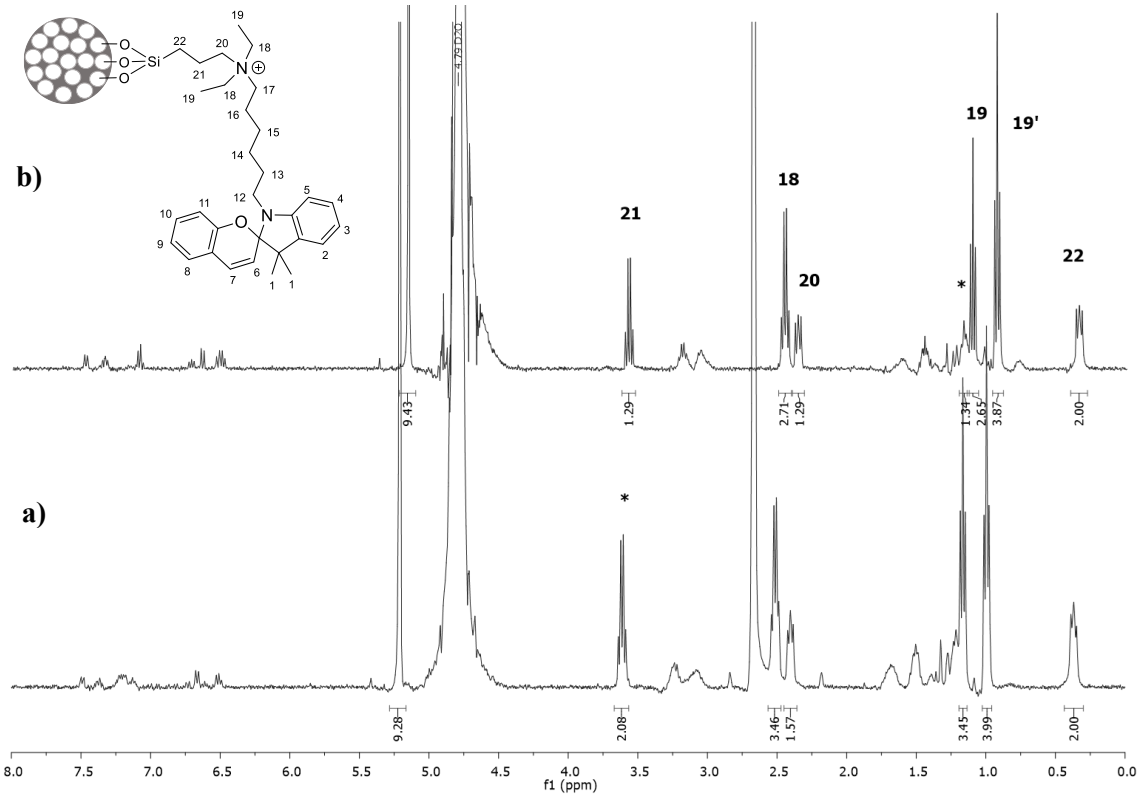


**Figure 4.17** MSN-Compound 5 $^{1}$H NMR spectra in $D_2O$+NaOH: **a)** microwave-assisted heating production; **b)** reflux production.

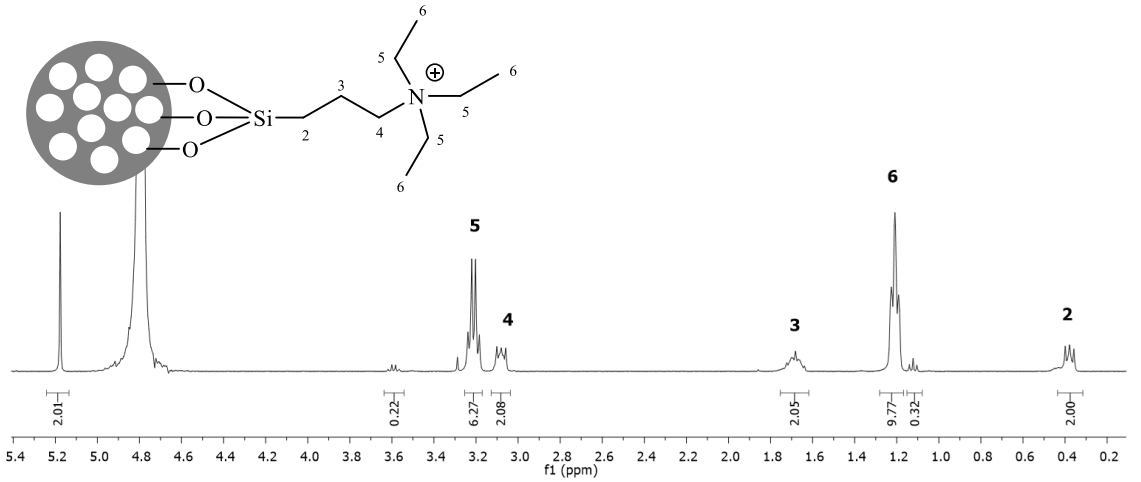


**Figure 4.18** MSN-TESPAI $^{1}$H NMR spectra in $D_2O$+NaOH.

Comparing MSN-Compound 5-M/W with MSN-Compound 5-Reflux, and considering the performed FTIR and $^{1}$H NMR analysis, both materials possess similar peak distribution. The first method is known for being more sustainable when compared to conventional reflux because it is faster [81] and allows higher yields. In this case, the reaction with M/W took 2h, while reflux took 24h, and the products obtained share similar properties. Therefore, it was developed a green method for the functionalization of MSNs with Compound 5.

Regarding Nitrogen adsorption isotherms analysis, it allows to determine the pores volume and the surface area of the MSNs prepared. As can be seen in **Figure 4.19**, the isotherms obtained on MSN-Compound 5-Reflux and MSN-TESPAI are type IV according to IUPAC classification through BET's method [82]. It can also be observed a reduced adsorption for those MSNs functionalized with TESPAI. The lower the gas adsorption, the more limited the availability of surface pores in MSNs, indicating a higher degree of functionalization, supporting NMR quantification's results.

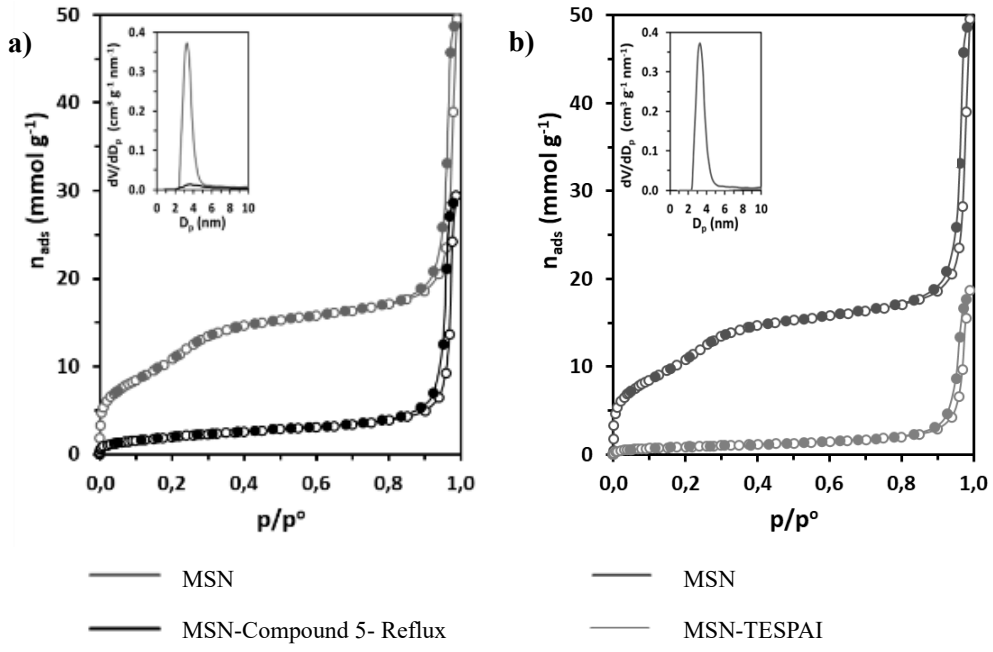


**Figure 4.19** Nitrogen adsorption isotherms ($n_{abs}$) determined at 77 K on MSN in comparison with **a)** MSN-Compound 5-Reflux and **b)** MSN-TESPAI as a function of the relative pressure (p/pº). NLDFT pore size distributions are inserted into the figures.

Functionalized materials are expected to present smaller values of surface areas and pore volumes, and a decrease in the pore size distributions when compared to the precursor materials [83]. This is primarily attributed to a reduction in the amount of pores available for nitrogen gas adsorption, as **Table 4.2** may show. The results suggest, once again, a higher degree of functionalization for MSN-TESPAI.

**Table 4.2** Textural characteristics of the mesoporous silica nanoparticles obtained by analysis of the Nitrogen adsorption isotherms determined at 77 K.

| Sample | $A_{BET}$ ($m^2 g^{-1}$) | $D_p$ (nm) | $V_p$ ($cm^3 g^{-1}$) |
|---|---|---|---|
| MSN | 820 | 3.3 | 0.46 |
| MSN-Compound 5-Reflux | 160 | 3.6 | 0.04 |
| MSN-TESPAI | 73 | - | - |

* $A_{BET}$ – specific surface area; $D_p$ – pore diameter; Vp – cumulative pore volume

X-Ray diffraction analysis (XRD), in **Figure 4.20**, provides detailed information about the crystallographic structure, chemical composition, and physical properties of materials [84]. The starting MSNs show a main peak in the low-angle region at 2θ = 2º and another with much lower intensity and broader around 2θ = 4º, which, according to the literature, indicate some ordering of the pores with reasonably uniform pore size [83], [85]. Both MSN-Compound 5-Reflux and MSN-TESPAI have a main peak in the low-angle region at around 2θ = 2°, which is consistent with the literature [5]. In addition, although with different intensities, these results are indicative of the presence of some remaining ordered mesopores after functionalization [83].

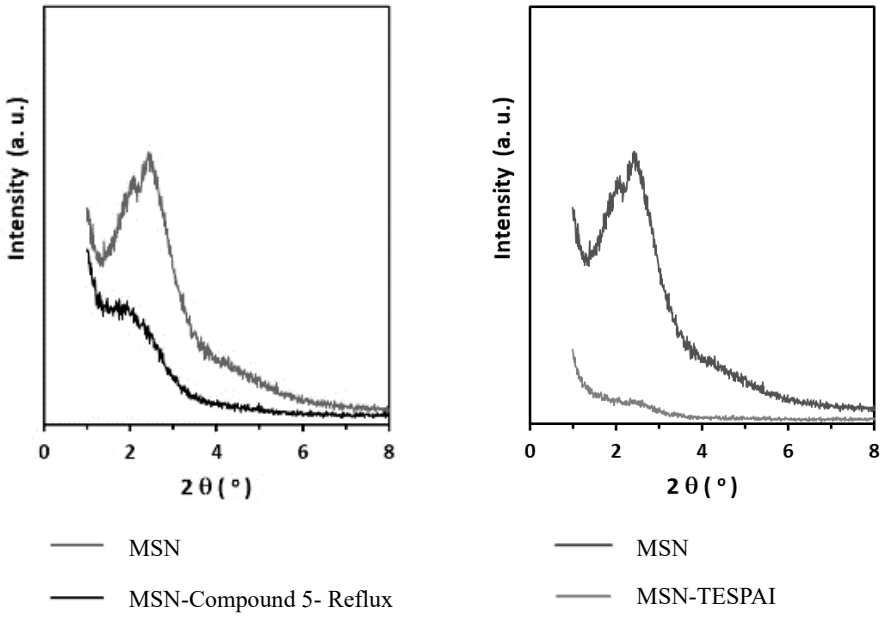


**Figure 4.20** X-ray diffraction patterns of MSN-Compound 5-Reflux and MSN-TESPAI, in comparison with the precursor MSNs.

Elemental analysis allowed us to ascertain if the production of the MSN materials was a success and to determine the functionalization loading [85]. Based in nitrogen and carbon percentages, this analysis suggests that the MSN-Compound 5-Reflux have a loading of ≈0.57mmol/g, which is according to the $^1$H NMR quantification results (0.55 mmol/g).

Thermogravimetry analysis (TGA), in this case represented in **Figure 4.21**, is usually used to determine materials' thermal stability and composition [86]. It can be described as the change in weight of a substance as a function of temperature, which yields a decomposition curve that provides parameters that may be indicative of material quality or the presence of impurities [87], [88].

At temperatures below 200 ºC, the mass loss can be related to water molecules, surface silanols and volatile impurities. Above 200 °C, Δm values can be considered due to surface functionalization [89], [90]. In the range of 150-600 ºC the thermal decomposition of the organic molecules occurred with a weight loss of 20.7 and 31.0% for MSN-Compound 5-Reflux and MSN-TESPAI, respectively, which is consistent with the content obtained by elemental analysis.

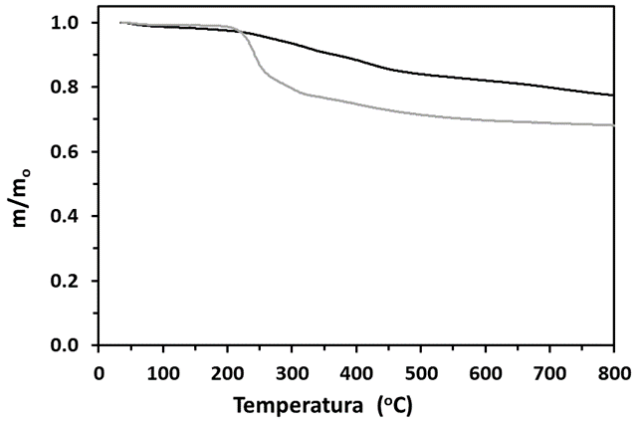


**Figure 4.21** Thermogravimetric analysis (TGA) of MSN-Compound 5-Reflux and MSN-TESPAI, where the mass variation ($m/m_o$) is measured as a function of temperature (ºC). Mass variation values are normalized to the initial mass ($m_o$) at 35 ºC.

The images obtained by TEM (**Figure 4.22**), with the help of the software Image J, allowed us to establish the size of both unmodified and functionalized MSNs with more precision. Besides, it can also give some information about the appearance of the MSNs as well as their functionalization.

According to the data obtained, the precursor MSNs have a mean size of 62.22 ± 16.02 nm and the ones functionalized with TESPAI a size of 64.27 ± 13.61 nm. The MSN-Compound 5 produced resorting to microwave-assisted heating present a mean size of 66.17 ± 14.57 nm, while the refluxed ones 68.57 ± 14.24 nm. Considering the experimental protocol used, the precursor MSNs were supposed to present 45 nm, which is roughly the size of the smaller MSNs in stock. We can consider the observed size augmentation normal since even a slight alteration of the production conditions can highly influence the results [32].

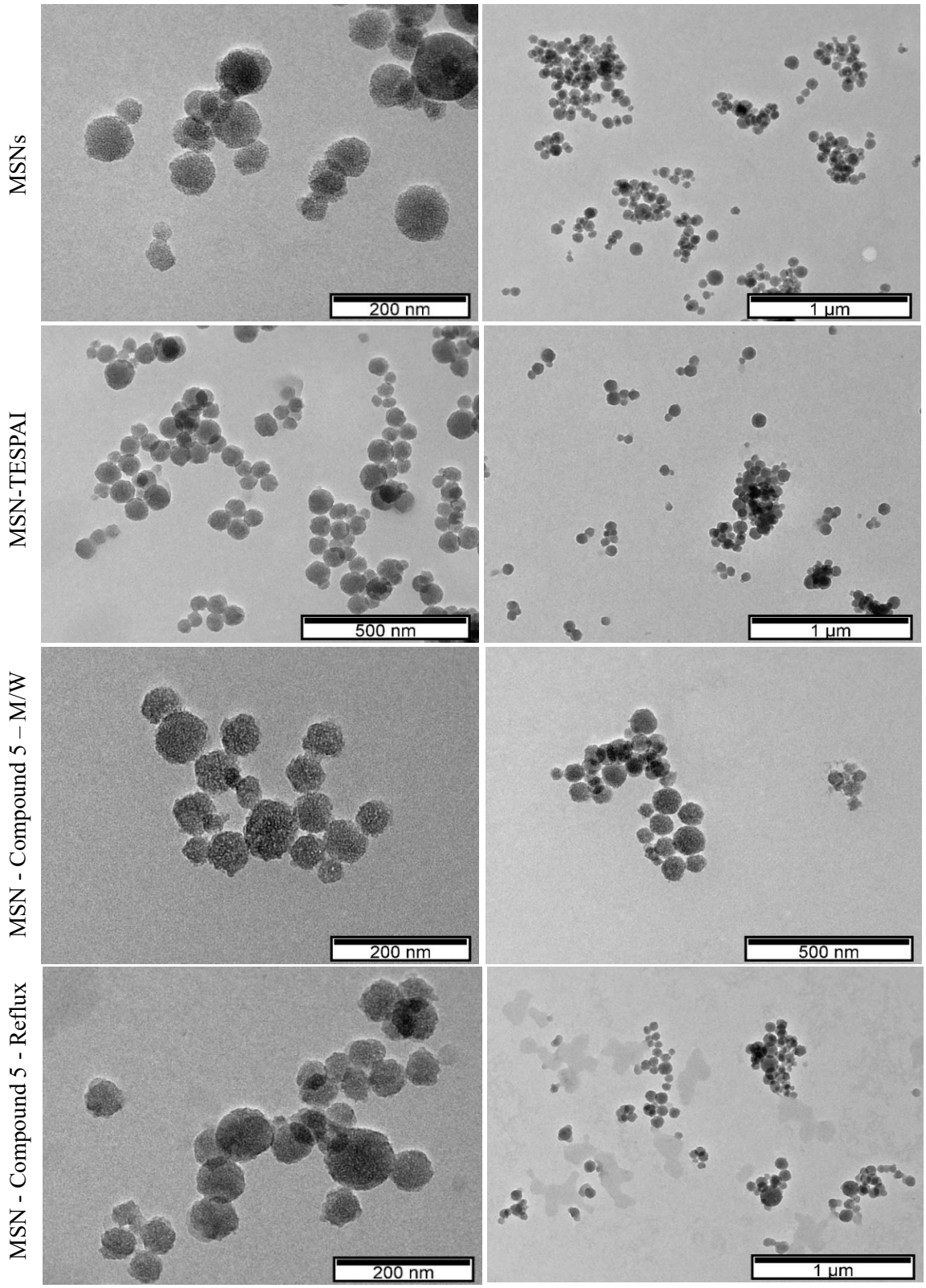


**Figure 4.22** Transmission electron microscopy images of the precursor MSNs (MSNs) and the functionalized MSNs (MSN-TESPAI, MSN-Compound 5-M/W and MSN-Compound 5-Reflux) produced with and with no functionalization, magnified to 1µm, 500 nm, 200 nm and 100 nm, using ethanol as solvent.

The MSNs prepared were suspended in water by sonication and their colloidal stability was monitored by DLS. The table below (**Table 4.3**), shows the results of the three main parameters of DLS analysis: size (peak mean size), z-average and zeta potential (ζ-potential).

DLS is an optical measurement technique for the analysis of suspension's colloidal stability, a feature that affects nanoparticles' (NPs)' hydrodynamic diameter and might have a profound impact on a future therapy's success. This analysis is performed through the quantification of the Brownian motion of individual particles in liquids [91], [92]. The size distribution of each sample is represented in **Figure 4.23**.

While in TEM we analyze the core size of each NP, DLS represents the core size plus the electric dipole layer that adheres to its surface. Hydrodynamic diameter hence refers to the size of a particle in a fluidic medium, considering its interactions with the surrounding solvent molecules giving information about the dynamic behavior of the particles in solution [93].

Z-average and peak mean size are both measurements used to describe the size distribution of particles in a sample, but they represent different aspects of the distribution. Regarding z-average, this parameter determines the average hydrodynamic diameter of particles in a solution from an autocorrelation analysis of scattered light, considering all particles in the sample. Peak mean size on the other hand represents the size of the most abundant population. Finally, ζ-potential is indicative of the particles' charge.

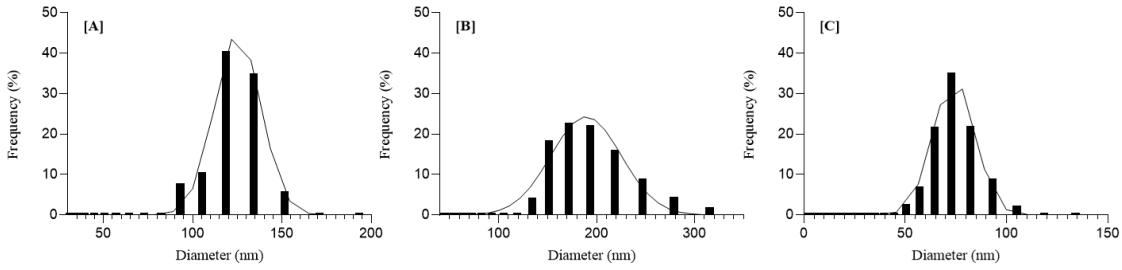


**Figure 4.23** DLS analysis of the Mesoporous Silica Nanoparticles size distribution with five measurements: **[A]** unmodified and functionalized with **[B]** Compound 5 and **[C]** TESPAI, in water.

**Table 4.3** DLS results of MSNs: **[A]** unmodified and functionalized with **[B]** Compound 5 and **[C]** TESPAI, in water.

| | Sample | Size (nm) | Z-Average (nm) | ζ-Potential (mV) | PDI |
|---|---|---|---|---|---|
| **A** | MSN | 115.4 | 594.3 | -57.06 | 0.76 |
| **B** | MSN-Compound 5-M/W | 183.3 | 382.5 | 41.68 | 0.54 |
| **C** | MSN-TESPAI | 69.7 | 143.4 | 44.34 | 0.44 |

The ζ-potential results obtained were the ones we expected. MSN have a negative charge due to their terminal silanol groups (Si-O-H) and both funcionalized MSN present a positive charge owing to the ammonium groups in their composition, also considering that the values of pH of the solutions in water were 5.18, 5.21 and 6.21 for the precursor MSNs, the MSN-TESPAI and the MSN-Compound 5, respectively.

Looking at the results we may observe that in all samples the z-average is way higher than the mean size which is indicative of a polydisperse suspension in the presence of aggregates, agglomerates or a secondary population of larger particles within the sample. These results corroborate what was verified through the TEM images, where we can observe some differences between the NPs' sizes and some aggregations as well.

As is known, smaller particles, due to their higher surface energy, are more prone to aggregate due to their attempt to lower the system's energy [83]. That is why, unmodified MSNs have higher values of hydrodynamic diameter when compared with the functionalized ones, as represented in **Table 4.3**.

It is important to mention that there are several factors that influence NPs' stability, starting with their synthesis method. For example, a complete removal of the surfactant used as a template results in more stable suspensions. Besides, there are articles proposing that the template removal technique used (calcination), could lead to less stable suspensions due to interparticle dehydration of surface silanol groups [7]. These factors could have influenced the stability and, in consequence, the z-average values obtained.

During this analysis, MSN-Compound 5 suspension was the only one that, even after long periods under vortex and sonication, seemed not to get stable. So we tried to change its original pH (pH=5.20) to a pH=4, which in photochemical experiments was determined as one the most stable pHs. This alteration visually seemed to slightly stabilize the suspension, hence the above results related to the MSN functionalized with SP are already represented at pH=4.

The figure below (**Figure 4.24**) shows the peak mean size plots of the NP functionalized with Compound 5 before and after the addition of CB7. Apparently, CB7 decrease the size dispersion in the medium, which is favourable to the system proposed.

In conclusion, the components of the system (MCH and CB7) might help stabilize the NPs. However, more studies have to be done to understand if, in the future, might be needed the addition of coatings, for example, polymers like PEG which is one of the most used polymers in DDS to improve the stability [94].

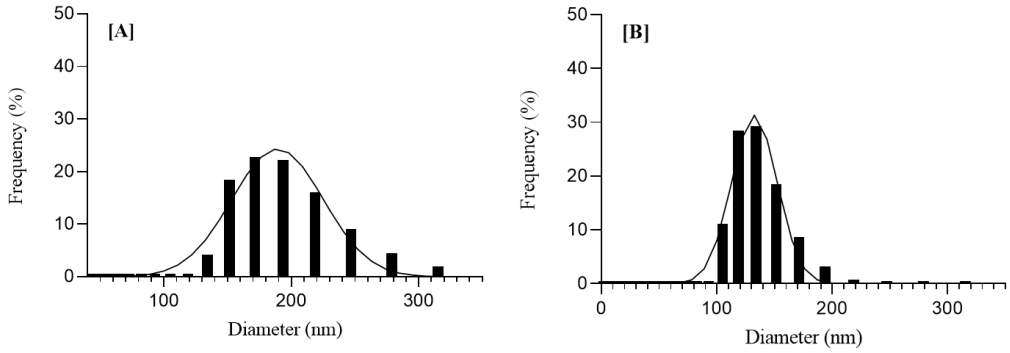


**Figure 4.24** DLS size distribution of MSN-Compound 5-M/W (**A**) before and (**B**) after the addition of 500 µL of a ≈2 mM CB7 solution, in water.

## 4.3 Spiropyran in suspension

### 4.3.1 Photochemistry of MSN-Compound 5

The image below (**Figure 4.25**) shows the UV-Vis absorption spectra of the aqueous suspensions of the hybrid material MSN-Compound 5 prepared at different pH values (1<pH<9). The changing colours correspond to the distinct forms assumed by the molecule at different pH levels, which illustrates its acid-base behaviour. As can be observed, the functionalized material has a similar behaviour to its homogenous analogue (Compound 4, **Figure 4.3**).

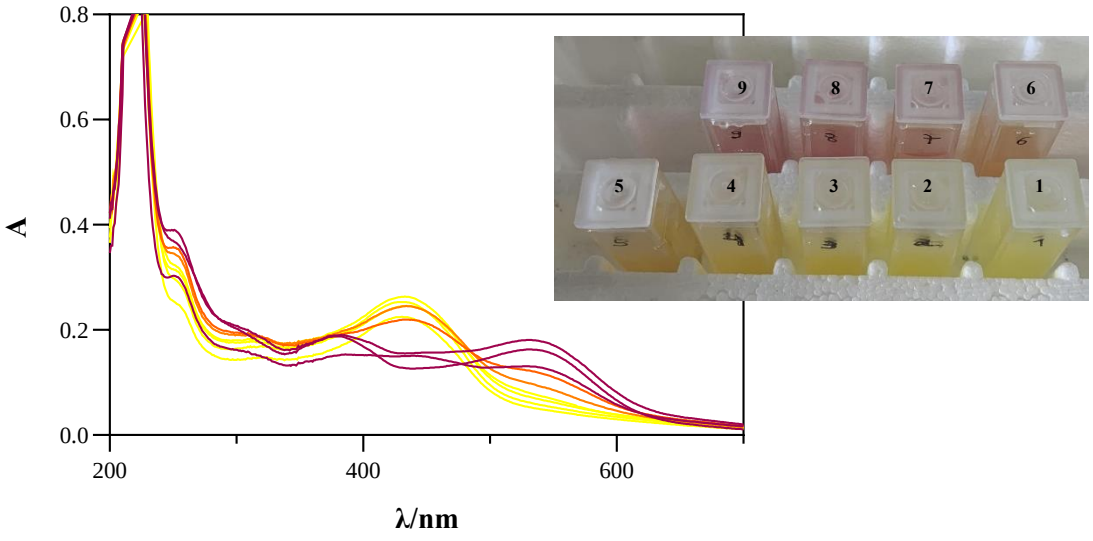


**Figure 4.25** UV-Vis spectra of MSN-Compound 5 as a function of pH at different pHs in water, from pH = 1 to pH = 9, and the progression of colours respective to the different forms that this molecule can have. The colour of each UV-Vis spectrum is represented with the corresponding coloured solution (yellow at a lower pH – higher absorbance at 420 nm – and pink/red at a higher pH – higher absorbance at 530 nm).

In the future, tests with CB7 should also be done for the MSN-Compound 5 complex to explore its potential.

### 4.3.2 Stability in a PBS suspension

A PBS pH=7.4 solution can better mimic a physiological medium like blood [95], rather than water. Therefore, suspensions with PBS at different conditions were done: **1)** 5 mg of MSN-Compound 5 in 4 mL of PBS and **2)** 2 mg of MSN-Compound 5 for 4 mL.

The suspension with the highest concentration, in its original pH (7.32), formed huge nanoclusters, and, even after long periods of vortex and sonication, the precipitation was almost instant, as represented in **Figure 4.26a**. Nevertheless, the results observed corroborate previous statements [96]. He and his colleagues reported that in a pH=7.4 PBS solution, silica NPs functionalized with SP derivatives form nanoclusters due to hydrophobic interactions. Being hydrophobic, when in aqueous solutions, they tend to aggregate to minimize the exposure to the surrounding water, resulting in nanoclusters' formation. At low pHs ($4.5<pH<5.5$), the hydrophobic SP form is converted to the hydrophilic MCH form, thus resulting in cluster dissociation (**Figure A.8**) [96], [97].

The suspension prepared with few NPs had the intention to observe if the aggregation could also be related to a saturation of the medium, and what was observed was an instant precipitation as well (**Figure 4.26b**).

In conclusion, all these results denote the importance of studies regarding the improvement of this system's stability.

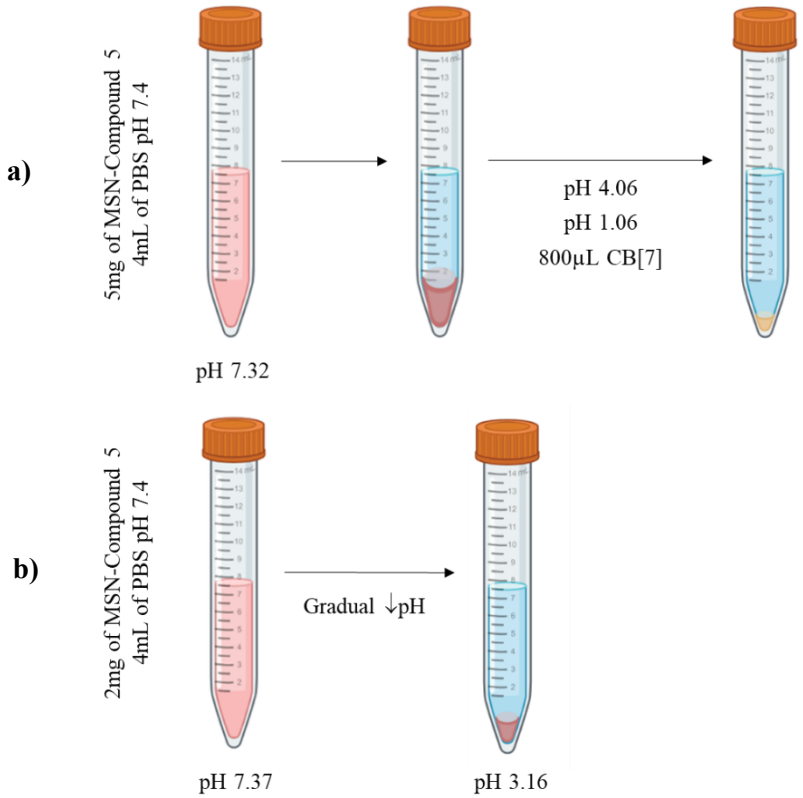


**Figure 4.26** Stability of MSN-Compound 5-M/W suspensions at different pHs, with and without CB[7]. **a)** 5 mg of MSN-Compound 5 resuspended in 4 mL of PBS pH=7.4; **b)** 2 mg of MSN-Compound 5 resuspended in 4 mL of PBS pH=7.4.

## 4.4 DNA tests with MSN-TESPAI

The reason why TESPAI was chosen for these DNA tests, instead of Compound 5, is owed to the fact that, besides being positively charged like SP, it has a less complex structure. The molecule chosen allowed us to corroborate what is already in the literature and also test CB7 influence, so, in the future, forward tests with the SPs' derivatives themselves could be done. Their positive charge makes them able to establish interactions with DNA, which is negative due to its phosphate groups ($PO_4^{3-}$).

### 4.4.1 DNA adsorption capacity

Several DNA solutions were prepared at different concentrations (10, 100, 500, 2000 and 5000 µg/mL - $C_o$) based on previous reports [69]–[72].

It is known that nucleic acids have an absorbance peak at 260 nm [71]. Taking this into account, a correlation plot (**Figure A.9**) was calculated with the absorbances at that wavelength in all DNA solutions prepared. An equation was obtained and used to calculate the concentration of the supernatant after the centrifugations ($C_f$).

To obtain the adsorption percentage, the following expression was used, as it was already used in some other articles [70].

$$Adsorption = \frac{(C0-Cf)}{C0} x100$$

The adsorption results were 69.53, 28.98 and 8.52% respectively for 100, 500 and 2000 µg/mL of DNA concentration ([DNA]). Since some articles state that per 1µg of DNA, there are 3 nmol of phosphate [98], and considering both the concentrations added and the percentages obtained, we can estimate the amount of $PO_4^{3-}$ adsorbed: 834.36, 1738.8 and 2044.8 nmol, respectively. So, although there is a decrease in the adsorption percentages, which could have suggested a saturation of the MSNs at a concentration of <100 µg/mL, that is not what is actually occurring.

Taking into account that the NPs used have 3.636 mmol of TESPAI in 1g of MSNs, according to the $^1$H NMR quantification, in the 5mg used for the suspensions are ≈18000 nmol of the molecule. So, to saturate TESPAI molecules with DNA, it would be necessary the addition of a ≈1500 µg/mL solution, maintaining 4 mL of solution added.

Moreover, nanoparticles pores' diameter can influence DNA adsorption. It was reported that pores greater than 5.4 nm promote a higher DNA adsorption as the molecules could likely enter the pores without significant intermolecular interactions [99]. In general, larger pores can adsorb a higher amount of DNA [72].

### 4.4.2 DLS analysis

As gene therapy has emerged as a promising treatment for several diseases, DLS tests were performed to give suggestions about a future integration of this type of system in gene therapy strategies or even conjugated therapies. Tests were done to observe if the DNA adsorbed or not onto the NPs and if the addition of CB7 could create competition with DNA allowing its release.

DLS analysis results are represented in **Table 4.4**, where ζ-potential values demonstrate that the adsorption does happen, due to a decrease of mV.

As mentioned, we considered the possibility of CB7 to compete with DNA. However, looking at **Table 4.4** CB7 results, there is no significant effect of the macromolecule in DNA, at least resorting to the method used. In fact, during the preparation of the suspensions, they should have been washed to remove the extra DNA that could be influencing the ζ-potential detected by the DLS equipment. Performing the washes we might be able to obtain the results of just the molecules attached.

**Table 4.4** DLS results onto MSN-TESPAI with DNA after agitation (a.a) and after washes (a.w) before and after the addition of the 500 µL of CB7.

| | **Size (nm)** | **Z-average (nm)** | **ζ-Potential (mV)** | **PDI** |
|---|---|---|---|---|
| MSN-TESPAI | 69.7 | 143.4 | **44.34** | 0.44 |
| With DNA a.a | 563.7 | 4567.4 | **-4.84** | 0.85 |
| With DNA a.w | 2815.5 | 3586.9 | - | 0.35 |
| With 500 µL CB7 | 2908.0 | 3120.0 | -2.32 | 0.45 |

An analysis that could also be done in the future, to take conclusions about CB7 potential in gene therapy, is the preparation of a few batches with the same amount of particles and DNA for different volumes of CB7. Finally, it could also be interesting to verify the adsorption capacity of DNA onto CB7 complexed MSNs, to see if the DNA can be adsorbed even in the presence of CB7 onto the surface.

Even though CB7 might not be able to provide DNA release by competition, the isomeric switching properties of SP derivatives are reported to possess dramatically different DNA-binding properties, enabling photoswitched DNA binding. The article showed that the closed form of SP derivates has no interaction with DNA. However, after UV exposure, SP chromene opens and the molecule becomes able to bind to DNA by intercalation. As the SP structure switching is reversible also is DNA binding affinity, in this case [100].

# 5. CONCLUSIONS

In this work, MSNs based on SP derivatives (MSN-Compound 5-M/W and MSN-Compound 5-Reflux) and ammonium groups (MSN-TESPAI) were prepared and characterized, and their interactions with CB7 studied, with the aim of building a new photoswitchable drug delivery system in the future.

Irradiation and thermal recovery tests proved SP's capacity to be included in a reversible system that rapidly returns to its initial structure. Since the acid-base behaviour of the SP model molecule (Compound 4) remains when complexed with the MSNs (MSN-Compound 5), it might suggest that the verified reversible properties may remain as well. SP acid-base behaviour in solution and suspension was accessed at different pHs, where MCH form predominates at pH=4 and the $pK_a$ is around 7, which can be used in favour of some physiological mediums. Stability and degradability tests showed that SP's derivatives seemed to remain stable in methanol, which, in the future, can be used as a stock solvent.

In addition to its capability of enabling controlled release, we also hypothesized its role in gene therapy, using a model cationic molecule, in this case, TESPAI.

All materials were extensively characterized through several techniques, including FTIR, $^1$H NMR, Nitrogen adsorption, Elemental analysis, XRD and TGA to prove the successful preparations. Regarding DLS results, those showed that, when in suspension with MSNs, the MSN-SP complex barely remains stable, in PBS and water, although CB7 and a pH=4 appear to help. ITC tests made it possible to verify that SP-CB7 complex have a $K_A$ of $1.445 \times 10^7$ $M^{-1}$ at pH=4.2 and in the range of $10^5$ for pH=7.5. The synthesis and functionalizations prepared were a success, where we obtained loadings of ≈0.55 and ≈3.6 mmol/g for MSN-Compound 5 and MSN-TESPAI, respectively. In particular to the MSN-Compound 5, we developed a greener method for MSN functionalization with SPs, using microwave-assited heating instead of heating under reflux.

TEM images showed sizes of 62.22 ± 16.02nm for the starting MSNs. Regarding the modified MSNs, the ones with TESPAI measure 64.27 ± 13.61nm while the ones with Compound 5 have 66.17 ± 14.57 and 68.57 ± 14.24nm (M/W and reflux, respectively).

In conclusion, although its potential, in the future further testing should be done and more improvements should be considered and analysed.

# BIBLIOGRAPHY


[1] M. Kester, K. D. Karpa, and K. E. Vrana, "Pharmacokinetics," in *Elsevier's Integrated Review Pharmacology*, Elsevier, 2012, pp. 1–15. doi: 10.1016/B978-0-323-07445-2.00001-X.

[2] M. W. Tibbitt, J. E. Dahlman, and R. Langer, "Emerging Frontiers in Drug Delivery," *J Am Chem Soc*, vol. 138, no. 3, pp. 704–717, Jan. 2016, doi: 10.1021/jacs.5b09974.

[3] M. Nasrollahzadeh, S. M. Sajadi, M. Sajjadi, and Z. Issaabadi, "An Introduction to Nanotechnology," 2019, pp. 1–27. doi: 10.1016/B978-0-12-813586-0.00001-8.

[4] R. R. Castillo, L. de la Torre, F. García-Ochoa, M. Ladero, and M. Vallet-Regí, "Production of MCM-41 Nanoparticles with Control of Particle Size and Structural Properties: Optimizing Operational Conditions during Scale-Up," *Int J Mol Sci*, vol. 21, no. 21, p. 7899, Oct. 2020, doi: 10.3390/ijms21217899.

[5] M. Bouchoucha, M.-F. Côté, R. C.-Gaudreault, M.-A. Fortin, and F. Kleitz, "Size-Controlled Functionalized Mesoporous Silica Nanoparticles for Tunable Drug Release and Enhanced Anti-Tumoral Activity," *Chemistry of Materials*, vol. 28, no. 12, pp. 4243–4258, Jun. 2016, doi: 10.1021/acs.chemmater.6b00877.

[6] L. Pan, Q. He, J. Liu, Y. Chen, M. Ma, L. Zhang, and J. Shi, "Nuclear-Targeted Drug Delivery of TAT Peptide-Conjugated Monodisperse Mesoporous Silica Nanoparticles," *J Am Chem Soc*, vol. 134, no. 13, pp. 5722–5725, Apr. 2012, doi: 10.1021/ja211035w.

[7] F. Lu, S.-H. Wu, Y. Hung, and C.-Y. Mou, "Size Effect on Cell Uptake in Well-Suspended, Uniform Mesoporous Silica Nanoparticles," *Small*, vol. 5, no. 12, pp. 1408–1413, Jun. 2009, doi: 10.1002/smll.200900005.

[8] Q. Gan, D. Dai, Y. Yuan, J. Qian, S. Sha, J. Shi, C. Liu*et*, "Effect of size on the cellular endocytosis and controlled release of mesoporous silica nanoparticles for intracellular delivery," *Biomed Microdevices*, vol. 14, no. 2, pp. 259–270, Apr. 2012, doi: 10.1007/s10544-011-9604-9.

[9] H. L. Kim, S. B. Lee, H. J. Jeong, and D. W. Kim, "Enhanced tumor targetability of PEGylated mesoporous silica nanoparticles on in vivo optical imaging according to their size," *RSC Adv.*, vol. 4, no. 59, pp. 31318–31322, 2014, doi: 10.1039/C4RA03905J.

[10] A. Yusuf, A. R. Z. Almotairy, H. Henidi, O. Y. Alshehri, and M. S. Aldughaim, "Nanoparticles as Drug Delivery Systems: A Review of the Implication of Nanoparticles' Physicochemical Properties on Responses in Biological Systems," *Polymers (Basel)*, vol. 15, no. 7, p. 1596, Mar. 2023, doi: 10.3390/polym15071596.

[11] M. J. Mitchell, M. M. Billingsley, R. M. Haley, M. E. Wechsler, N. A. Peppas, and R. Langer, "Engineering precision nanoparticles for drug delivery," *Nat Rev Drug Discov*, vol. 20, no. 2, pp. 101–124, Feb. 2021, doi: 10.1038/s41573-020-0090-8.

[12] L. R. Volpatti, M. A. Matranga, A. B. Cortinas, D. Delcassian, K. B. Daniel, R. Langer, D. G. Anderson, "Glucose-Responsive Nanoparticles for Rapid and Extended Self-Regulated Insulin Delivery," *ACS Nano*, vol. 14, no. 1, pp. 488–497, Jan. 2020, doi: 10.1021/acsnano.9b06395.

[13] A. Geraili, M. Xing, and K. Mequanint, “Design and fabrication of drug-delivery systems toward adjustable release profiles for personalized treatment,” *VIEW*, vol. 2, no. 5, Oct. 2021, doi: 10.1002/VIW.20200126.

[14] P. Mi, “Stimuli-responsive nanocarriers for drug delivery, tumor imaging, therapy and theranostics,” *Theranostics*, vol. 10, no. 10, pp. 4557–4588, 2020, doi: 10.7150/thno.38069.

[15] Z. Li, N. Song, and Y.-W. Yang, “Stimuli-Responsive Drug-Delivery Systems Based on Supramolecular Nanovalves,” *Matter*, vol. 1, no. 2, pp. 345–368, Aug. 2019, doi: 10.1016/j.matt.2019.05.019.

[16] S. Anu Mary Ealia and M. P. Saravanakumar, “A review on the classification, characterisation, synthesis of nanoparticles and their application,” *IOP Conf Ser Mater Sci Eng*, vol. 263, p. 032019, Nov. 2017, doi: 10.1088/1757-899X/263/3/032019.

[17] W. Paul and C. P. Sharma, “Inorganic nanoparticles for targeted drug delivery,” in *Biointegration of Medical Implant Materials*, Elsevier, 2020, pp. 333–373. doi: 10.1016/B978-0-08-102680-9.00013-5.

[18] J. Liu and X. Du, “pH- and competitor-driven nanovalves of cucurbit[7]uril pseudorotaxanes based on mesoporous silica supports for controlled release,” *J Mater Chem*, vol. 20, no. 18, p. 3642, 2010, doi: 10.1039/b915510d.

[19] P. Kazemzadeh, K. Sayadi, A. Toolabi, J. Sayadi, M. Zeraati, N. P. S. Chauhan, G. Sargazi, “Structure-Property Relationship for Different Mesoporous Silica Nanoparticles and its Drug Delivery Applications: A Review,” *Front Chem*, vol. 10, Mar. 2022, doi: 10.3389/fchem.2022.823785.

[20] A. Popat, S. B. Hartono, F. Stahr, J. Liu, S. Z. Qiao, and G. Qing (Max) Lu, “Mesoporous silica nanoparticles for bioadsorption, enzyme immobilisation, and delivery carriers,” *Nanoscale*, vol. 3, no. 7, p. 2801, 2011, doi: 10.1039/c1nr10224a.

[21] S. N. Harun, H. Ahmad, H. N. Lim, S. L. Chia, and M. R. Gill, “Synthesis and Optimization of Mesoporous Silica Nanoparticles for Ruthenium Polypyridyl Drug Delivery,” *Pharmaceutics*, vol. 13, no. 2, p. 150, Jan. 2021, doi: 10.3390/pharmaceutics13020150.

[22] Y. Wang, Q. Zhao, N. Han, L. Bai, J. Li, J. Liu, E. Che, L. Hu, Q. Zhang, T. Jiang, S. Wang, “Mesoporous silica nanoparticles in drug delivery and biomedical applications,” *Nanomedicine*, vol. 11, no. 2, pp. 313–327, Feb. 2015, doi: 10.1016/j.nano.2014.09.014.

[23] Y. Zhang, J. Wang, X. Bai, T. Jiang, Q. Zhang, and S. Wang, “Mesoporous Silica Nanoparticles for Increasing the Oral Bioavailability and Permeation of Poorly Water Soluble Drugs,” *Mol Pharm*, vol. 9, no. 3, pp. 505–513, Mar. 2012, doi: 10.1021/mp200287c.

[24] Y. Zhou, G. Quan, Q. Wu, X. Zhang, B. Niu, B. Wu, Y. Huang, X. Pan, C. Wu, “Mesoporous silica nanoparticles for drug and gene delivery,” *Acta Pharm Sin B*, vol. 8, no. 2, pp. 165–177, Mar. 2018, doi: 10.1016/j.apsb.2018.01.007.

[25] Q. Qu, G. Zhou, Y. Ding, S. Feng, and Z. Gu, “Adjustment of the morphology of MCM-41 silica in basic solution,” *J Non Cryst Solids*, vol. 405, pp. 104–115, Dec. 2014, doi: 10.1016/j.jnoncrysol.2014.09.012.

[26] G. Martínez-Edo, A. Balmori, I. Pontón, A. Martí del Rio, and D. Sánchez-García, "Functionalized Ordered Mesoporous Silicas (MCM-41): Synthesis and Applications in Catalysis," *Catalysts*, vol. 8, no. 12, p. 617, Dec. 2018, doi: 10.3390/catal8120617.

[27] Z. Li, A. J. González, V. B. Heeralal, and D.-Y. Wang, "Covalent assembly of MCM-41 nanospheres on graphene oxide for improving fire retardancy and mechanical property of epoxy resin," *Compos B Eng*, vol. 138, pp. 101–112, Apr. 2018, doi: 10.1016/j.compositesb.2017.11.001.

[28] J. Xu, Z. Luan, H. He, W. Zhou, and L. Kevan, "A Reliable Synthesis of Cubic Mesoporous MCM-48 Molecular Sieve," *Chemistry of Materials*, vol. 10, no. 11, pp. 3690–3698, Nov. 1998, doi: 10.1021/cm980440d.

[29] M. Vallet-Regi, A. Rámila, R. P. del Real, and J. Pérez-Pariente, "A New Property of MCM-41: Drug Delivery System," *Chemistry of Materials*, vol. 13, no. 2, pp. 308–311, Feb. 2001, doi: 10.1021/cm0011559.

[30] J. S. Beck, J. C. Vartuli, W. J. Roth, M. E. Leonowicz, C. T. Kresge, K. D. Schmitt, C. T. W. Chu, D. H. Olson, E. W. Sheppard, S. B. McCullen, J. B. Higgins, and J. L. Schlenker, "A new family of mesoporous molecular sieves prepared with liquid crystal templates," *J Am Chem Soc*, vol. 114, no. 27, pp. 10834–10843, Dec. 1992, doi: 10.1021/ja00053a020.

[31] E. Valiey, M. G. Dekamin, and Z. Alirezvani, "Sulfamic acid pyromellitic diamide-functionalized MCM-41 as a multifunctional hybrid catalyst for melting-assisted solvent-free synthesis of bioactive 3,4-dihydropyrimidin-2-(1H)-ones," *Sci Rep*, vol. 11, no. 1, p. 11199, May 2021, doi: 10.1038/s41598-021-89572-y.

[32] G. J. Owens, R. K. Singh, F. Foroutan, M. Alqaysi, C-M Han, C. Mahapatra, H-W Kim, J. C. Knowles, "Sol–gel based materials for biomedical applications," *Prog Mater Sci*, vol. 77, pp. 1–79, Apr. 2016, doi: 10.1016/j.pmatsci.2015.12.001.

[33] H. Ghaedi and M. Zhao, "Review on Template Removal Techniques for Synthesis of Mesoporous Silica Materials," *Energy & Fuels*, vol. 36, no. 5, pp. 2424–2446, Mar. 2022, doi: 10.1021/acs.energyfuels.1c04435.

[34] T. T. Hoang Thi, V. Du Cao, T. N. Q. Nguyen, D. T. Hoang, V. C. Ngo, and D. H. Nguyen, "Functionalized mesoporous silica nanoparticles and biomedical applications," *Materials Science and Engineering: C*, vol. 99, pp. 631–656, Jun. 2019, doi: 10.1016/j.msec.2019.01.129.

[35] U. Wiedemann, W. Alt, and D. Meschede, "Switching photochromic molecules adsorbed on optical microfibres," *Opt Express*, vol. 20, no. 12, p. 12710, Jun. 2012, doi: 10.1364/OE.20.012710.

[36] H. Dürr and H. Bouas-Laurent, *Photochromism: Molecules and Systems*, vol. 116. 2005. doi: 10.1016/j.ijleo.2005.01.001.

[37] B. S. Lukyanov and M. B. Lukyanova, "Spiropyrans: Synthesis, Properties, and Application. (Review)," *Chem Heterocycl Compd (N Y)*, vol. 41, no. 3, pp. 281–311, Mar. 2005, doi: 10.1007/s10593-005-0148-x.

[38] I. V. Ozhogin, A. D. Pugachev, N. I. Makarova, A. A. Belanova, A. S. Kozlenko, I. A. Rostovtseva, P. V. Zolotukhin, O. P. Demidov, I. M. El-Sewify, G. S. Borodkin, A. V. Metelitsa, B. S. Lukyanov, "Novel Indoline Spiropyrans Based on Human Hormones β-Estradiol and Estrone: Synthesis, Structure, Chromogenic and Cytotoxic Properties," *Molecules*, vol. 28, no. 9, p. 3866, May 2023, doi: 10.3390/molecules28093866.

[39] S. Heng, M.-C. Nguyen, R. Kostecki, T. M. Monro, and A. D. Abell, “Nanoliter-scale, regenerable ion sensor: sensing with a surface functionalized microstructured optical fibre,” *RSC Adv*, vol. 3, no. 22, p. 8308, 2013, doi: 10.1039/c3ra40321a.

[40] R. Klajn, “Spiropyran-based dynamic materials,” *Chem. Soc. Rev.*, vol. 43, no. 1, pp. 148–184, 2014, doi: 10.1039/C3CS60181A.

[41] T. Halbritter, C. Kaiser, J. Wachtveitl, and A. Heckel, “Pyridine–Spiropyran Derivative as a Persistent, Reversible Photoacid in Water,” *J Org Chem*, vol. 82, no. 15, pp. 8040–8047, Aug. 2017, doi: 10.1021/acs.joc.7b01268.

[42] L. Wimberger, S. K. K. Prasad, M. D. Peeks, J. Andréasson, T. W. Schmidt, and J. E. Beves, “Large, Tunable, and Reversible pH Changes by Merocyanine Photoacids,” *J Am Chem Soc*, vol. 143, no. 49, pp. 20758–20768, Dec. 2021, doi: 10.1021/jacs.1c08810.

[43] Z. Miskolczy and L. Biczók, “Selective Acceleration of the Protonated Merocyanine-Spiropyran Photochromic Transformation by Inclusion in Cucurbit[7]uril,” *Photochem Photobiol*, vol. 88, no. 6, pp. 1461–1466, Nov. 2012, doi: 10.1111/j.1751-1097.2012.01183.x.

[44] T. D. Nguyen, Y. Liu, S. Saha, K. C.-F. Leung, J. F. Stoddart, and J. I. Zink, “Design and Optimization of Molecular Nanovalves Based on Redox-Switchable Bistable Rotaxanes,” *J Am Chem Soc*, vol. 129, no. 3, pp. 626–634, Jan. 2007, doi: 10.1021/ja065485r.

[45] J. Lagona, P. Mukhopadhyay, S. Chakrabarti, and L. Isaacs, “The Cucurbit[n]uril Family,” *Angewandte Chemie International Edition*, vol. 44, no. 31, pp. 4844–4870, Aug. 2005, doi: 10.1002/anie.200460675.

[46] W. A. Freeman, W. L. Mock, and N. Y. Shih, “Cucurbituril,” *J Am Chem Soc*, vol. 103, no. 24, pp. 7367–7368, Dec. 1981, doi: 10.1021/ja00414a070.

[47] H. Tang, D. Fuentealba, Y. H. Ko, N. Selvapalam, K. Kim, and C. Bohne, “Guest Binding Dynamics with Cucurbit[7]uril in the Presence of Cations,” *J Am Chem Soc*, vol. 133, no. 50, pp. 20623–20633, Dec. 2011, doi: 10.1021/ja209266x.

[48] X. Du, X. Liu, H. Su, X. Cheng, L. Li, H. Gu, X. Xing, D. Qiu, H. Hao, “A simple AIEgen photosensitizer with cucurbit[7]uril selective detection amantadine and application in mitochondrion imaging,” *Microchemical Journal*, vol. 182, p. 107942, Nov. 2022, doi: 10.1016/j.microc.2022.107942.

[49] D. Das, K. I. Assaf, and W. M. Nau, “Applications of Cucurbiturils in Medicinal Chemistry and Chemical Biology,” *Front Chem*, vol. 7, Sep. 2019, doi: 10.3389/fchem.2019.00619.

[50] L. Cao, M. Šekutor, P. Y. Zavalij, K. Mlinarić-Majerski, R. Glaser, and L. Isaacs, “Cucurbit[7]uril·Guest Pair with an Attomolar Dissociation Constant,” *Angewandte Chemie International Edition*, vol. 53, no. 4, pp. 988–993, Jan. 2014, doi: 10.1002/anie.201309635.

[51] A. L. Koner and W. M. Nau, “Cucurbituril Encapsulation of Fluorescent Dyes,” *Supramol Chem*, vol. 19, no. 1–2, pp. 55–66, Mar. 2007, doi: 10.1080/10610270600910749.

[52] K. I. Assaf, M. Florea, J. Antony, N. M. Henriksen, J. Yin, A. Hansen, Z-W Qu, R. Sure, D. Klapstein, M. K. Gilson, S. Grimme, W. M. Nau, “HYDROPHOBE Challenge: A Joint Experimental and Computational Study on the Host–Guest Binding of Hydrocarbons to Cucurbiturils, Allowing Explicit Evaluation of Guest Hydration Free-Energy

Contributions," *J Phys Chem B*, vol. 121, no. 49, pp. 11144–11162, Dec. 2017, doi: 10.1021/acs.jpcb.7b09175.

[53] H. Tang, D. Fuentealba, Y. H. Ko, N. Selvapalam, K. Kim, and C. Bohne, "Guest Binding Dynamics with Cucurbit[7]uril in the Presence of Cations," *J Am Chem Soc*, vol. 133, no. 50, pp. 20623–20633, Dec. 2011, doi: 10.1021/ja209266x.

[54] L. Qi, R. Wang, and H.-Z. Yu, "Supramolecular Cucurbit[7]uril@Ferrocene Complexation on Surface: From Nanostructure Differentiation to Guest Quantitation," *Acc Mater Res*, vol. 4, no. 5, pp. 457–466, May 2023, doi: 10.1021/accountsmr.3c00025.

[55] J. W. Lee, S. Samal, N. Selvapalam, H.-J. Kim, and K. Kim, "Cucurbituril Homologues and Derivatives: New Opportunities in Supramolecular Chemistry," *Acc Chem Res*, vol. 36, no. 8, pp. 621–630, Aug. 2003, doi: 10.1021/ar020254k.

[56] D. Shetty, J. K. Khedkar, K. M. Park, and K. Kim, "Can we beat the biotin–avidin pair?: cucurbit[7]uril-based ultrahigh affinity host–guest complexes and their applications," *Chem Soc Rev*, vol. 44, no. 23, pp. 8747–8761, 2015, doi: 10.1039/C5CS00631G.

[57] N. M. Green, "Avidin," 1975, pp. 85–133. doi: 10.1016/S0065-3233(08)60411-8.

[58] I. J. General, R. Dragomirova, and H. Meirovitch, "Absolute Free Energy of Binding of Avidin/Biotin, Revisited," *J Phys Chem B*, vol. 116, no. 23, pp. 6628–6636, Jun. 2012, doi: 10.1021/jp212276m.

[59] F. Biedermann, V. D. Uzunova, O. A. Scherman, W. M. Nau, and A. De Simone, "Release of High-Energy Water as an Essential Driving Force for the High-Affinity Binding of Cucurbit[ *n* ]urils," *J Am Chem Soc*, vol. 134, no. 37, pp. 15318–15323, Sep. 2012, doi: 10.1021/ja303309e.

[60] H. Lambert, Y.-W. Zhang, and T.-C. Lee, "Supramolecular Catalysis of *m* -Xylene Isomerization by Cucurbiturils: Transition State Stabilization, Vibrational Coupling, and Dynamic Binding Equilibrium," *The Journal of Physical Chemistry C*, vol. 124, no. 21, pp. 11469–11479, May 2020, doi: 10.1021/acs.jpcc.0c02012.

[61] W. Ong and A. E. Kaifer, "Salt Effects on the Apparent Stability of the Cucurbit[7]uril-Methyl Viologen Inclusion Complex SCHEME 1. Formation of a 1:1 Inclusion Complex between Host CB7 and Guest MV 2+," *Proc. Natl. Acad. Sci. U.S.A*, vol. 66, no. 4, pp. 1383–1385, 2001, doi: 10.1021/jo035030.

[62] A. R. Sharma, Y.-H. Lee, A. Bat-Ulzii, M. Bhattacharya, C. Chakraborty, and S.-S. Lee, "Recent advances of metal-based nanoparticles in nucleic acid delivery for therapeutic applications," *J Nanobiotechnology*, vol. 20, no. 1, p. 501, Nov. 2022, doi: 10.1186/s12951-022-01650-z.

[63] B. B. Mendes, J. Conniot, A. Avital, D. Yao, X. Jiang, X. Zhou, N. Sharf-Pauker, Y. Xiao, O. Adir, H. Liang, J. Shi, A. Schroeder, J. Conde, "Nanodelivery of nucleic acids," *Nature Reviews Methods Primers*, vol. 2, no. 1, p. 24, Apr. 2022, doi: 10.1038/s43586-022-00104-y.

[64] M. S. Al-Dosari and X. Gao, "Nonviral Gene Delivery: Principle, Limitations, and Recent Progress," *AAPS J*, vol. 11, no. 4, p. 671, Dec. 2009, doi: 10.1208/s12248-009-9143-y.

[65] S. T. Eberhart, A. Hatzis, and R. Rothchild, "Quantitative NMR assay for aspirin, phenacetin, and caffeine mixtures with 1,3,5-trioxane as internal standard," *J Pharm Biomed Anal*, vol. 4, no. 2, pp. 147–154, Jan. 1986, doi: 10.1016/0731-7085(86)80036-X.

[66] Carla Nunes, Anabela Valente, Martyn Pillinger, and Isabel Gonçalves, "Síntese e análise estrutural de um suporte mesoporoso: MCM — 41," *Boletim da Sociedade Portuguesa de Química*, p. 73, Jun. 2002, doi: 10.52590/M3.P610.A30001059.

[67] A. P. Thomas, L. Palanikumar, M. T. Jeena, K. Kim, and J.-H. Ryu, "Cancer-mitochondria-targeted photodynamic therapy with supramolecular assembly of HA and a water soluble NIR cyanine dye," *Chem Sci*, vol. 8, no. 12, pp. 8351–8356, 2017, doi: 10.1039/C7SC03169F.

[68] N. and S. V. Rad, "A Light-Gated Molecular Shuttle With Catalyzing, Reacting and Regulatory Functions," *The Royal Society of Chemistry*, 2022.

[69] Y. Li, M. Hei, Y. Xu, X. Qian, and W. Zhu, "Ammonium salt modified mesoporous silica nanoparticles for dual intracellular-responsive gene delivery," *Int J Pharm*, vol. 511, no. 2, pp. 689–702, Sep. 2016, doi: 10.1016/j.ijpharm.2016.07.029.

[70] J. Xu, D. Chen, Y. Yang, H. Gong, W. Gao, and H. Xiao, "A one step method for isolation of genomic DNA using multi-amino modified magnetic nanoparticles," *RSC Adv*, vol. 11, no. 6, pp. 3324–3332, 2021, doi: 10.1039/D0RA09409A.

[71] A. G. Pershina, A. E. Sazonov, and L. M. Ogorodova, "Investigation of the interaction between DNA and cobalt ferrite nanoparticles by FTIR spectroscopy," *Russ J Bioorg Chem*, vol. 35, no. 5, pp. 607–613, Sep. 2009, doi: 10.1134/S1068162009050112.

[72] X. Li, J. Zhang, and H. Gu, "Study on the Adsorption Mechanism of DNA with Mesoporous Silica Nanoparticles in Aqueous Solution," *Langmuir*, vol. 28, no. 5, pp. 2827–2834, Feb. 2012, doi: 10.1021/la204443j.

[73] P. L. Kastritis and A. M. J. J. Bonvin, "On the binding affinity of macromolecular interactions: daring to ask why proteins interact," *J R Soc Interface*, vol. 10, no. 79, p. 20120835, Feb. 2013, doi: 10.1098/rsif.2012.0835.

[74] S. A. Ahmed and D. Seth, "Thermodynamic analysis of binding of benzimidazole derivative with cucurbit[7]uril: A isothermal titration calorimetry study," *J Mol Liq*, vol. 254, pp. 70–75, Mar. 2018, doi: 10.1016/j.molliq.2018.01.082.

[75] K. I. Assaf and W. M. Nau, "Cucurbiturils: from synthesis to high-affinity binding and catalysis," *Chem Soc Rev*, vol. 44, no. 2, pp. 394–418, 2015, doi: 10.1039/C4CS00273C.

[76] A. Schön, N. Madani, A. B. Smith, J. M. Lalonde, and E. Freire, "Some Binding-Related Drug Properties are Dependent on Thermodynamic Signature," *Chem Biol Drug Des*, vol. 77, no. 3, pp. 161–165, Mar. 2011, doi: 10.1111/j.1747-0285.2010.01075.x.

[77] G. Anbalagan, A. R. Prabakaran, and S. Gunasekaran, "Spectroscopic characterization of indian standard sand," *J Appl Spectrosc*, vol. 77, no. 1, pp. 86–94, Mar. 2010, doi: 10.1007/s10812-010-9297-5.

[78] D. Lin-Vien, N. B. Colthup, W. G. Fateley, and J. G. Grasselli, "Alkanes," in *The Handbook of Infrared and Raman Characteristic Frequencies of Organic Molecules*, Elsevier, 1991, pp. 9–28. doi: 10.1016/B978-0-08-057116-4.50008-0.

[79] M. Hamidinasab, M. A. Bodaghifard, and A. Mobinikhaledi, "Green synthesis of 1H-pyrazolo[1,2-b]phthalazine-2- carbonitrile derivatives using a new bifunctional base–ionic liquid hybrid magnetic nanocatalyst," *Appl Organomet Chem*, vol. 34, no. 2, Feb. 2020, doi: 10.1002/aoc.5386.

[80] C. I. C. Crucho, C. Baleizão, and J. P. S. Farinha, "Functional Group Coverage and Conversion Quantification in Nanostructured Silica by $^{1}$ H NMR," *Anal Chem*, vol. 89, no. 1, pp. 681–687, Jan. 2017, doi: 10.1021/acs.analchem.6b03117.

[81] D. Adam, "Out of the kitchen," *Nature*, vol. 421, no. 6923, pp. 571–572, Feb. 2003, doi: 10.1038/421571a.

[82] F. Rouquerol, J. Rouquerol and K. Sing, "Adsorption by Powders and Porous Solids Principles, Methodology and Applications." *Academic Press*, pp. 1-26, 1999. https://doi.org/10.1016/B978-012598920-6/50002-6.

[83] A. Forte, S. Gago, M. R. Carrot, P. Carrot, C. Alves, F. Teodoro, R. Pedrosa, I.M. Marrucho and L. C. Branco, "Mesoporous silica nanoparticles with manganese and lanthanide salts: synthesis, characterization and cytotoxicity studies," *Dalton Transactions*, vol. 50, no. 24, pp. 8588–8599, 2021, doi: 10.1039/D1DT00605C.

[84] P. B. Raja, K. R. Munusamy, V. Perumal, and M. N. M. Ibrahim, "Characterization of nanomaterial used in nanobioremediation," in *Nano-Bioremediation : Fundamentals and Applications*, Elsevier, 2022, pp. 57–83. doi: 10.1016/B978-0-12-823962-9.00037-4.

[85] L. Filipe, T. de Sousa, D. Silva, M.M. Santos, M.R. Carrot, P. Poeta, L.C. Branco and S. Gago, "In Vitro Antimicrobial Studies of Mesoporous Silica Nanoparticles Comprising Anionic Ciprofloxacin Ionic Liquids and Organic Salts," *Pharmaceutics*, vol. 15, no. 7, p. 1934, Jul. 2023, doi: 10.3390/pharmaceutics15071934.

[86] K. R. Rajisha, B. Deepa, L. A. Pothan, and S. Thomas, "Thermomechanical and spectroscopic characterization of natural fibre composites," in *Interface Engineering of Natural Fibre Composites for Maximum Performance*, Elsevier, 2011, pp. 241–274. doi: 10.1533/9780857092281.2.241.

[87] F. Kunc, V. Balhara, Y. Sun, M. Daroszewska, Z. J. Jakubek, M. Hill, A. Brinkmann and L. J. Johnston, "Quantification of surface functional groups on silica nanoparticles: comparison of thermogravimetric analysis and quantitative NMR," *Analyst*, vol. 144, no. 18, pp. 5589–5599, 2019, doi: 10.1039/C9AN01080G.

[88] F. Kunc, M. Gallerneault, O. Kodra, A. Brinkmann, G. P. Lopinski, and L. J. Johnston, "Surface chemistry of metal oxide nanoparticles: NMR and TGA quantification," *Anal Bioanal Chem*, vol. 414, no. 15, pp. 4409–4425, Jun. 2022, doi: 10.1007/s00216-022-03906-x.

[89] C. Das, N. N. Ghosh, V. Pulhani, G. Biswas, and P. Singhal, "Bio-functionalized magnetic nanoparticles for cost-effective adsorption of U( <scp>vi</scp> ): experimental and theoretical investigation," *RSC Adv*, vol. 13, no. 22, pp. 15015–15023, 2023, doi: 10.1039/D3RA00799E.

[90] V. Nairi, S. Medda, M. Piludu, M. F. Casula, M. Vallet-Regì, M. Monduzzi and A. Salis, "Interactions between bovine serum albumin and mesoporous silica nanoparticles functionalized with biopolymers," *Chemical Engineering Journal*, vol. 340, pp. 42–50, May 2018, doi: 10.1016/j.cej.2018.01.011.

[91] V. Ayala, A. P. Herrera, M. Latorre-Esteves, M. Torres-Lugo, and C. Rinaldi, "Effect of surface charge on the colloidal stability and in vitro uptake of carboxymethyl dextran-coated iron oxide nanoparticles," *Journal of Nanoparticle Research*, vol. 15, no. 8, p. 1874, Aug. 2013, doi: 10.1007/s11051-013-1874-0.

[92] F. Babick, “Dynamic light scattering (DLS),” in *Characterization of Nanoparticles*, Elsevier, 2020, pp. 137–172. doi: 10.1016/B978-0-12-814182-3.00010-9.

[93] P. S. Popovetskiy and A. N. Kolodin, “Hydrodynamic Diameter of Silver Nanoparticles in Solutions of Nonionic Surfactants,” *Russian Journal of Physical Chemistry A*, vol. 94, no. 10, pp. 2126–2134, Oct. 2020, doi: 10.1134/S0036024420100246.

[94] J. V Jokerst, T. Lobovkina, R. N. Zare, and S. S. Gambhir, “Nanoparticle PEGylation for imaging and therapy,” *Nanomedicine*, vol. 6, no. 4, pp. 715–728, Jun. 2011, doi: 10.2217/nnm.11.19.

[95] I. Neri, S. Laneri, R. Di Lorenzo, I. Dini, G. Russo, and L. Grumetto, “Parabens Permeation through Biological Membranes: A Comparative Study Using Franz Cell Diffusion System and Biomimetic Liquid Chromatography,” *Molecules*, vol. 27, no. 13, p. 4263, Jul. 2022, doi: 10.3390/molecules27134263.

[96] Y. He, L. Shao, I. Usman, Y. Hu, A. Pan, S. Lianga and H. Xu, “A pH-responsive dissociable mesoporous silica-based nanoplatform enabling efficient dual-drug co-delivery and rapid clearance for cancer therapy,” *Biomater Sci*, vol. 8, no. 12, pp. 3418–3429, 2020, doi: 10.1039/D0BM00204F.

[97] A. Fagan, M. Bartkowski, and S. Giordani, “Spiropyran-Based Drug Delivery Systems,” *Front Chem*, vol. 9, Jul. 2021, doi: 10.3389/fchem.2021.720087.

[98] Mohsen M. Mady, “Interaction of DNA and polyethylenimine: Fourier-transform infrared (FTIR) and differential scanning calorimetry (DSC) studies,” *International Journal of the Physical Sciences*, vol. 6, no. 32, Dec. 2011, doi: 10.5897/IJPS11.1005.

[99] Sean M. Solberg and Christopher C. Landry, “Adsorption of DNA into Mesoporous Silica,” *J Phys Chem B*, vol. 110, no. 31, pp. 15261–15268, 2006.

[100] J. Andersson, S. Li, P. Lincoln, and J. Andréasson, “Photoswitched DNA-Binding of a Photochromic Spiropyran,” *J Am Chem Soc*, vol. 130, no. 36, pp. 11836–11837, Sep. 2008, doi: 10.1021/ja801968f.

# A. APPENDIX

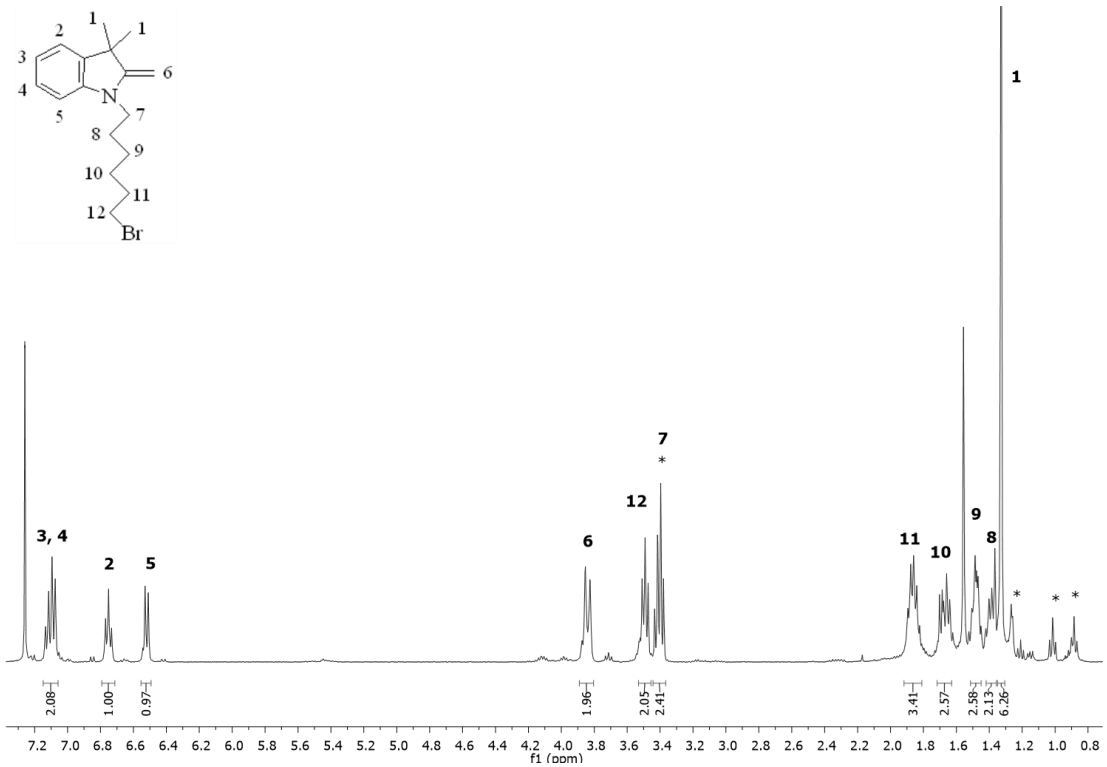


**Figure A.1** $^{1}$H NMR of Compound 2; solvent peaks are market with a *.

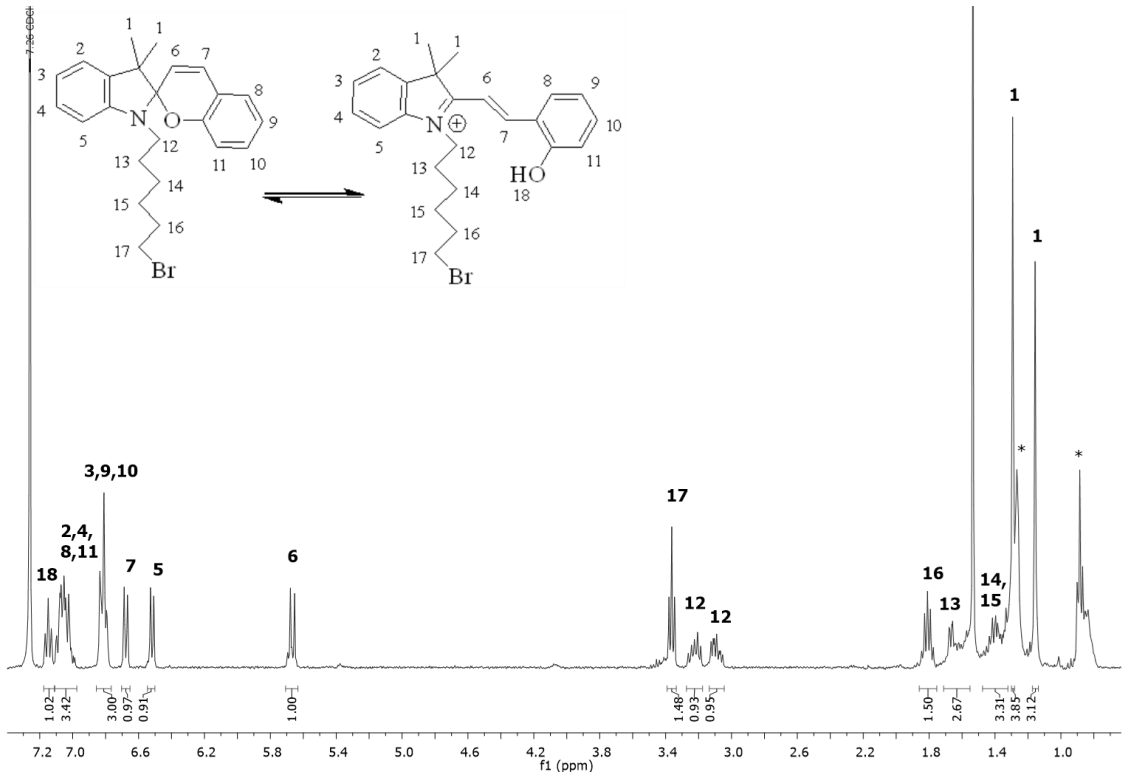


**Figure A.2** $^{1}$H NMR of Compound 2; solvent peaks are market with a *.

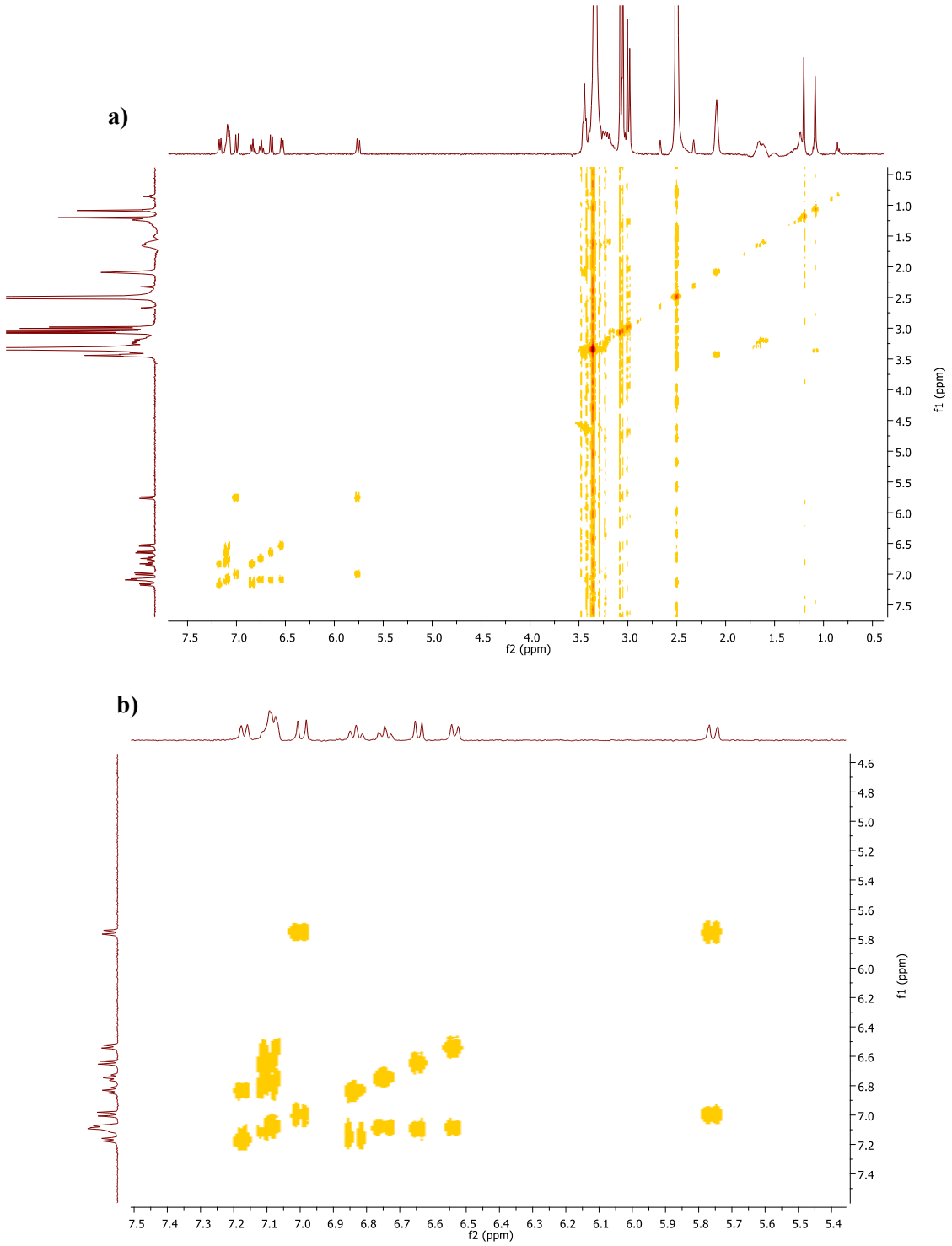


**Figure A.3** COSY 2D NMR spectrum of Compound 4: **a)** all spectrum; **b)** aromatic region.

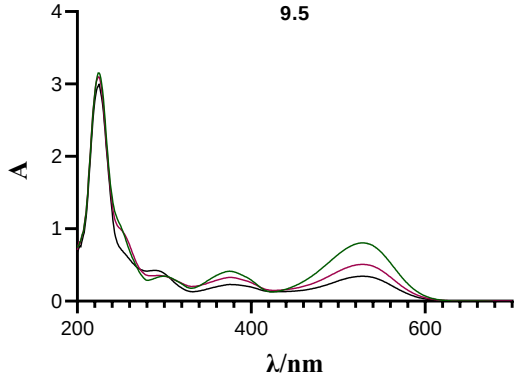
9.5
A
λ/nm
0
1
2
3
4
200
400
600

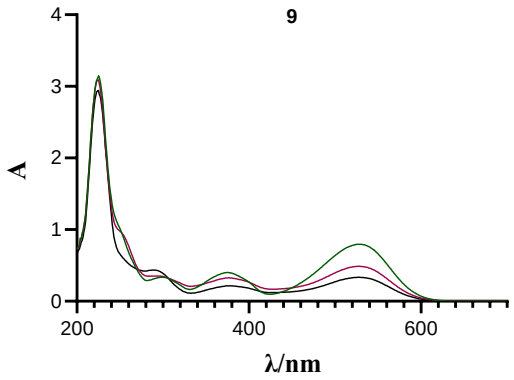
9
A
λ/nm
0
1
2
3
4
200
400
600

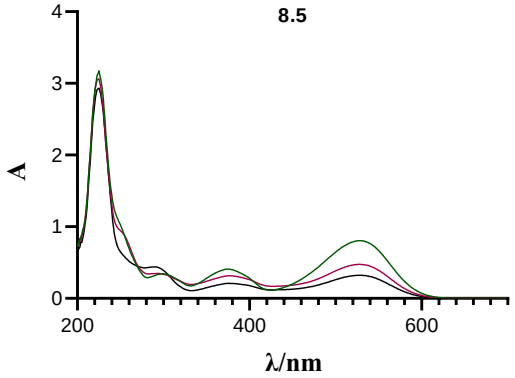
8.5
A
λ/nm
0
1
2
3
4
200
400
600

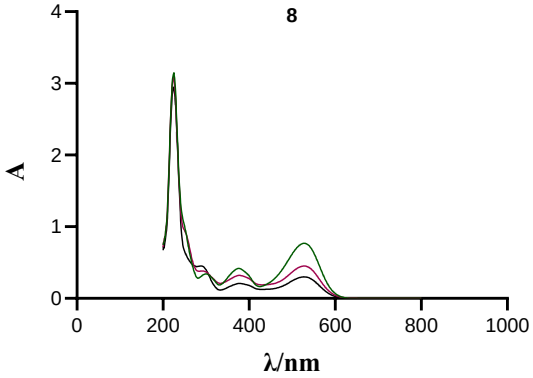
8
A
λ/nm
0
1
2
3
4
0
200
400
600
800
1000

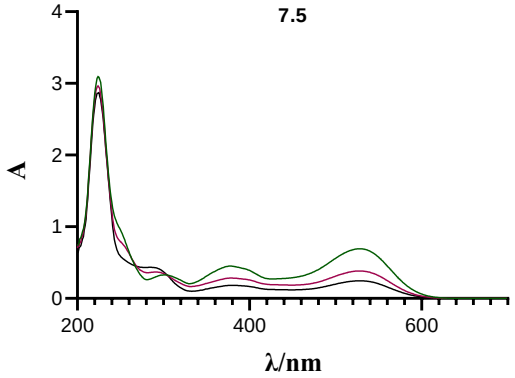
7.5
A
λ/nm
0
1
2
3
4
200
400
600

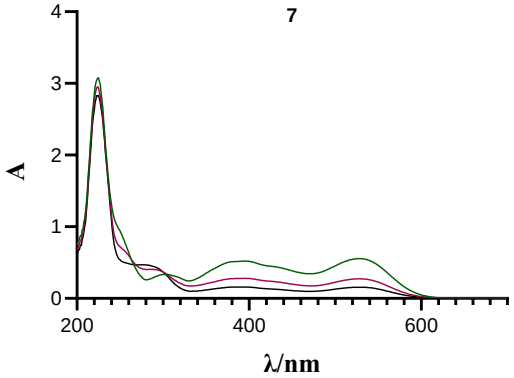
7
A
λ/nm
0
1
2
3
4
200
400
600

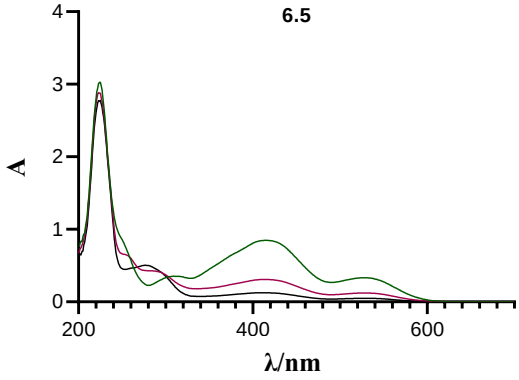
6.5
A
λ/nm
0
1
2
3
4
200
400
600

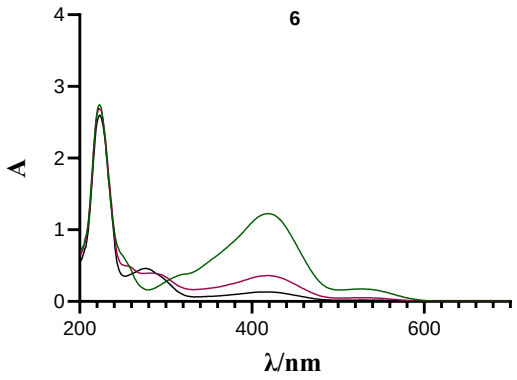
6
A
λ/nm
0
1
2
3
4
200
400
600

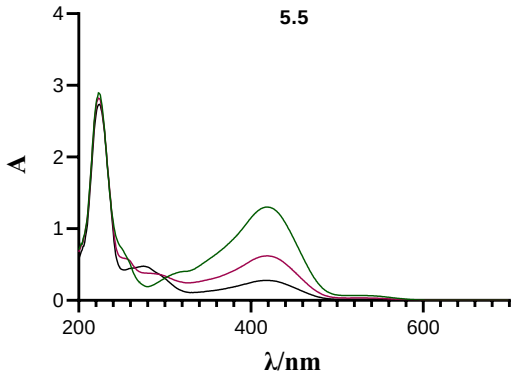
5.5
A
λ/nm
0
1
2
3
4
200
400
600

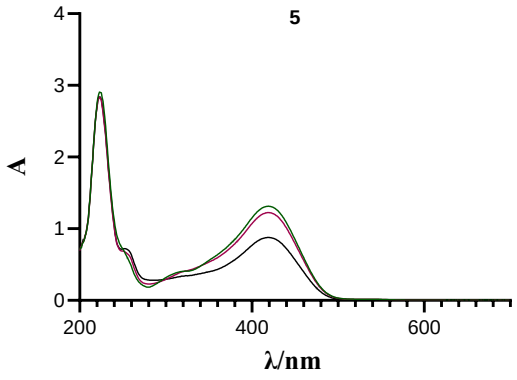
5
A
λ/nm
0
1
2
3
4
200
400
600

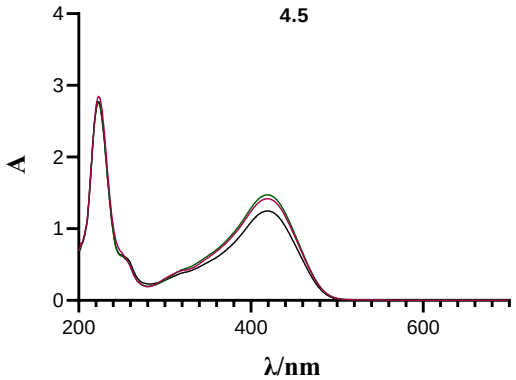
4.5
A
λ/nm
0
1
2
3
4
200
400
600

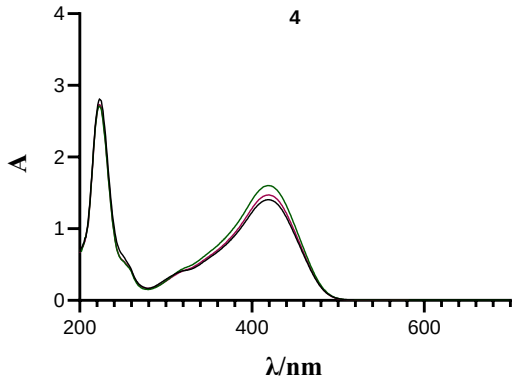
4
A
λ/nm
0
1
2
3
4
200
400
600

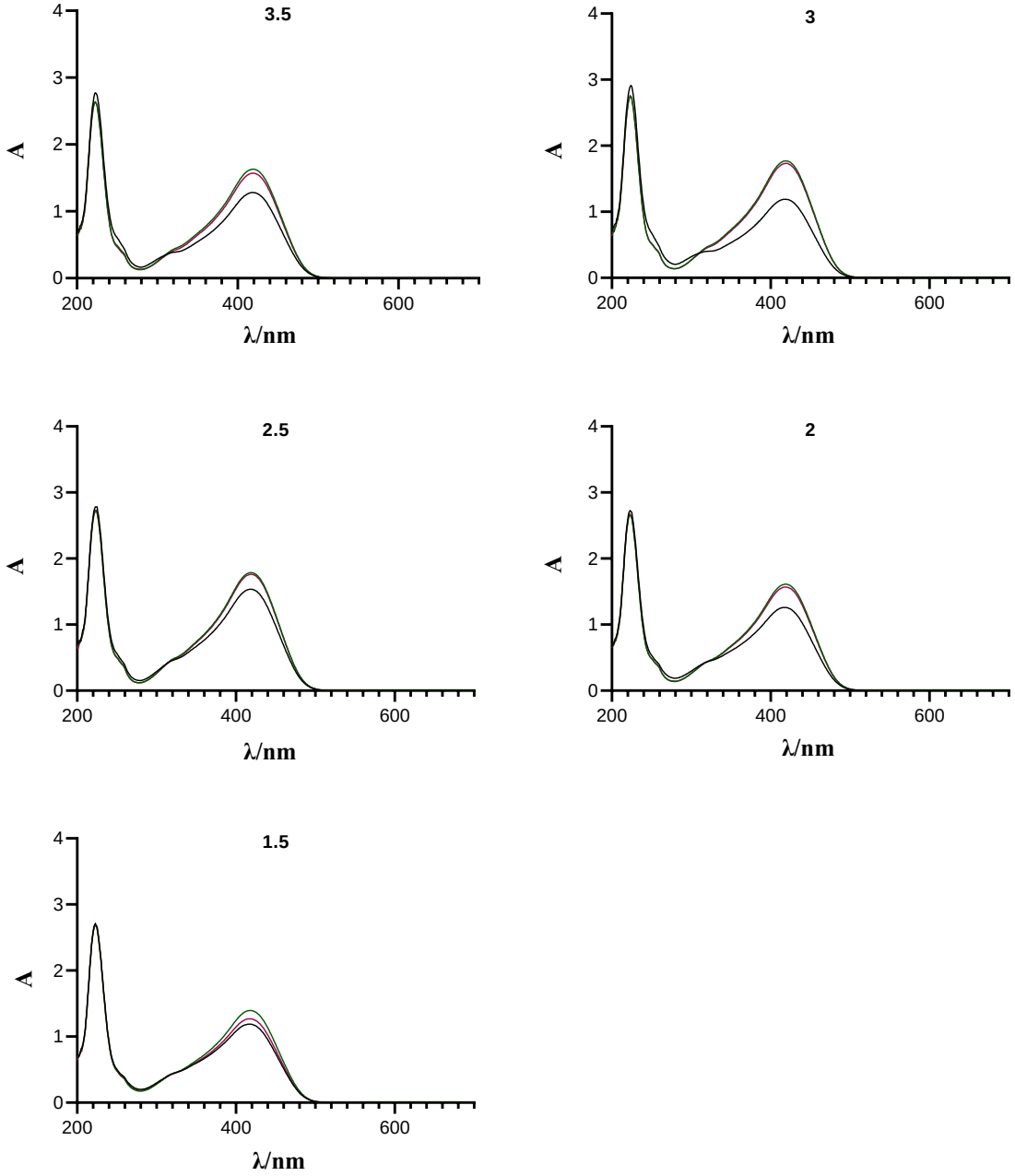


**Figure A.4** SP solutions UV-Vis spectra at different pHs in water. The pH range is from 9.5 to 1.5 with an interval of 0.5un. It it possible to observe SP degradation throught time at different pHs where there is a decrease in absorbance: Day 1 - inicial absorbance (higher absorbance at green); Day 4 - second absorbance (medium absorbance at pink); Day 6 - last absorbance (lower absorbance at black).

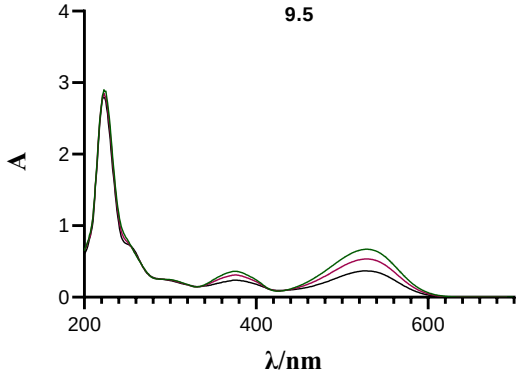
9.5
A
λ/nm

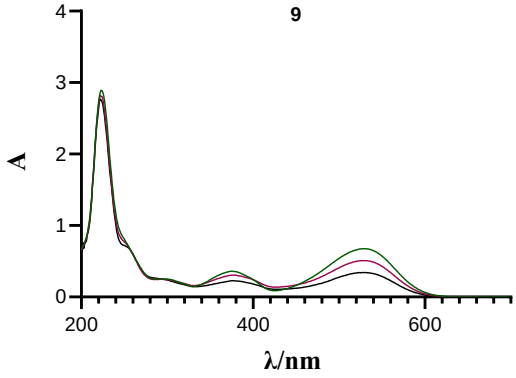
9
A
λ/nm

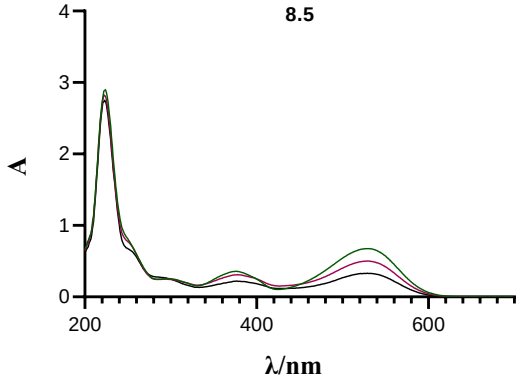
8.5
A
λ/nm

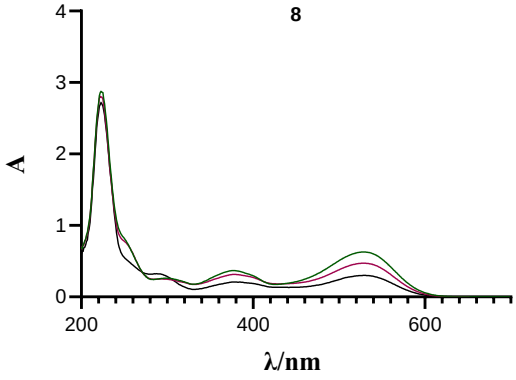
8
A
λ/nm

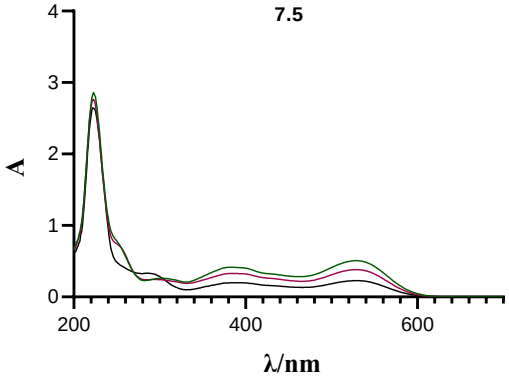
7.5
A
λ/nm

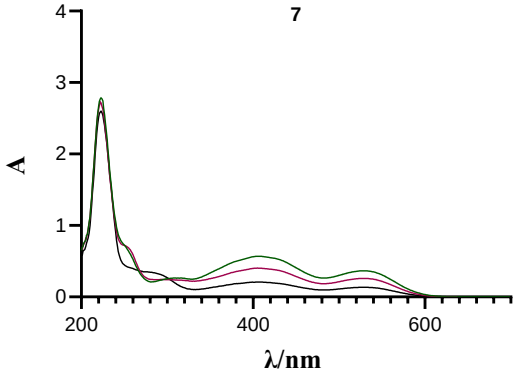
7
A
λ/nm

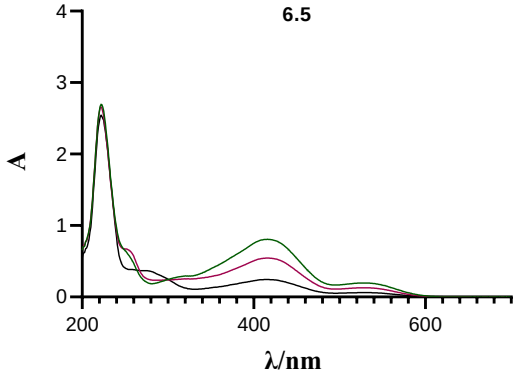
6.5
A
λ/nm
0
1
2
3
4
200
400
600

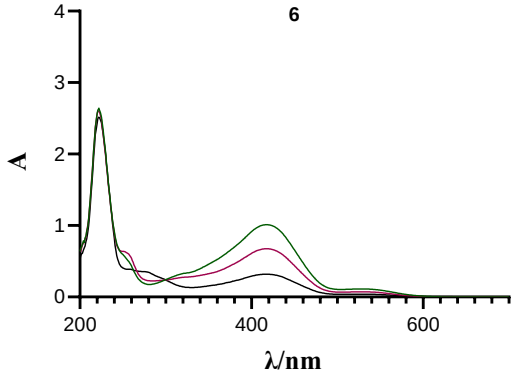
6
A
λ/nm
0
1
2
3
4
200
400
600

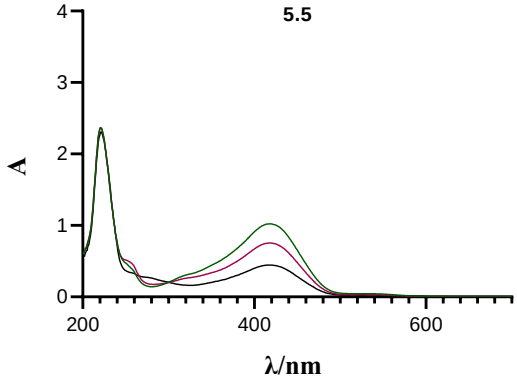
5.5
A
λ/nm
0
1
2
3
4
200
400
600

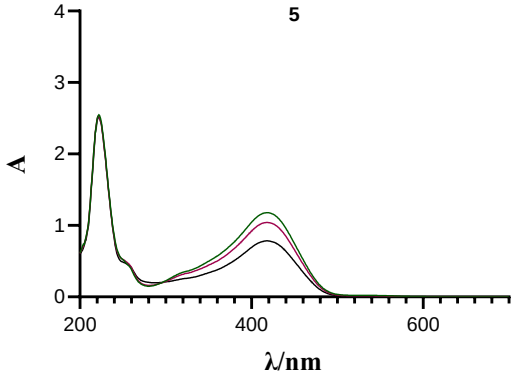
5
A
λ/nm
0
1
2
3
4
200
400
600

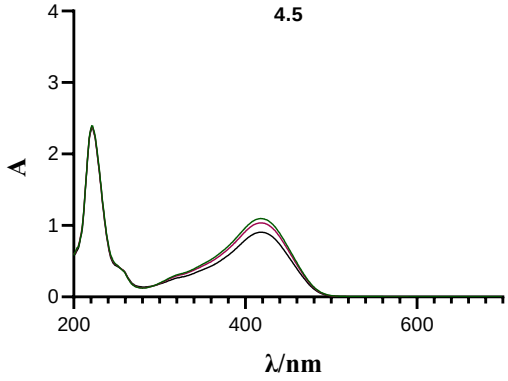
4.5
A
λ/nm
0
1
2
3
4
200
400
600

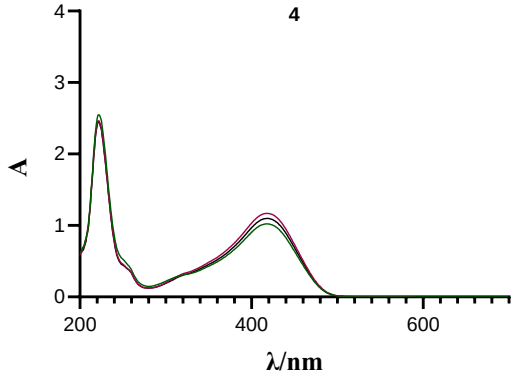
4
A
λ/nm
0
1
2
3
4
200
400
600

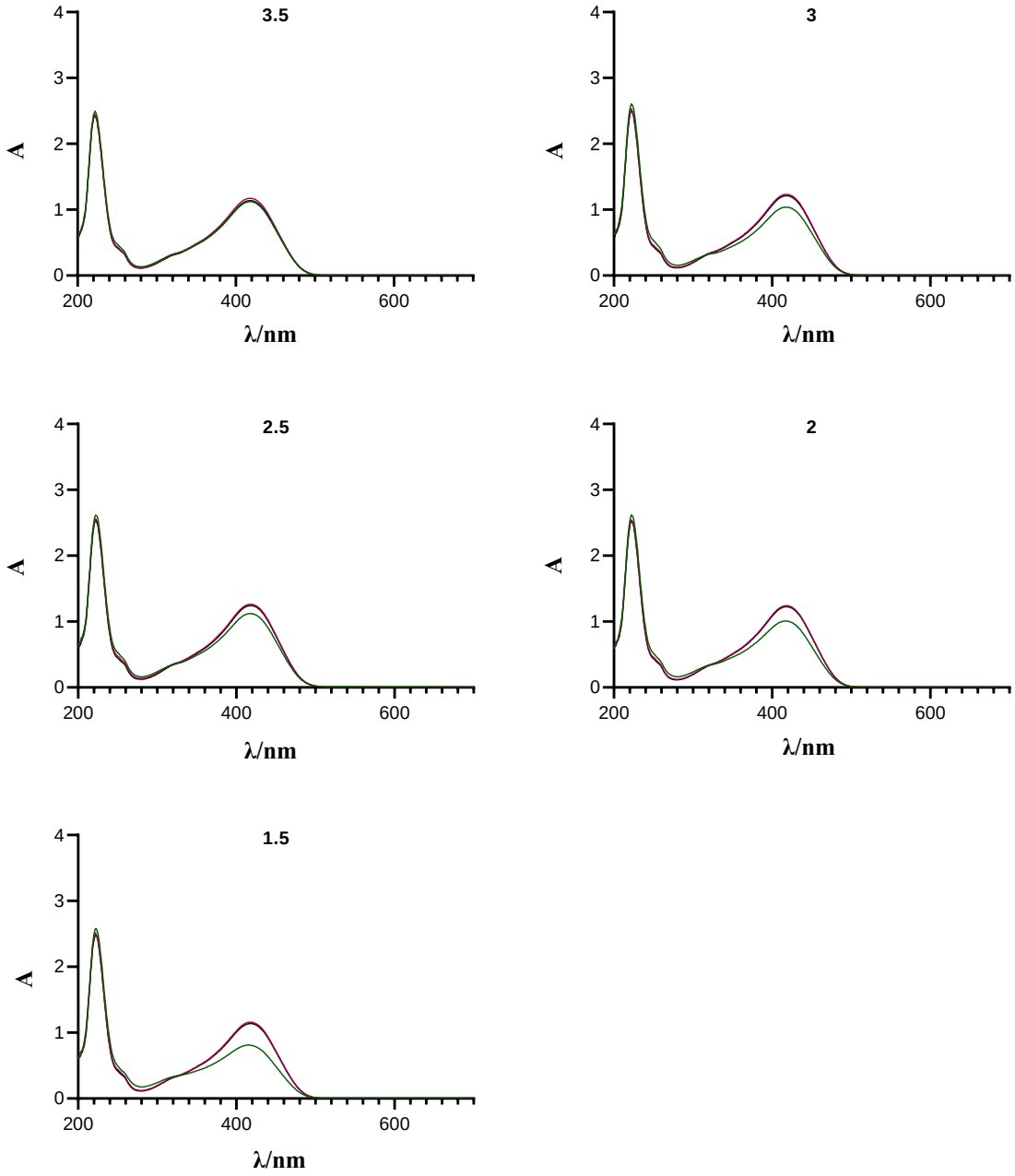


**Figure A.5** SP solutions UV-Vis spectra at different pHs in water, in the presence of a ≈2M solution of CB[7]. The pH range is from 9.5 to 1.5 with an interval of 0.5un. It it possible to observe SP degradation throught time at different pHs where there is a decrease in absorbance: Day 1 - inicial absorbance (higher absorbance at green); Day 2 - second absorbance (medium absorbance at pink); Day 4 - last absorbance (lower absorbance at black).

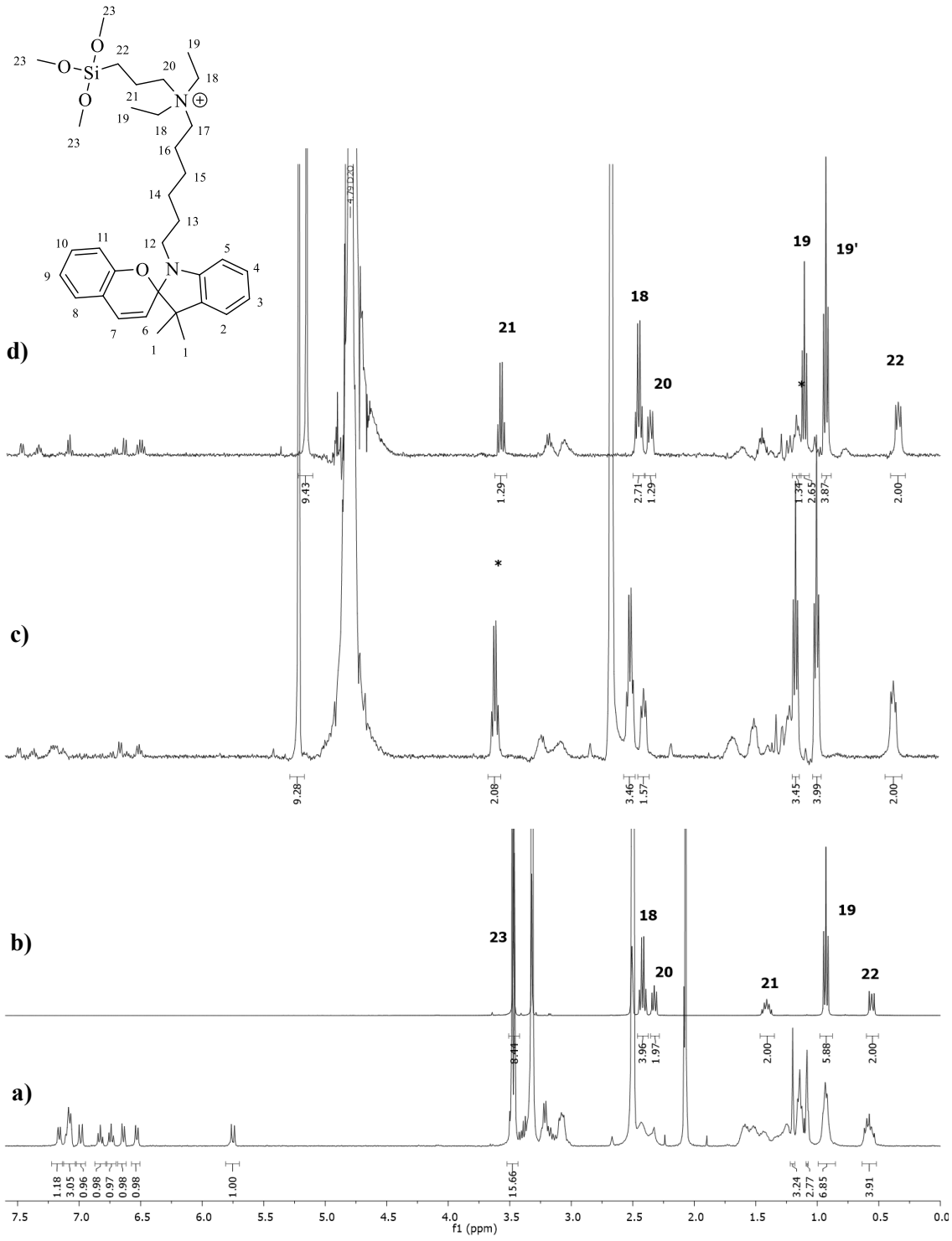


**Figure A.6** $^{1}$H NMR spectrum of a) Compound 5, b) DAPTS, c) MSN-Compound 5-MW and d) MSN-Compound 5-Reflux.

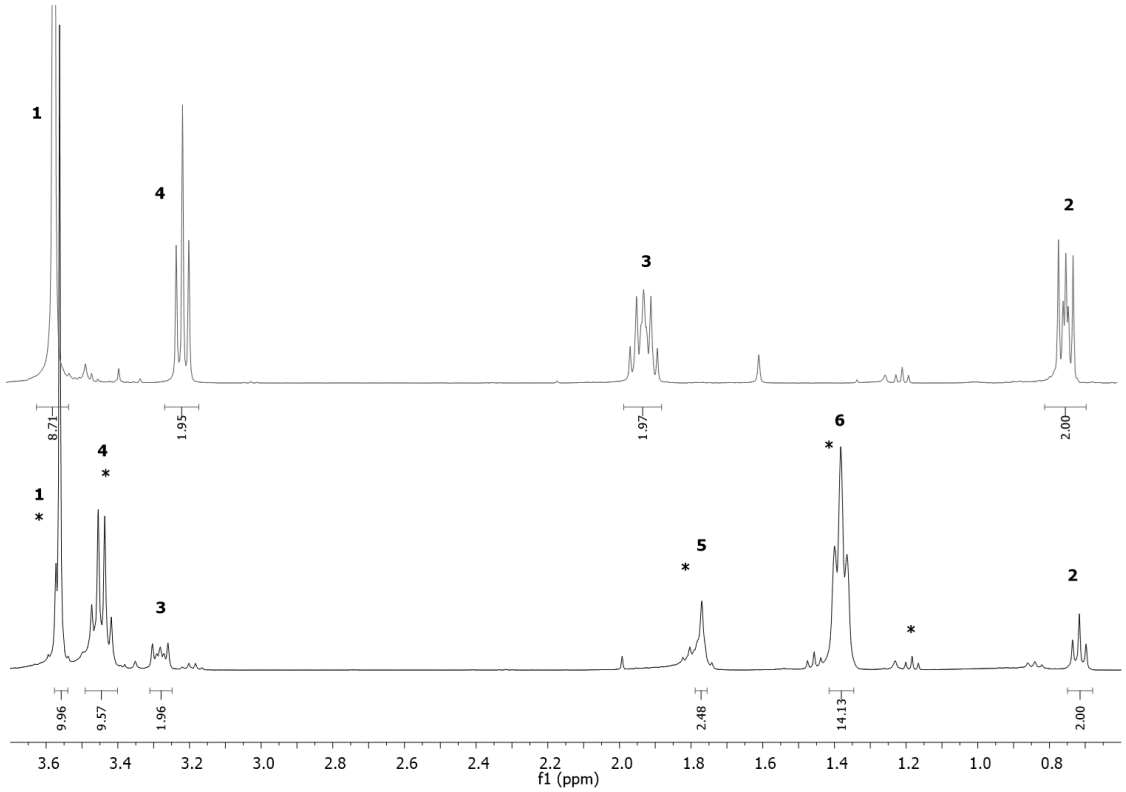


**Figure A.7** [1]H NMR spectrum of a) TESPAI in comparison with b) (3-Iodopropyl)trimethoxysilane.

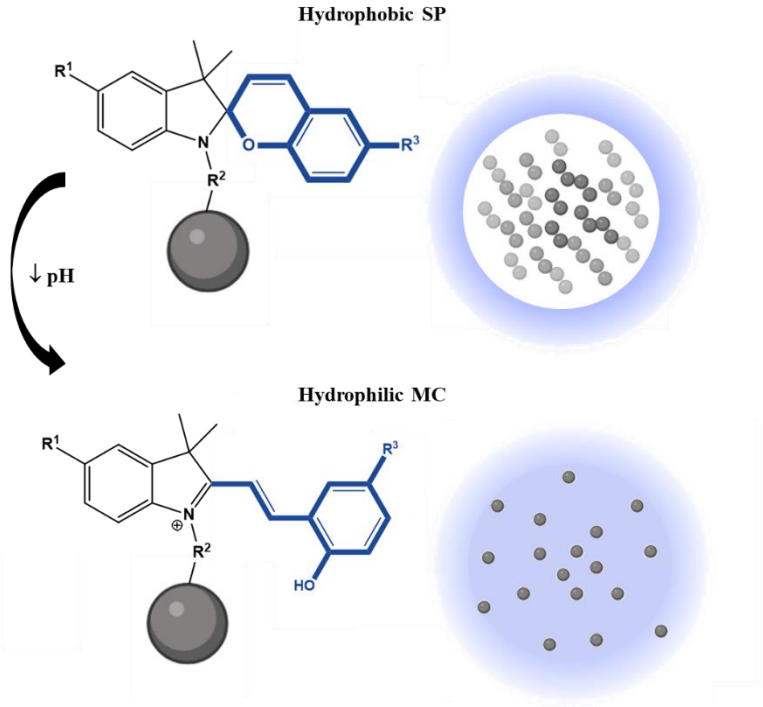


**Figure A.8** Effect of SP derivates on suspension's stability according to the pH.

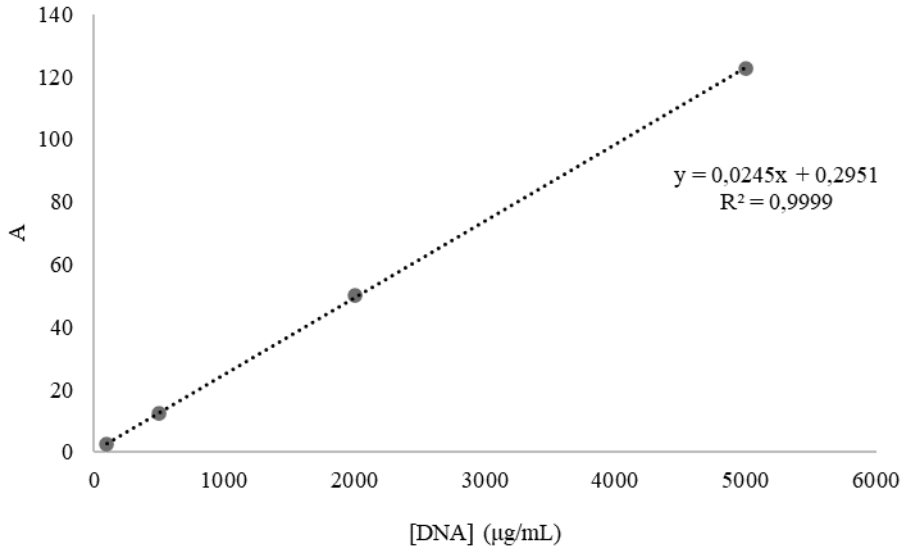


**Figure A.9** Absorbance as a function of the DNA concentration ([DNA]).

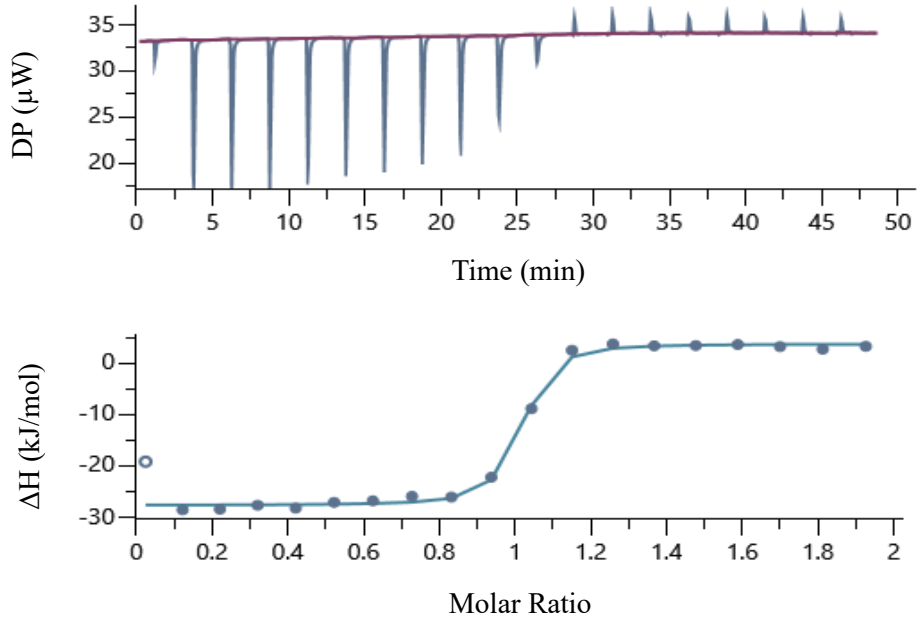


**Figure A.10** ITC binding profile: (**A**) Heat flow versus time for the injection of 2 mM CB7 solution in 0.2 mM solution of Compound 4 at 25 ºC and (**B**) data points represent heat/mol versus CB7/Compound 4 ratio. The solid line represents the best fitted curve at its original pH=7.5.

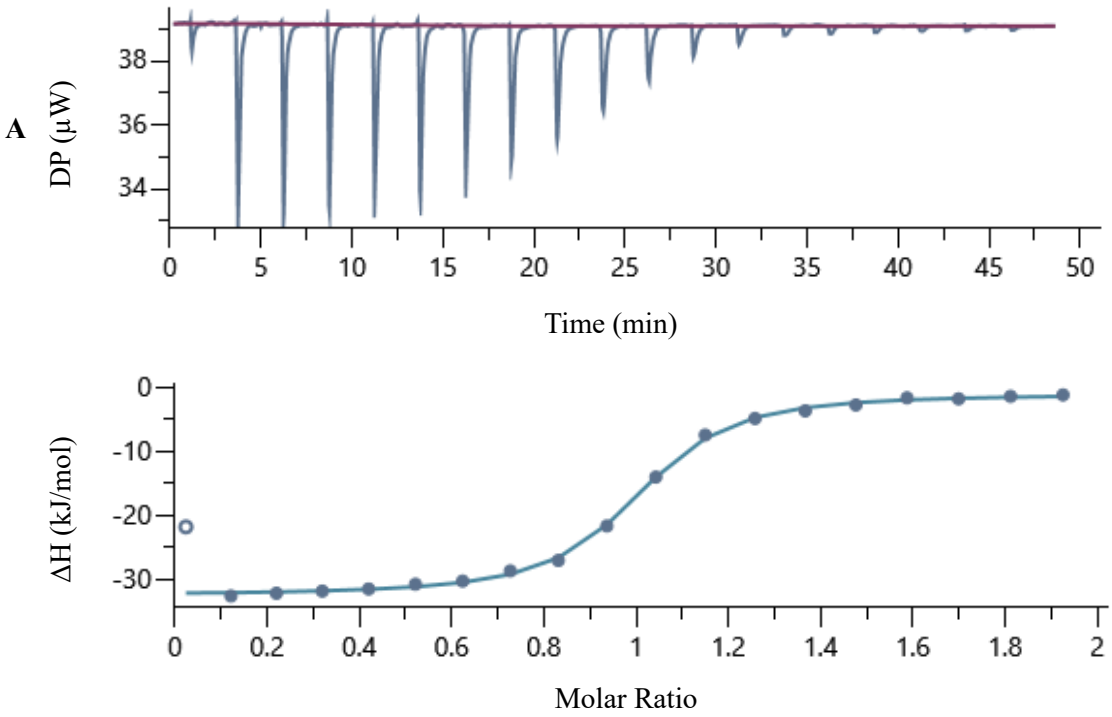


**Figure A.11** ITC binding profile: (**A**) Heat flow versus time for the injection of 1 mM CB7 solution in 0.2 mM solution of Compound 4 at 25 ºC and (**B**) data points represent heat/mol versus CB7/Compound 4 ratio. The solid line represents the best fitted curve at its original pH=7.5.

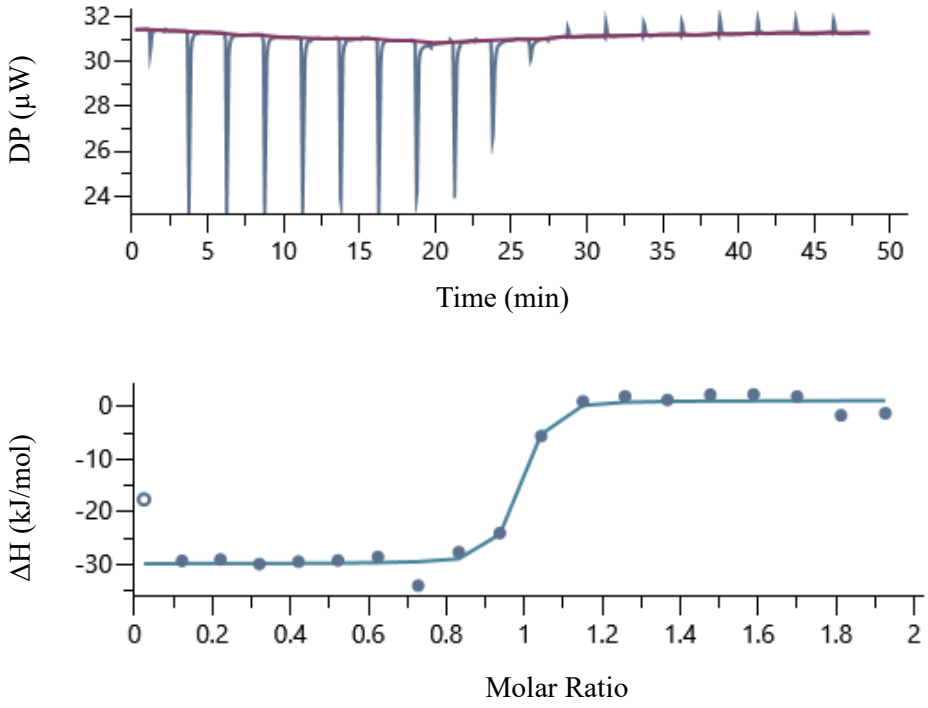


**Figure A.12** ITC binding profile: (**A**) Heat flow versus time for the injection of 1 mM CB7 solution in 0.1 mM solution of Compound 4 at 25 ºC and (**B**) data points represent heat/mol versus CB7/Compound 4 ratio. The solid line represents the best fitted curve at pH=4.2

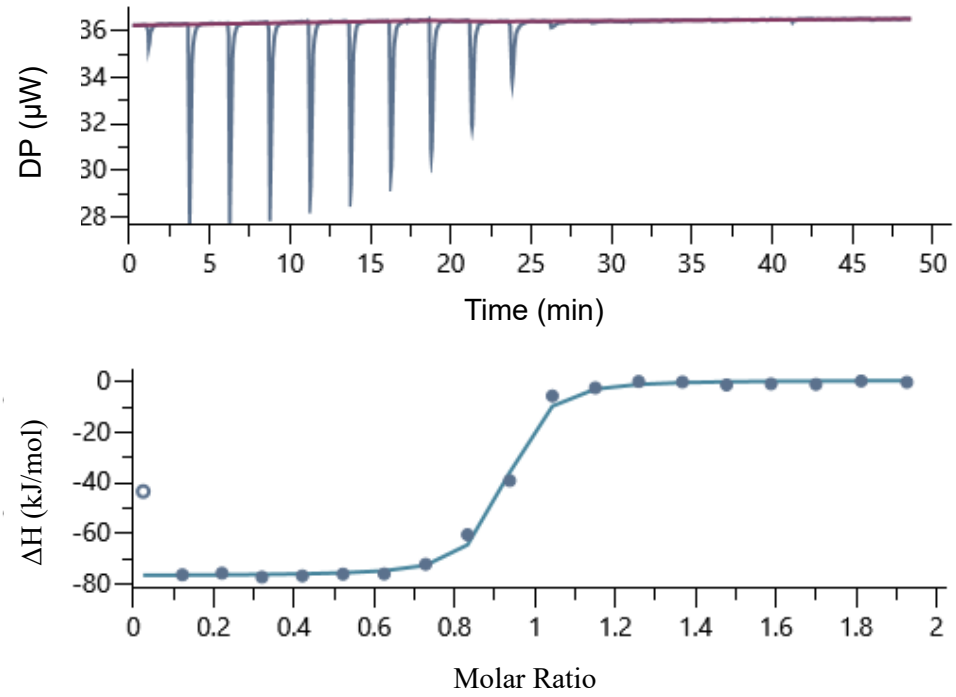


**Figure A.13** ITC binding profile: (**A**) Heat flow versus time for the injection of 0.5 mM CB7 solution in 0.05 mM solution of Adamantane 25 ºC and (**B**) data points represent heat/mol versus CB7/Compound 4 ratio. The solid line represents the best fitted curve at pH=4.5.

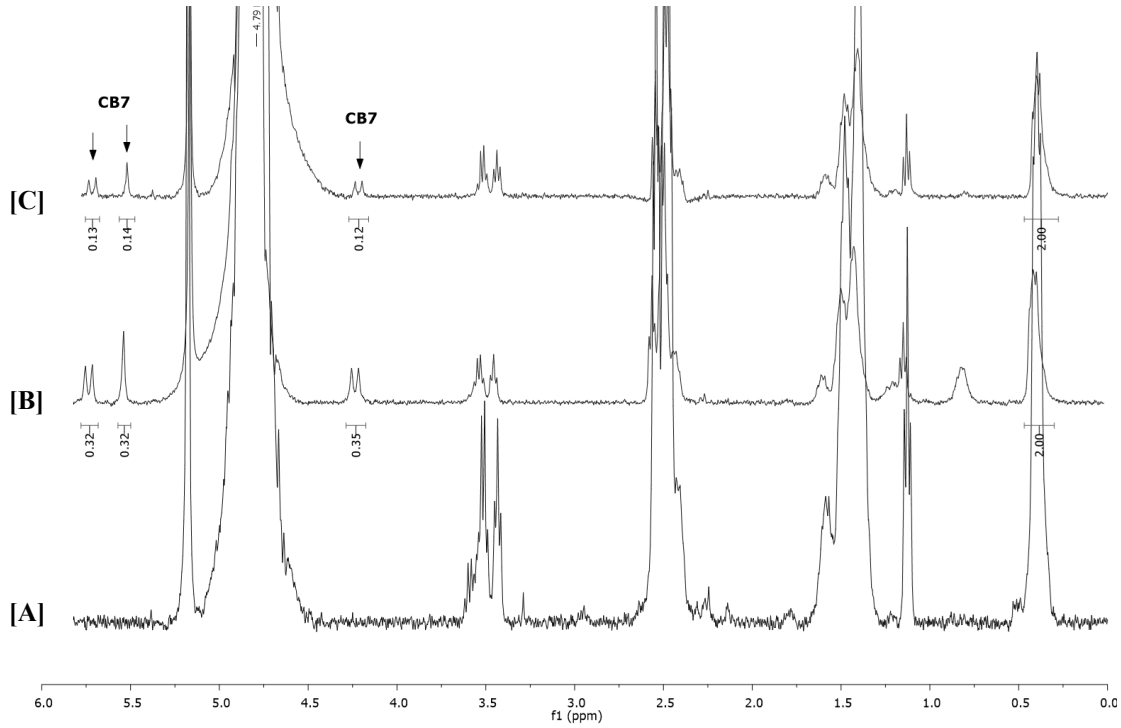


**Figure A.14** [1]H NMR spectra (D2O+NaOH) of the first batch prepared in section 3.6.1: **[A]** NMR prepared after MCM-41 functionalization with butanediamine; **[B]** 20mg of MCM-41+butanediamine with 1.5 mL of a ≈2mM CB[7] solution and no washes; **[C]** previous sample but with a triple washing.

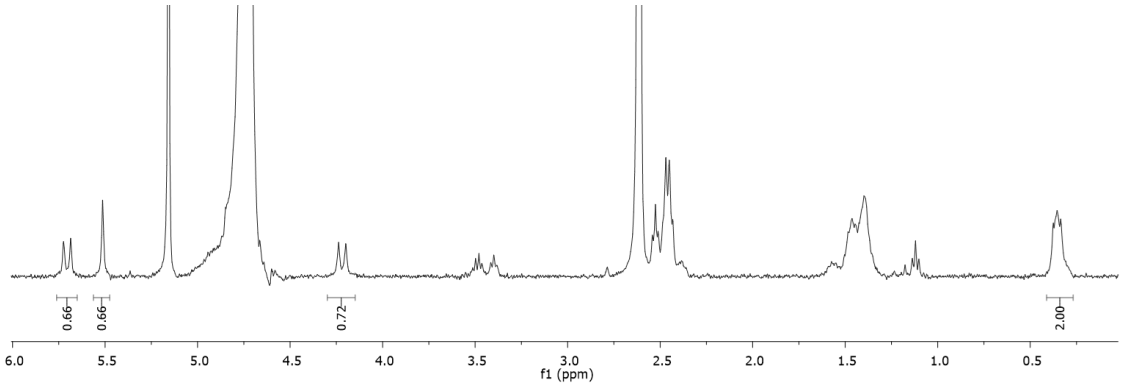


**Figure A.15** [1]H NMR spectrums of MCM-41+butanediamine with 5 mL of a ≈2mM CB[7] solution (second batch). NMR in D2O+NaOH.

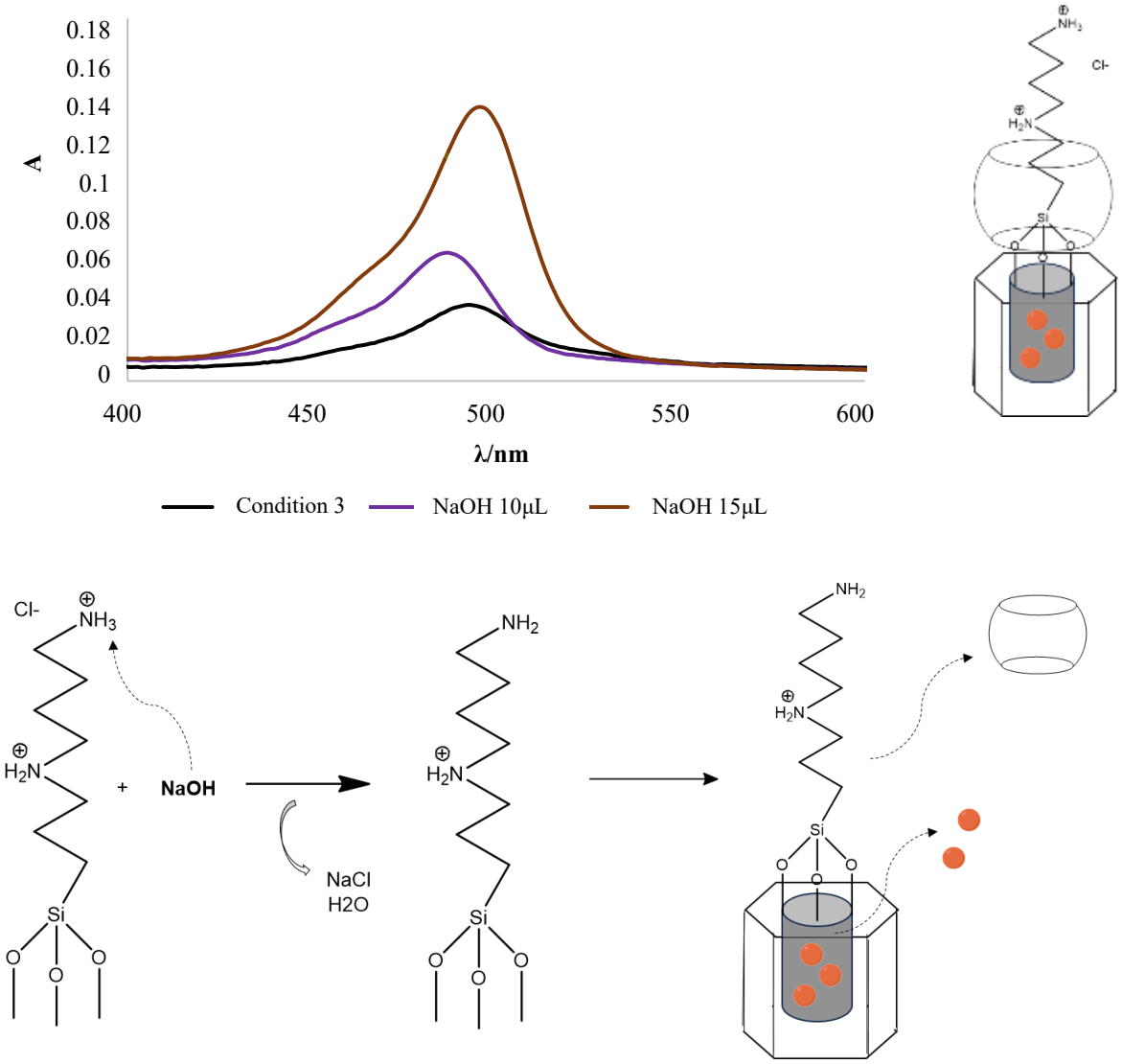


**Figure A.16** Release tests with MCM41-butanediamine: UV-Vis spectrum of condition 3 (MCM-41+calcein+CB7+3 washes) in the presence of a 1M NaOH solution followed by a representative scheme of the deprotonation of butanediamine and detachment of CB7 after NaOH addition.

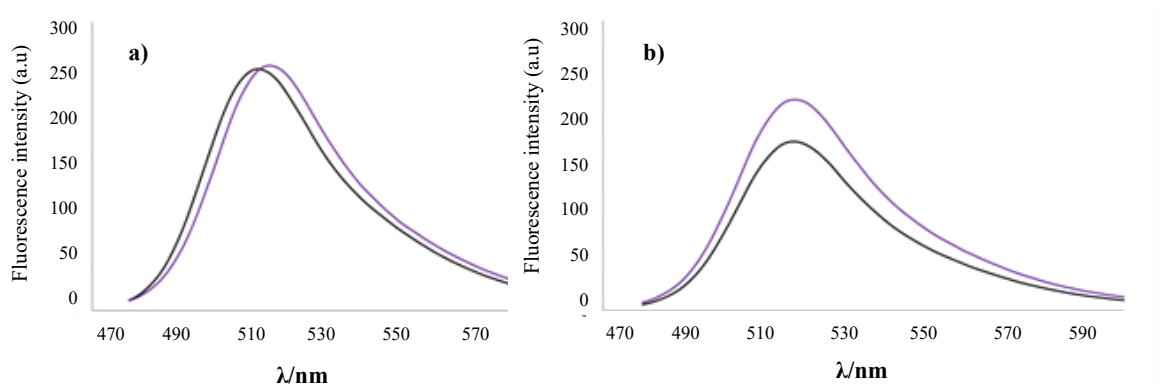


**Figure A.17** Fluorescence emission spectra of condition 4 (**a**) respective to MCM41-butanediamine and calcein washed until no absorbance is observed and condition 3 (**b**) - MCM41-butanediamine with calcein and CB7 after 5 washes -, both with the addition of 3μL of a 0.859M of adamantane solution.